CHALMERS
UNIVERSITY OF TECHNOLOGY

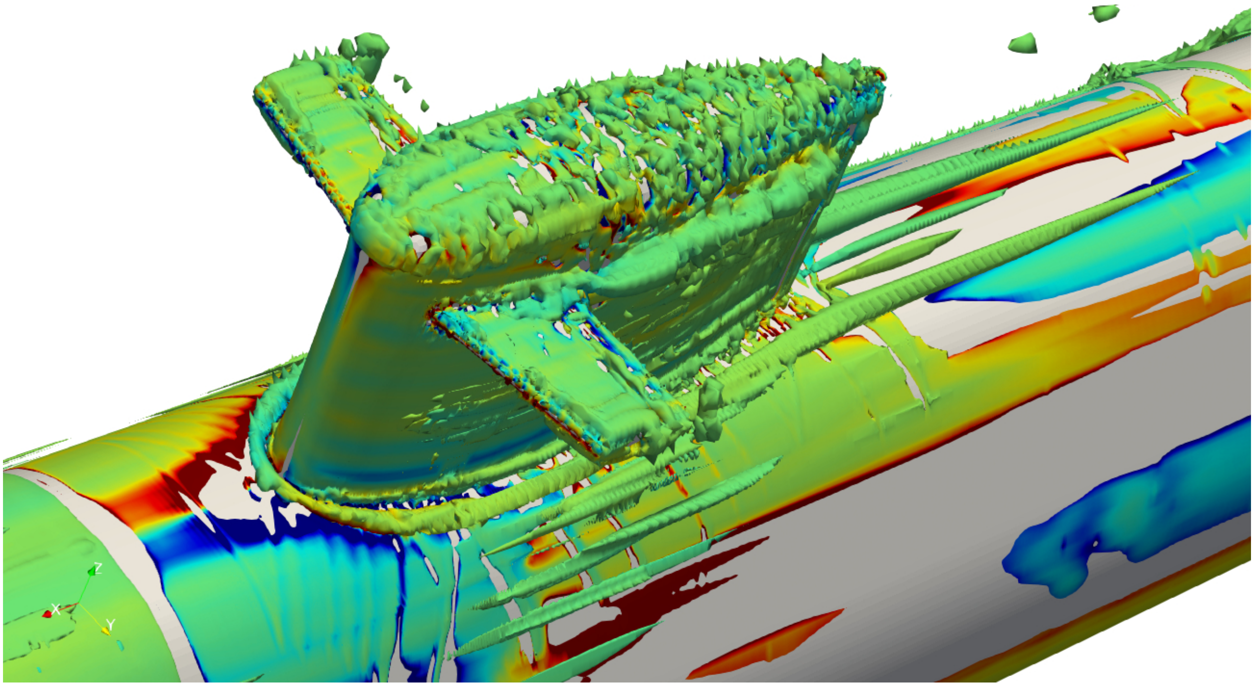

A PANS implementation of k-ω SST turbulence model

Applied to a Submarine flow

Master's thesis in Naval Architecture and Ocean Engineering

SKANDA SUBRAMANYA

DEPARTMENT OF MECHANINCS AND MARITIME SCIENCES

CHALMERS UNIVERSITY OF TECHNOLOGY
Gothenburg, Sweden 2022
www.chalmers.se

Master's thesis 2022

A PANS implementation of k-ω SST turbulence model

SKANDA SUBRAMANYA

CHALMERS
UNIVERSITY OF TECHNOLOGY

Department of Mechanics and Maritime Sciences
Division of Marine technology
Chalmers University of Technology
Gothenburg, Sweden 2022

A PANS implementation of k-ω SST turbulence model

SKANDA SUBRAMANYA

Supervisor: Rickard Bensow, Chalmers University of Technology
Examiner: Rickard Bensow, Chalmers University of Technology

Report Number: 2022:02

Master's Thesis 2022
Department of Mechanics and Maritime Sciences
Chalmers University of Technology
SE-412 96 Gothenburg
Telephone +46 764419005

Typeset in LaTeX
Printed by Chalmers Reproservice
Gothenburg, Sweden 2022

A PANS implementation of k-ω SST turbulence model

SKANDA SUBRAMANYA
Department of Mechanics and Maritime Sciences
Chalmers University of Technology

Abstract

In this thesis, a Partially Averaged Navier Stokes (PANS) turbulence model is implemented for the standard k-ω Shear Stress model (SST). The source code for the PANS implementation of the k-ω SST turbulence model was developed using the C++ programming language. The dynamic PANS turbulence model consists of the active filter function f_k, responsible for the transition from the Reynolds Averaged Navier Stokes (RANS) region to the Large Eddy Simulation (LES) region provided with a smoother transition for refined mesh when compared to coarser mesh. The developed turbulence model was first validated by studying the flow around a cylinder. After validation, the PANS turbulence model was used to investigate the flow quantities around BB2 Generic Submarine hull form.

The outcome of this study is that the PANS model simulations predicted the flow around the circular cylinder better than the k-ω SST model. The validation was performed for different cylinder grid resolutions for comparison. CFD simulations were then carried out for the submarine hull model at straight flight and 10-degree yaw. The PANS model had better flow prediction along the surface of the submarine when compared to the standard SST model for a straight flight, whereas for the 10-degree yaw, both PANS and SST turbulence model had similar flow predictions.

Keywords: Partially Averaged Navier Stokes (PANS), k-ω Shear Stress model (SST), Turbulence model, C++ programming language, Computational Fluid Dynamics (CFD), Reynolds Averaged Navier Stokes (RANS) and Large Eddy Simulation (LES).

Acknowledgements

This master's thesis is part of the Naval Architecture and Ocean Engineering master's programme, part of the Department of Mechanics and Maritime Sciences, Chalmers University of Technology.

The author of this thesis would like to thank and acknowledge the help and contribution of the following:

- Professor Rickard E. Bensow, examiner and supervisor of this master's thesis and Head of Research in Hydrodynamics at the Department of Mechanics and Maritime Sciences at Chalmers University of Technology.
- To everyone on the internet platform and the community for their continuing support.
- Family and friends for their support during the master's programme.

Skanda Subramanya, Gothenburg, November 2021

Contents

List of Figures xi

List of Tables xv

1 Introduction 1
- 1.1 Turbulence Models 1
- 1.2 Hybrid-Turbulence models 3
- 1.3 Thesis Objective and Outline 4

2 Numerical Models 5
- 2.1 k-ω Shear Stress Model 6
- 2.2 PANS implementation for k-ωSST model 7
  - 2.2.1 Computing f_k 8

3 Circular Cylinder at Re=3,900 9
- 3.1 Computational Domain and Boundary Conditions 9
- 3.2 Numerical Settings and Measurements 10
  - 3.2.1 Prism Layers 10
  - 3.2.2 Solving 11
  - 3.2.3 Post-Processing 12
- 3.3 Results 12

4 BB02 Generic Submarine 33
- 4.1 Submarine Geometry and Flow Properties 34
- 4.2 Solving 34
- 4.3 Post-Processing 35
- 4.4 Submarine with Straight Flight 35
- 4.5 Submarine with 10 degree yaw 41

5 Conclusion and Future Work 49

A Appendix 1 I
- A.1 Cylinder I
  - A.1.1 Velocity profile for Mesh 1 II
  - A.1.2 Unresolved Turbulent Kinetic Energy for Mesh 1 III
  - A.1.3 Velocity profile for Mesh 2 V
  - A.1.4 Unresolved Turbulent Kinetic Energy for Mesh 2 VI

A.2 Submarine Straight VIII
A.2.1 Vorticies VIII
A.2.2 Skin Friction IX
A.2.3 Unresolved Turbulent Kinetic Energy XI
A.3 Submarine 10 Degree Yaw XII
A.3.1 Co-Ordinates XII
A.3.2 Vorticies XIII
A.3.3 Skin Friction XV
A.3.4 fK Variation XVI

List of Figures

1.1 Energy Spectrum 2

3.1 Computational Domain 10
3.2 Spatial Grid Resolution 10
3.3 Prism Layers 11
3.4 Mesh1 Grid Refinement 13
3.5 Drag Coefficient for Mesh-1 14
3.6 Lift Coefficient for Mesh-1 14
3.7 Stream-lines of SST and dynamic PANS 15
3.8 Stream-lines of $f_k = 0.3$ and 0.7 15
3.9 M1 Q-criterion for dynamic PANS and SST 16
3.10 M1 Q-criterion for static PANS at 0.3 and 0.7 16
3.11 SST and Static PANS $f_k = 1.0$ Streamwise Comparison 17
3.12 SST and Static PANS $f_k = 1.0$ Spanwise Comparison 17
3.13 X-Magnitude with Experimental Data at 1.06 18
3.14 Z-Magnitude with Experimental Data at 1.06 18
3.15 X-Magnitude without Experimental Data at 1.06 19
3.16 X-Magnitude without Experimental Data Zoomed at 1.06 19
3.17 Z-Magnitude without Experimental Data at 1.06 20
3.18 X-Magnitude with Experimental Data at 1.54 20
3.19 Z-Magnitude with Experimental Data at 1.54 21
3.20 X-Magnitude at 1.54 21
3.21 X-Magnitude zoomed at 1.54 22
3.22 X-Magnitude with Experimental Data at 2.02 22
3.23 Z-Magnitude with Experimental Data at 2.02 23
3.24 X-Magnitude Zoomed at 2.02 23
3.25 Z-Magnitude at 2.02 24
3.26 Mesh2 Grid Refinement 25
3.27 Drag Coefficient for Mesh-2 25
3.28 Lift Coefficient for Mesh-2 26
3.29 Stream Lines of SST and dynamic PANS for Mesh 2 27
3.30 Stream Lines for fk = 0.3 and 0.7 for Mesh 2 27
3.31 M2 Q-criterion for dynamic PANS and SST 28
3.32 M2 Q-criterion for static PANS at 0.3 and 0.7 28
3.33 X-Magnitude at 1.06 M2 29
3.34 Z-Magnitude at 1.06 M2 29

3.35 f_k Variation Comparison 31

4.1 Hull Form 33
4.2 BB2 Flow Quantities 35
4.3 BB2 Grid resolution for Straight Flight 36
4.4 Drag Force for straight flight 36
4.5 Lift Force for straight flight 37
4.6 Vorticity x for dynamic PANS and SST Straight Flight 37
4.7 Vorticity x for static PANS at 0.3 and 0.7 Straight Flight 38
4.8 Pressure for dynamic PANS and SST Straight Flight 38
4.9 Pressure for static PANS at 0.3 and 0.7 Straight Flight 39
4.10 taux for dynamic PANS and SST Straight Flight 39
4.11 taux for static PANS at 0.3 and 0.7 Straight Flight 40
4.12 Q Criterion for dynamic PANS and SST Straight Flight 40
4.13 Q Criterion for static PANS at 0.3 and 0.7 Straight Flight 41
4.14 BB2 Grid resolution for 10 degree yaw Flight 41
4.15 Drag Force for SST for 10 degree yaw Flight 42
4.16 Yaw for SST for 10 degree yaw Flight 43
4.17 Vorticity x for SST for 10 degree yaw Flight 43
4.18 Vorticity x for static PANS at 0.3 and 0.7 for 10 degree yaw Flight . . 44
4.19 Pressure for SST for 10 degree yaw Flight 44
4.20 Pressure for static PANS at 0.3 and 0.7 for 10 degree yaw Flight . . . 45
4.21 taux for SST for 10 degree yaw Flight 45
4.22 taux for static PANS at 0.3 and 0.7 for 10 degree yaw Flight 46
4.23 Q-Criterion for SST for 10 degree yaw Flight 46
4.24 Q-Criterion for static PANS at 0.3 and 0.7 for 10 degree yaw Flight . 47

A.1 X-Magnitude with Experimental Data at 1.54m for Mesh 2 I
A.2 Z-Magnitude with Experimental Data at 1.54m for Mesh 2 I
A.3 X-Magnitude with Experimental Data at 2.02m for Mesh 2 II
A.4 Z-Magnitude with Experimental Data at 2.02m for Mesh 2 II
A.5 Velocity profile for SST Turbulence model for Mesh 1 II
A.6 Velocity profile for dynamic PANS Turbulence model for Mesh 1 . . . III
A.7 Velocity profile for static PANS at 0.3 Turbulence model for Mesh 1 . III
A.8 Velocity profile for static PANS at 0.7 Turbulence model for Mesh 1 . III
A.9 Turbulent Kinetic Energy for SST Turbulence model for Mesh 1 . . . IV
A.10 Unresolved Turbulent Kinetic Energy for dynamic PANS Turbulence model for Mesh 1 IV
A.11 Unresolved Turbulent Kinetic Energy for static PANS at 0.3 Turbulence model for Mesh 1 IV
A.12 Unresolved Turbulent Kinetic Energy for static PANS at 0.7 Turbulence model for Mesh 1 V
A.13 Velocity profile for SST Turbulence model for Mesh 2 V
A.14 Velocity profile for dynamic PANS Turbulence model for Mesh 2 . . . V
A.15 Velocity profile for static PANS at 0.3 Turbulence model for Mesh 2 . VI
A.16 Velocity profile for static PANS at 0.7 Turbulence model for Mesh 2 . VI
A.17 Turbulent Kinetic Energy for SST Turbulence model for Mesh 2 . . . VI

A.18 Unresolved Turbulent Kinetic Energy for dynamic PANS Turbulence model for Mesh 2 VII
A.19 Unresolved Turbulent Kinetic Energy for static PANS at 0.3 Turbulence model for Mesh 2 VII
A.20 Unresolved Turbulent Kinetic Energy for static PANS at 0.7 Turbulence model for Mesh 2 VII
A.21 vorty for dynamicPANS and SST VIII
A.22 vorty for staticPANS at 0.3 and 0.7 VIII
A.23 vortz for dynamicPANS and SST IX
A.24 vortz for staticPANS at 0.3 and 0.7 IX
A.25 tauy for dynamicPANS and SST X
A.26 tauy for staticPANS at 0.3 and 0.7 X
A.27 tauz for dynamicPANS and SST X
A.28 tauz for staticPANS at 0.3 and 0.7 XI
A.29 Unresolved Turbulent Kinetic Energy for Dynamic PANS XI
A.30 Unresolved Turbulent Kinetic Energy for staticPANS at 0.3 and 0.7 . XI
A.31 y Co-Ordinate for SST 10 degree yaw XII
A.32 y Co-Ordinates for staticPANS at 0.3 and 0.7 10 degree yaw XII
A.33 z Co-Ordinate for SST 10 degree yaw XII
A.34 z Co-Ordinates for staticPANS at 0.3 and 0.7 10 degree yaw XIII
A.35 vorty for SST 10 degree yaw XIII
A.36 vorty for staticPANS at 0.3 and 0.7 10 degree yaw XIV
A.37 vortz for SST 10 degree yaw XIV
A.38 vortz for staticPANS at 0.3 and 0.7 10 degree yaw XIV
A.39 tauy for SST 10 degree yaw XV
A.40 tauy for staticPANS at 0.3 and 0.7 10 degree yaw XV
A.41 tauz for SST 10 degree yaw XV
A.42 tauz for staticPANS at 0.3 and 0.7 10 degree yaw XVI
A.43 fk variation XVI

List of Tables

2.1 Coefficients of the k - ω SST closure model 7

3.1 Comparison of forces for the cylinder 30

4.1 Particulars of BB2 34
4.2 Flow properties of BB2 34
4.3 Comparison of forces for the Submarine 47

1

Introduction

CFD, or Computational fluid dynamics, is the study or analysis of fluid flow, heat transfer, or any other type of phenomena, such as chemical reactions, using computed simulations. These computations are performed using modern computer-based simulations [14]. One of the many challenging aspects considered while performing a CFD analysis is the turbulence modelling for the specific flow type. According to [9], many researchers have been addressing turbulence flow through Direct Numerical Simulation(DNS)and Large Eddy Simulation(LES) for nearly decades. Similarly, many engineers approach this problem based on intuition in which an appropriate mathematical model is derived to simulate and examine the flow of some beneficial interests since DNS and LES simulations are time consuming and expensive. These simulations are typically constrained by walls and are performed at high Reynolds numbers (typically above 10^5).

1.1 Turbulence Models

Almost all fluids encountered on a day-to-day basis are turbulent. In turbulent flow, the velocities are divided into two parts: the time-averaged part independent of time, while the other is the fluctuating part in space and time. The energy transfer in turbulence is based on the cascade process, where the energy is transferred from large turbulent scales to small scales. These scales extract the kinetic energy from the mean flow, which contains the time scale. The most miniature scale where dissipation occurs is called the Kolmogorov scale. It is assumed that these scales are determined by viscosity and dissipation.
As mentioned above, turbulent fluctuations are composed of energy at different scales. We can think of these structures as eddies. The spectrum of the turbulent fluctuations can be understood better when looking at the energy spectrum graph. Figure 1.1 shows the spectrum for the turbulent kinetic energy, k. The wavenumber, κ, is proportional to the inverse of the length scale of a turbulent eddy. The initial region I, we have the large eddies which carry most of the energy. These eddies then interact with the main flow and extract energy from mean flow. This energy transfer takes place by the production term present in the transport equation for the turbulent kinetic energy. The region II in figure 1.1 is called the inertial subrange. For the existence of this region, the Reynolds number should be high (fully turbulent flow). The eddies in this region represent the mid-region. This region is considered as the transport region in the cascade process. This region consists of isotropic turbulence which means that the average eddies have no preferred direction i.e. the fluctuations

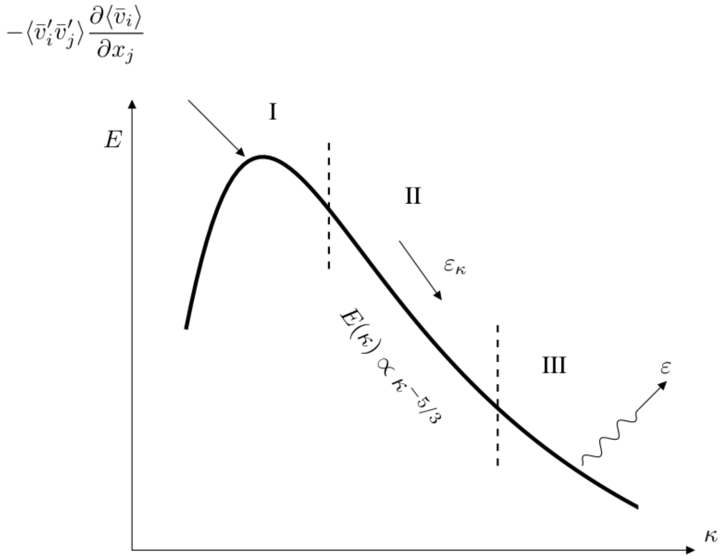

Figure 1.1: Energy Spectrum

in all directions are same. The last region III in the figure is called the dissipation region. The eddies are small and isotropic like region II. In this region, the energy is transferred form the turbulent kinetic energy into thermal energy i.e. increased temperature.
When we consider the implementation of turbulence models, the most accurate model that can be considered in predicting the flows is the DNS method. According to [8], DNS involves solving the Navier-Stokes equation directly. It is said to have very high resolving capabilities considering even the smallest eddies and the turbulent time scales of the flow. Similar to the DNS model is the LES model, which is also considered to provide highly accurate simulation results. The only drawbacks of these turbulence models are that they are costly and time-consuming. Therefore, it is not feasible to use DNS and LES models for day-to-day simulations or implement them for industrial purposes. Hence, to overcome this, engineers had to develop a turbulence model with a sure accuracy in the flow prediction and reduced cost and time.

This led to the Reynolds Averaged Navier-Stokes Equation(RANS). The popular RANS turbulence models are mainly two equation models, with one being the 'k-ω' turbulence model and the other being the 'k-ϵ' model. These turbulence models are used based on their desired criteria. There are also four equations turbulence models available, but the most widely used turbulence models are the 'k-ω' and the 'k-ϵ' models. As mentioned before that these turbulence models are used based on specific criteria. The 'k-ω' turbulence model is used when predicting the flow for a near-wall/boundary layer region. The accuracy of the prediction near-wall region is the highest under this model. Simultaneously, while predicting the flow for a region away from the wall/free shear flow, the k-ϵ model is the most accurate. Hence, the turbulence model accommodation during the CFD analysis is purely based on the desired flow prediction.
The main drawback of using either the 'k-ω' or 'k-ϵ' model during flow prediction

is that these turbulence models have sure prediction accuracy at a specific region within the computational domain. Hence, it was impossible to correctly predict the flow at both the near-wall region and far away from the wall region in the same simulation. To overcome this, a new turbulence model was created is called the 'k-ω SST' model. Here the term 'SST' stands for shear stress transport. The SST model combines the 'k-ω' and the 'k-ϵ'.

1.2 Hybrid-Turbulence models

Simulations of bluff body flow is an ideal example for the LES method as bluff body flows are dominated by large turbulent scales, which can be resolved using the LES method without fine resolution. However, it becomes challenging to accurately predict the flow in the near-wall region since the grid spacing should be about one wall unit in the wall-normal direction. This is similar to the requirement in RANS using low-Re number models. At low to medium Reynolds numbers the streak process is responsible for the major part of the turbulence production. These structures must be resolved in an LES in order to achieve accurate results. The idea to overcome this problem led to the development of hybrid turbulence models which is to eliminate the requirement of high near-wall resolution in wall-parallel planes.
Hybrid turbulence models are developed based on combining the advantages of RANS and LES models in a zonal manner according to [10]. Hybrid turbulence models are used to switch between RANS and LES models during the computational analysis. In the near-wall region (the URANS region), a low-Re number RANS turbulence model (usually an eddy-viscosity model) is used. In the outer region (the LES region), the usual LES is used. The idea is that the effect of the near-wall turbulent structures should be modeled by the RANS turbulence model rather than being resolved. In the LES region, coarser grid spacing in wall-parallel planes can be used.
The RANS model, when compared to the LES model, yields lesser information than required for flow prediction, whereas the LES model gives a lot more information than required. Hence, a hybrid turbulence model is developed to yield the right amount of information throughout the computational domain to predict flows.
One of the hybrid models used is the Partially Averaged Navier Stokes (PANS) model, Detached Eddy Simulation (DES) model, and the Delayed Detached-Eddy Simulation (DDES). The PANS approach towards merging the RANS and LES models uses a parameter called "f_k". The parameter "f_k" is used to replace the turbulent length scales. When f_k=1, it is said to be the RANS region, whereas, for f_k=0, it is said to be DNS. For f_k ranging from 0.5-0.1, it is in the LES region. The development of this model is mainly focused on this specific parameter. The f_k parameter is the ratio of the unresolved kinetic energy to the total kinetic energy. When hybrid models are considered, it is required to close these equations because the turbulent length scale present in the dissipation term of the governing equations will be replaced by different parameters. Like the PANS, the DES and the DDES use a similar parameter to switch between RANS and LES.
The main advantages of the hybrid turbulence models over LES and RANS models are as follows,

- They provide more accurate results than the RANS models.
- They are cost effective when compared to DNS or LES approaches.
- They are less time consuming when compared to DNS or LES approaches.

1.3 Thesis Objective and Outline

This dissertation investigates the validation of turbulent external flow for the k-ω. SST PANS model. The source code for the k-ω SST PANS model is created using the open-source CFD software OpenFOAM. It is then validated by investigating the external turbulent flow around a simple cylinder. The PANS validation is performed for multiple parameters "f_k" variants. The investigation is performed for a dynamic f_k and static f_k at 0.3, 0.7, and 1.0. Once the model is validated, the PANS turbulent model is applied to a BB02 generic submarine. The simulations are performed, and all the results are provided later.
Chapter 2 of this dissertation provides a detailed description of the k-ω SST model and the PANS model. Chapter 3 discusses the flow around a cylinder at Re = 3900. This test case is considered to conduct a comprehensive investigation of the selected methods and flow. Once validation is performed in chapter 4, discussions for PANS flow around a submarine is performed, and the results are compared. Chapter 5 deals with the conclusion of the entire study performed.

2

Numerical Models

In order to understand the implementation of the PANS model using the bridging factor, it is necessary to understand the various types of turbulence models present and their computational advantages and disadvantages. Once these models are comprehensible it becomes easier to understand the need for PANS model. This chapter contains a detailed description of RANS model k-ω SST and the hybrid model PANS.
Before getting into the detailed description of the above mentioned turbulence models it is important to understand the equations governing these models. When the flow is turbulent it is preferred to decompose the instantaneous variables such as the velocity and the pressure into two different components where one of the component being the mean value and the other being the fluctuating value. The general notation for this can be written as,

$$\Phi = \overline{\Phi} + \Phi\,', \tag{2.1}$$

where Φ can be considered as any component such as temperature or velocity. It is then split into mean part or time averaged which is $\overline{\Phi}$ and the fluctuating part which is $\Phi\,'$. The time average can then be defined as

$$\overline{\Phi} = \frac{1}{2T}\int_{-T}^{T} \Phi \, dt \ , \tag{2.2}$$

The main equations governing the turbulence models are the continuity equation and the momentum equation which then give rise to the Navier-Stokes equation. The continuity equation equation for an incompressible flow (ρ = constant) is

$$\frac{\partial v_i}{\partial x_i} = 0, \tag{2.3}$$

The next equation that has to be considered is the momentum equation. The momentum equation for the "v" can be written as

$$\frac{\partial v_i}{\partial t} + \frac{\partial (v_i v_j)}{\partial x_j} = -\frac{1}{\rho}\frac{\partial p}{\partial x_i} + \frac{\partial}{\partial x_j}[(\nu)\frac{\partial v_i}{\partial x_j}], \tag{2.4}$$

where v_i is the initial velocity, ν is the kinematic viscosity and ν_T is the turbulent viscosity. The equation 2.4 is called the Navier-Stokes Equation.

2.1 k-ω Shear Stress Model

The k-ω SST model was developed by Menter[7] to overcome the excess dependencies of the k-ω and the k-ϵ models. According to [3], the SST model mainly has two differences,

- It is a combination of the k-ϵ (for region away from the boundary layer) and the k-ω (for regions inside the boundary layer) models .
- Shear stress limitaion in the adverse pressure gradient region.

Similar to the other RANS models the SST model is a two equation model, meaning it relies on the two transport equation to compute the turbulent kinetic energy and the dissipation rate. In the SST model, the k and the ω equations are determined respectively,

$$\frac{Dk}{Dt} = P_k - \beta^* \omega k + \frac{\partial}{\partial x_j}[(\nu + \nu_t \sigma_k)\frac{\partial k}{\partial x_j}], \tag{2.5}$$

$$\frac{D\omega}{Dt} = \frac{\alpha_{SST}}{\nu_t} P_k - \beta_{SST}\omega^2 + \frac{\partial}{\partial x_j}[(\nu + \nu_t \sigma_\omega)\frac{\partial \omega}{\partial x_j}] + 2(1 - F1)\frac{\sigma_{\omega 2}}{\omega}\frac{\partial k}{\partial x_j}\frac{\partial \omega}{\partial x_j}, \tag{2.6}$$

where $\frac{D}{Dt} = \frac{\partial}{\partial t} + \overline{v_j}\frac{\partial}{\partial x_j}$ denotes the material derivative.
In the above equations, P_k is the production term, β^* is a constant, σ_k and σ_ω are called the Prandtl numbers having a constant value. The last term in the equation 2.6 is called as the cross-diffusion term which is responsible for the SST model to alternate between the k-ω model and the k-ϵ model. This switch between the two models is governed by the blending functions $F1$ and $F2$. The expression to calculate the blending function $F1$ is given by,

$$F1 = \tanh(\min(\max(\frac{\sqrt{k}}{\beta^* \omega d}, \frac{500\nu}{d^2 \omega}), \frac{4\sigma_{\omega 2} k}{CDk\omega d^2})^4), \tag{2.7}$$

where,

$$CDk\omega = 2\sigma_{\omega 2}\frac{1}{\omega}\frac{\partial k}{\partial x_j}\frac{\partial \omega}{\partial x_j}, \tag{2.8}$$

The smooth transition of the coefficients from the k-ω model to the k-ϵ model is achieved when $F1 = 1$ at the near wall region and $F1 = 0$ at the outer region. The α_{SST} and the β_{SST} coefficients in the equation 2.6 are then computed as follows,

$$\alpha_{SST} = F1\alpha_{k-\omega} + (1 - F1)\alpha_{k-\epsilon}, \tag{2.9}$$

$$\beta_{SST} = F1\beta_{k-\omega} + (1 - F1)\beta_{k-\epsilon}, \tag{2.10}$$

and so on. To accurately predict the transition from the wall boundary region to the free stream region, another blending function is used, the expression for this blending function is given by,

$$F2 = \tanh(\max(\frac{2\sqrt{k}}{\beta^* \omega d}, \frac{500\ \nu}{d^2 \omega})^2), \tag{2.11}$$

Table 2.1: Coefficients of the k - ω SST closure model

α_1	α_2	a1	β_1	β_2	β^*	α_{k1}	α_{k2}	$\alpha_{\omega 1}$	$\alpha_{\omega 2}$
5/9	0.440	0.310	0.075	0.0828	0.090	0.850	1.000	0.500	0.856

The turbulent viscosity for the k-ω SST model is calculated using the following expression.

$$\nu_t = \frac{a_1 k}{\max(a_1\omega, sF2)}, \tag{2.12}$$

In the above equation, $a1$ is a constant and, s is the strain rate tensor denoted as,

$$s = s_{ij} = \frac{1}{2}\left(\frac{\partial \overline{v_i}}{\partial x_j} + \frac{\partial \overline{v_j}}{\partial x_i}\right), \tag{2.13}$$

The production term P_k in both the k and the ω equations are calculated using the following expression,

$$P_k = \min(\nu_t s^2, 10\beta^* k\omega). \tag{2.14}$$

In this k-ω SST closure model, the coefficients α, β, β^*, α_k and α_ω are calculated form the equations 2.9 and 2.10. The constant values for these coefficients are defined in table 2.1.

2.2 PANS implementation for k-ωSST model

The Partially-Averaged Navier Stokes (PANS) models engage single closure model for the entire computational domain without any explicit dependencies on the grid properties. [4] This bridging strategy mainly depends on two parameters when considering for the SST model. These parameters are used to define the range of the resolved scales. These are the modelled turbulent kinetic energy to the total turbulent kinetic energy f_k,

$$f_k = \frac{k}{k_{tot}}, \tag{2.15}$$

And the specific dissipation f_ω is given by

$$f_\omega = \frac{\omega}{\omega_{tot}},$$

where the subscript "tot" denotes the total turbulent quantities. This model is characterized by a rigorous mathematical and physical background (According to [4]). The parameters f_k and f_ω can be set to a constant value or can be made dynamic as well. The static values for the PANS parameters can be considered to avoid commutation error where as if the dynamic parameters are considered there can be some commutation errors encountered which can be rectified by implementing the Variable-Resolution model.
The PANS model relies on the closure of the RANS models to compute the unresolved turbulent stresses. Hence, the parameters f_k and f_ω were introduced onto

the governing equations of the RANS SST model. The PANS version for the SST model is developed with the help of Lakshmipathy and Girimaji [6] and Filipe Miguel Soares Pereira [11]. The transport equations for the PANS version of the SST model for the unresolved kinetic energy k_U and the unresolved specific dissipation rate ω_U are,

$$\frac{Dk_U}{Dt} = P_k - \beta^* \omega_U k_U + \frac{\partial}{\partial x_j}[(\nu + \nu_t \sigma_k \frac{f_\omega}{f_k})\frac{\partial k}{\partial x_j}], \tag{2.16}$$

$$\frac{D\omega_U}{Dt} = \frac{\alpha_{PANS-SST}}{\nu_t} P_k - (P\,' - \frac{P\,'}{f_\omega} + \frac{\beta_{PANS-SST}\omega_U}{f_\omega})\omega_U + \frac{\partial}{\partial x_j}[(\nu + \nu_t \sigma_k \frac{f_\omega}{f_k})\frac{\partial k}{\partial x_j}] + D_C, \tag{2.17}$$

where D_C for the SST model is given by,

$$D_C = 2\frac{\sigma_{\omega 2}}{\omega_U}\frac{f_\omega}{f_k}(1 - F_1)\frac{\partial k_U}{\partial x_j}\frac{\partial \omega_U}{\partial x_j}. \tag{2.18}$$

The material derivative is given $\frac{D}{Dt} = \frac{\partial}{\partial t} + \overline{v_j}\frac{\partial}{\partial x_j}$.
In the above equations the value for P_k is calculated using the equation 2.14.
In the D_C term the F_1 is the blending function calculated from the equation 2.7. k_U and ω_U denote the unresolved turbulent quantities.
The $P\,'$ term in the equation 2.17 is calculated as follows,

$$P\,' = \frac{\alpha_{PANS-SST}\beta^* k_U}{\nu_t}. \tag{2.19}$$

The turbulent viscosity ν_t is calculated from the equation 2.12.

2.2.1 Computing f_k

The physical meaning of f_k is the ratio of the modelled to the total turbulent kinetic energy. When the dynamic f_k is considered, according to [2], it is expected that the value of f_k should be smaller when the grid is refined. One such way for computing f_k was proposed by [1] where,

$$f_k = C_\mu^{\frac{-1}{2}}(\frac{\Delta}{L_t})^{\frac{2}{3}}, L_t = \frac{k_{tot}^{\frac{3}{2}}}{\omega_U}, \Delta = (\Delta V)^{\frac{1}{3}} \tag{2.20}$$

Kenjeres and Hanjalic [5] have slightly made a different proposal for computing the parameter f_k under dynamic conditions. According to them,

$$f_k = \frac{\Delta}{L_t}. \tag{2.21}$$

According to [2] it was found that the expression from 2.21 gave very low values of f_k. Hence the expression for f_k from 2.20 was chosen for evaluating under dynamic conditions.

3

Circular Cylinder at Re=3,900

In this chapter the investigation for the flow around a circular cylinder is carried out at a Reynolds number of Re = 3,900 using the SST model and the PANS version of the k-ω SST model. The meshing of the Cylinder is performed with the help of the open source CFD software OpenFOAM's dictionaries blockMesh and snappyHexMesh. The PANS version of the SST turbulence model was also developed using OpenFOAM.
It was first required to validate the PANS version of the SST turbulence model before applying it to the Submarine hull. Hence, a simple case of circular cylinder was considered. The flow around the cylinder can be classified into different regions based on the Reynolds Number,

$$Re = \frac{V_\infty D}{\nu}, \tag{3.1}$$

where, V_∞ is the free stream velocity, D is the diameter of the cylinder which is 0.4 m. The fluid considered in in this investigation is air. At very low Re the flow is considered to be laminar and as the Reynold's number increases the flow becomes more turbulent.

3.1 Computational Domain and Boundary Conditions

The computational domain is a rectangular geometry defined in the Cartesian coordinate system. The Cylinder is placed at the center of the axis. Figure, 3.1 shows the dimensions of the computational domain where the diameter 'D' of the cylinder is 0.4m. The inlet and the outlet are located at 5D upstream and 25D downstream from the center of cylinder respectively; the front and back symmetry plane are 10D and -10D distant from the cylinder center, whereas the top and bottom boundaries have slip boundary condition and are 1.1D apart. The velocity and turbulent quantities are set to constant at the inflow boundary. The pressure is deduced from the interior of the domain. At the outlet, all the dependent variables in the streamwise direction are set to zero, where as for outlet there is an imposed pressure, the remaining variables are set to zero. Symmetry boundary conditions are applied for front and back planes. Naturally, no-slip conditions are applied on the surface of the cylinder.

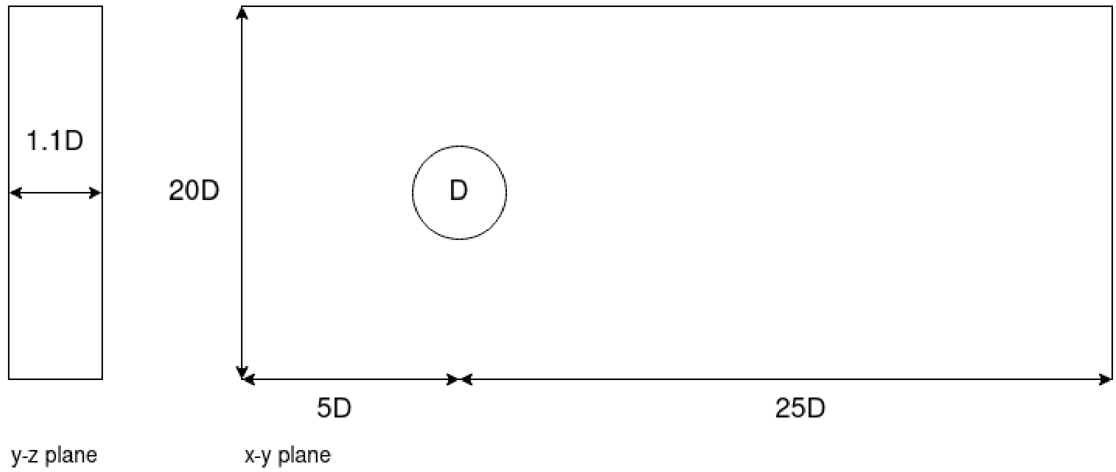

Figure 3.1: Computational Domain

3.2 Numerical Settings and Measurements

The numerical simulations are carried out on two spatial grids resolutions. The first grid resolution contains $9 * 10^6$ cells while the second contains $6 * 10^6$ cells. The investigation is carried out for the shear layer formation for the near wall region at the wake of the cylinder. Hence, a more finer mesh is made across the cylinder area. The grid resolution for the cylinder can be seen forn figure, 3.2.

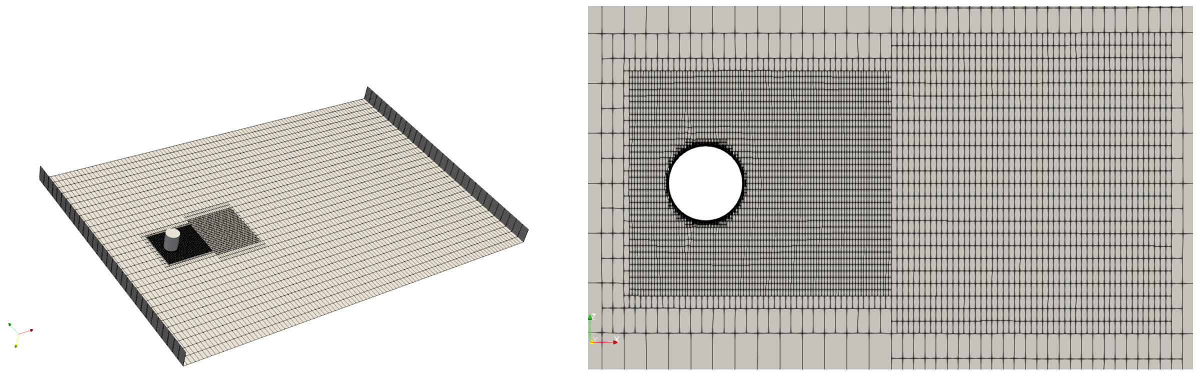

(a) Isometric view **(b)** top view

Figure 3.2: Spatial Grid Resolution

3.2.1 Prism Layers

The boundary condition for the cylinder surface is considered to be a no-slip condition. Hence, a region of viscous sublayer is considered around the surface of the cylinder to correctly predict the turbulent flow. To increase the prediction accuracy of the turbulent flow in the viscous sublayer region a suitable y+ value has to be considered, where y+ is a non-dimensional distance. While modelling turbulence, y+ helps in determining the proper cell distance or cell size near the domain walls.

Figure 3.3: Prism Layers

For this prediction a total number of 20 prism layers were considered with a calculated first wall distance of 0.001649 m from the cylinder to maintain a y+ less than 5 so that the simulation is performed in the viscous sub layer.Figure 3.3, shows the developed prism layer for the simulation.

3.2.2 Solving

In order to solve the integrated equations of the turbulence models, the equations first need to be discretized into algebraic equations. This is done with the help of numerical discretization schemes. The numerical discretization schemes used in this project are as follows:

- **Time-Derivative Scheme**: The time derivative scheme used for the SST and the PANS models is backward scheme which is second order accurate.
- **Gradient Scheme**: The gradient scheme used for the discretization of the integrated equations is Gauss linear scheme which is the Gaussian integration with central differencing, which is a second order, unbounded scheme.
- **Divergence Scheme**: The divergent scheme used in discretization for velocity, pressure, turbulent kinetic energy, turbulent frequency omega is Bounded Gauss Limited Linear scheme.
- **Laplacian Scheme** : The Laplacian scheme used in this project when discretising the equations for turbulence is Gauss Linear Corrected, which is Gaussian integration with central differencing and a blend of corrected and uncorrected numerical behaviour.
- **Interpolation Scheme**: Linear interpolations scheme which is also called as the central differencing scheme, which is second order accurate was used for

the interpolation of the discretized equations.

After the discretization of the integrated equations into algebraic equations, the discretized algebraic equations are solved in an iterative process using an algorithm called PIMPLE which is used for transient flows. The following linear solvers are used for the transient simulations:

- **Generalised algebraic multi-grid (GAMG)** with a Gauss-Seidel smoother for the pressure p.
- **Smoother solver** with a symmetric Gauss-Seidel smoother for the velocity U , the turbulent kinetic energy k and the specific dissipation rate ω.

When a transient simulation is considered, pressure correction has to be taken into account and for the pressure correction,

- **Generalised algebraic multi-grid (GAMG)** with a Diagonal incomplete-Cholesky with Gauss-Seidel (symmetric) smoother for pressure correction.

3.2.3 Post-Processing

The post processing of the simulation data was first visualised using an open source visualisation software Paraview. The data extracted from Paraview was then processed using Python.

- The quantities of interest taken into consideration from this study is the time-averaged velocity magnitude $< \overline{V_i} >$.
- The pressure field p.
- The unresolved kinetic energy kU and the unresolved turbulent frequency ωU.

To correctly predict the flow for regions where the dynamicPANS switches from RANS to LES, it is required to maintain a constant Courant number of 0.6 and this is achieved by maintaining a constant ΔT of 0.005.

3.3 Results

In this section, analysis of the time-averaged velocity of the two different grid resolutions considered is performed and the evaluation of the ability of these turbulence models to represent the flow around the circular cylinder at Reynolds number 3900. The numerical results are also compared against experimental results.

In order to understand the performance of the hybrid turbulence PANS model, a comparison was made between the following models:

- The standard k-ωSST model.
- The static PANS model with the filter function set to $f_k = 0.7$.
- The static PANS model with the filter function set to $f_k = 0.3$.
- The dynamic PANS model with the filter function f_k varying form 1.0 to 0.1.

In theory, the static PANS model with the filter function $f_k = 0.7$ should predict the velocity magnitude better than the k-ωSST model, whereas the static PANS model with the filter function $f_k = 0.3$ should predict the velocity magnitude better than $f_k = 0.7$. Similarly, the dynamic PANS with varying filter function based on the size of the cell should predict the the velocity magnitude better than $f_k = 0.3$.

Mesh-1

The initial comparison between the turbulence models was performed for the spatial grid resolution containing $9 * 10^6$ cells. To obtain a better prediction, the mesh at the wake of the cylinder was refined into 3 refinement stages by reducing the refinement zone of the mesh from the surface of the cylinder towards the outlet in the downstream direction. The grid refinement can be seen from the figure 3.4

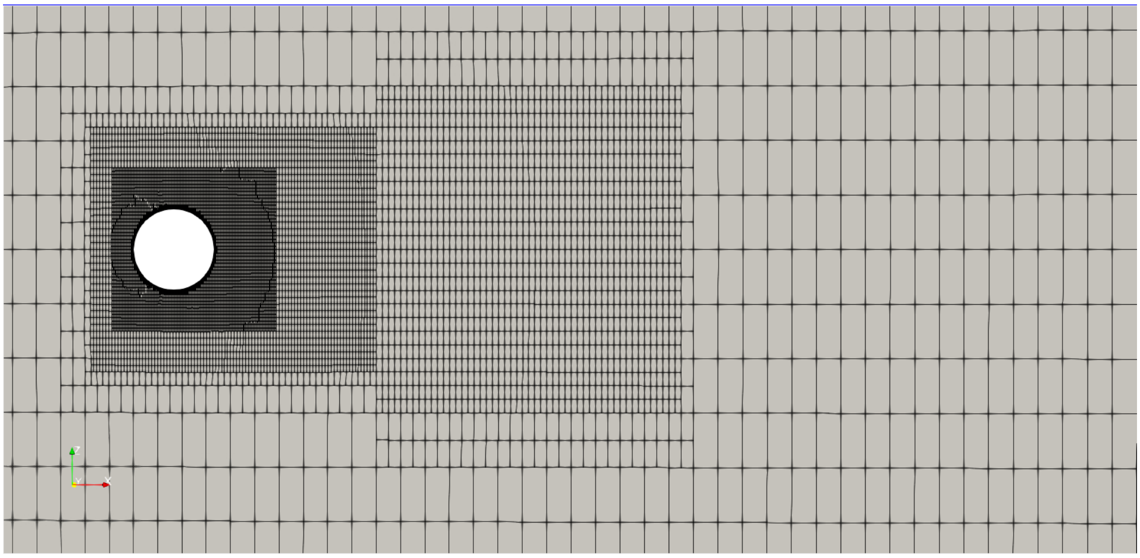

Figure 3.4: Mesh1 Grid Refinement

Drag and Lift Coefficients

The drag and lift coefficients were computed using the forced dictionary in OpenFOAM. The coefficients were calculated for all the turbulence models considered. Since the simulation is a transient simulation, in order to check if the results have been converged, the drag and lift coefficients were considered. From figures 3.5 and 3.6 it can be seen that the values have reached close to convergence. If the simulation was performed for more time duration, the results would have converged. Due to time and storage constraints the simulation was not performed for increased time duration.

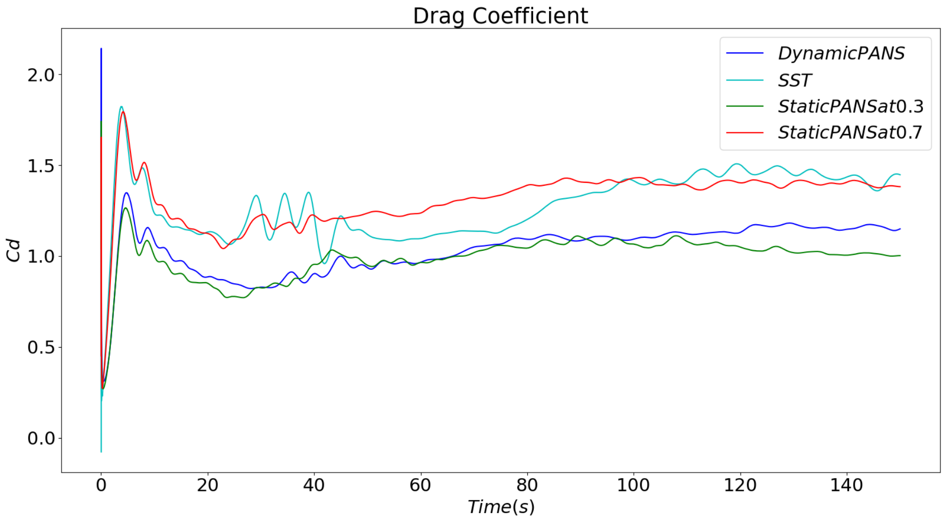

Figure 3.5: Drag Coefficient for Mesh-1

From figure 3.5, it can be seen that the drag coefficient of the SST model fluctuates between higher values of C_D when compared to other turbulence models considered. Whereas, the lowest fluctuations can be seen for the static PANS turbulence model with filter function $f_k = 0.3$. This can be because, at $f_k = 0.3$ the turbulence model should act as a LES simulation and hence a reduction in the drag coefficient can be seen which in turn suggests that there is minimum resistance. However, for SST model, the resistance around the cylinder is much higher.

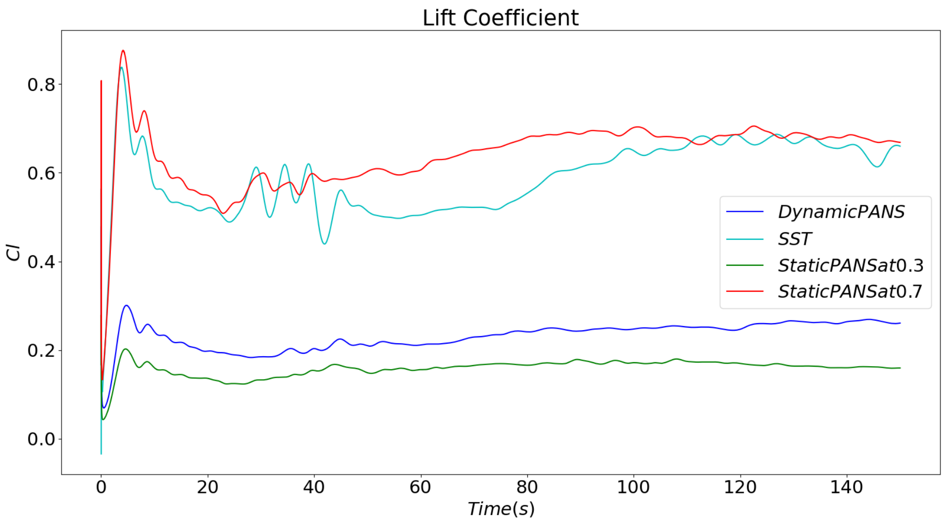

Figure 3.6: Lift Coefficient for Mesh-1

From figure 3.6, the lift coefficient is lowest for the static PANS model with filter function $f_k = 0.3$ followed by the dynamic PANS, SST and, static PANS with $f_k = 0.7$ respectively.

Stream-lines Comparison

Initially, the streamlines for all the four models were observed. The streamlines were first used to visualise the transition from laminar to turbulent in the re-circulation region at the wake of the cylinder. This helped in understanding the accuracy of the prediction of the shear layer development at the wake of the cylinder. From the figures 3.7 and 3.8, it can be seen that the dynamic PANS model predicts the re-circulation region at the wake better than the SST model and static $f_k = 0.7$ model. However, the static $f_k = 0.3$ which is in the LES regions provides with more detailed information regarding the re-circulations at the wake of the cylinder. The dynamic PANS model has a better prediction than the SST and the $f_k = 0.7$ model where as the $f_k = 0.3$ model predicts a more detailed re-circulation region at the wake as it should when looked at the theoretical aspect of the turbulence model. It can be observed that for dynamic PANS, the flow separation is slightly delayed when compared to the static PANS models.

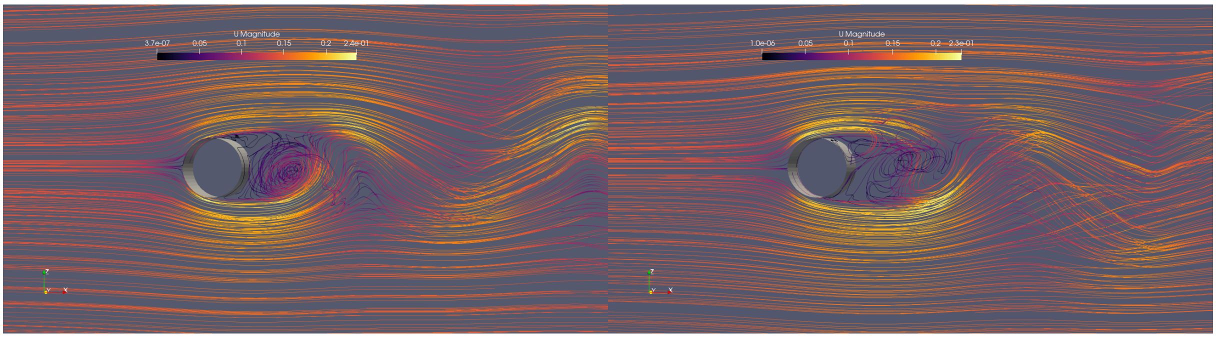

(a) Stream-lines for dynamic PANS model **(b)** Stream-lines for SST

Figure 3.7: Stream-lines of SST and dynamic PANS

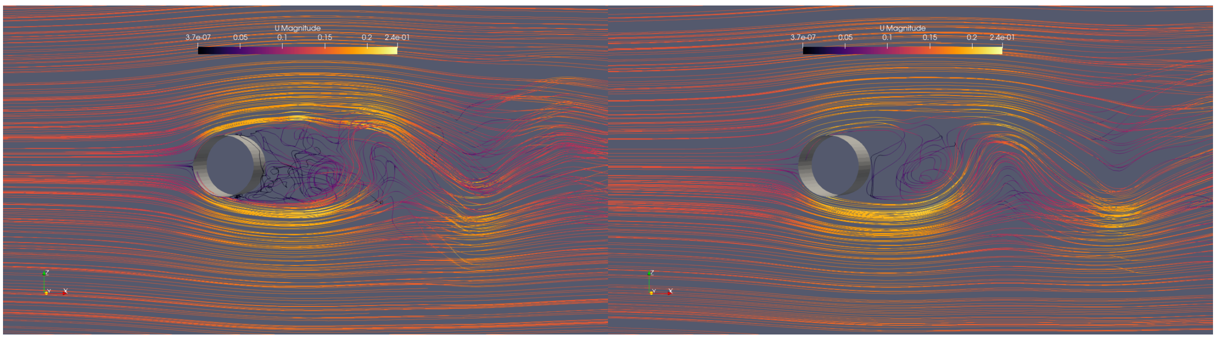

(a) Stream-lines for $f_k = 0.3$ **(b)** Stream-lines for $f_k = 0.7$

Figure 3.8: Stream-lines of $f_k = 0.3$ and 0.7

Q Criterion

The evaluation of a mathematical model's effective physical resolution should ideally be conducted using techniques such as energy spectra. However, given the purpose of this research and the difficulty of applying such methods to the current flow, we begin with a qualitative analysis of the instantaneous Q-criterion field predicted by various models.

$$Q = \frac{1}{2}[< \Omega_{ij} >< \Omega_{ij} > - < S_{ij} >< S_{ij} >] \tag{3.2}$$

Figure 3.9 and 3.10 depicts the iso-surface of the Q-criterion(Q = 0.1, Q = 0.2 and Q = 0.5) and as expected the SST model does not exhibit better flow structures since the turbulence is not entirely modelled. However, the dynamic PANS did provide with better flow structures. The static PANS at $f_k = 0.3$ and 0.7 provide with a better understanding of the PANS turbulence model in theory. At $f_k = 0.3$, the turbulence is modelled under LES condition and hence a more detailed flow structure has been captured at the wake. Similarly, at $f_k = 0.7$, the turbulence is still in the RANS region and hence the prediction of the fluid structure provides comparatively less information.
Overall, the PANS model developed predicts the flow structure better when compared to the k-ω SST turbulence model.

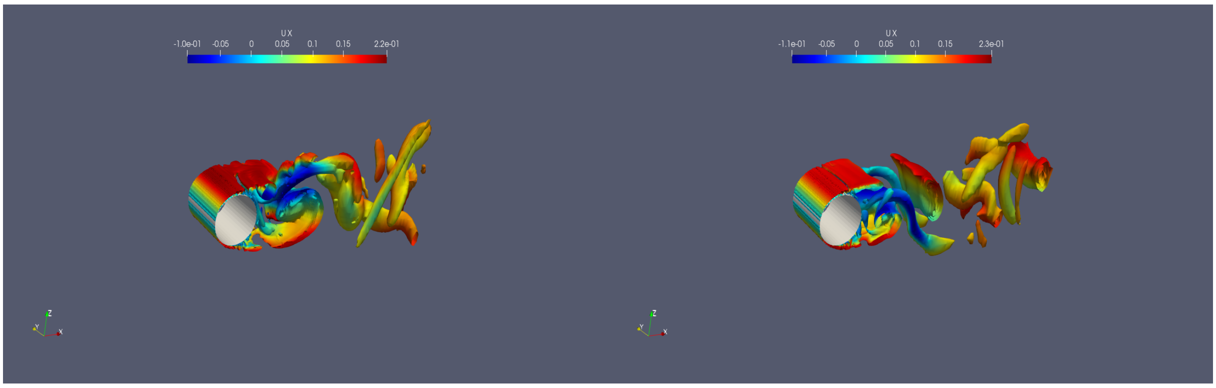

(a) M1 Q-criterion dynamic PANS **(b)** M1 Q-criterion SST

Figure 3.9: M1 Q-criterion for dynamic PANS and SST

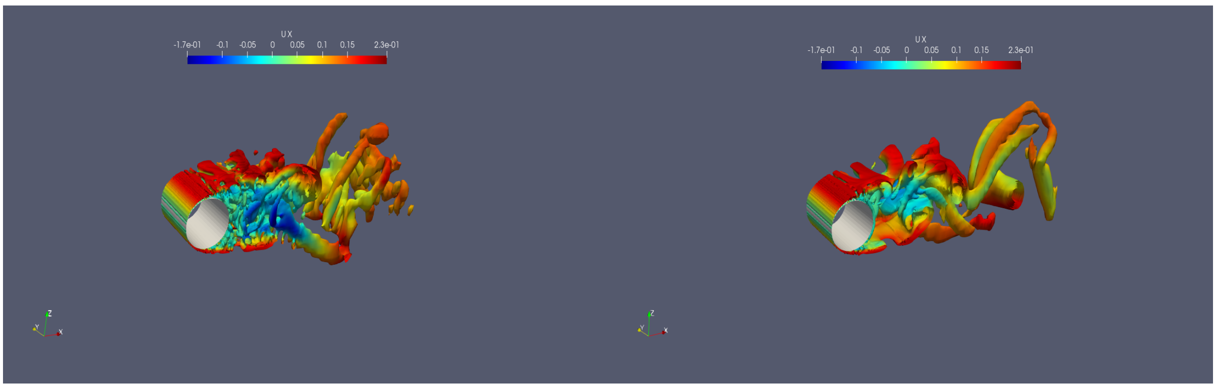

(a) M1 Q-criterion static PANS at 0.3 **(b)** M1 Q-criterion static PANS at 0.7

Figure 3.10: M1 Q-criterion for static PANS at 0.3 and 0.7

Time Averaged Velocity Comparison

The time averaged velocities were extracted using Paraview in streamwise and spanwise direction. In order to compare the results with the experimental data, the velocities were normalized and extracted at three different locations at the wake of the cylinder 1.06, 1.54 and 2.02 m in the streamwise direction from the center of the cylinder. Before the analysing the velocities at different location, validation of the source code developed for the PANS model was first performed with by analysing the time averaged velocity of SST model and PANS model at $f_k = 1.0$. When the PANS coefficient f_k is set 1, it mimics the SST model 3.11 and 3.12 for both the spanwise and the streamwise directions , hence validating the code developed.

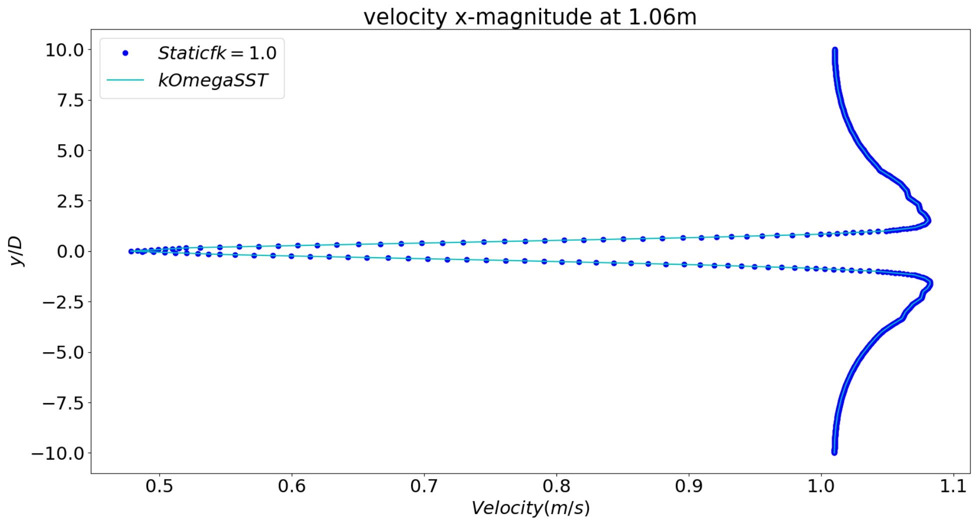

Figure 3.11: SST and Static PANS $f_k = 1.0$ Streamwise Comparison

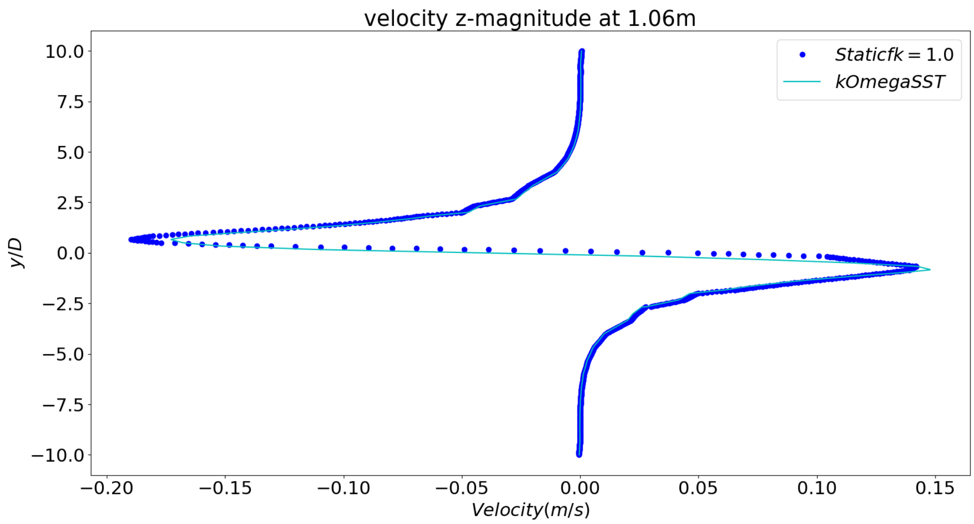

Figure 3.12: SST and Static PANS $f_k = 1.0$ Spanwise Comparison

Time Averaged Velocity Comparison at 1.06m

The comparison of the time averaged velocity for the turbulence models at a location of 1.06 m from the cylinder center in the streamwise direction was performed and compared.

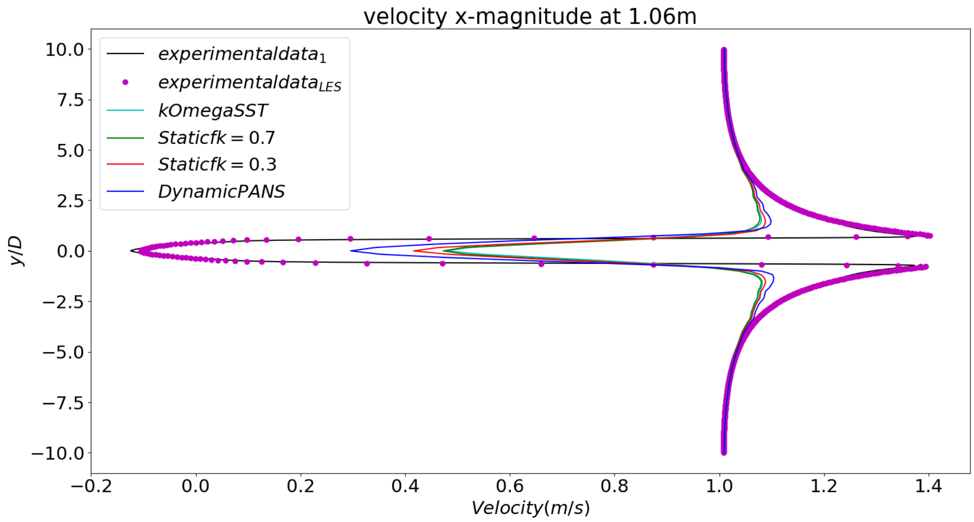

Figure 3.13: X-Magnitude with Experimental Data at 1.06

From figure 3.13, it can be seen that the model predicting the velocity in the x-magnitude closer to the experimental data is the Dynamic PANS. Where as for the velocity prediction in the z-magnitude 3.14, the experimental data show a better re-circulation of the fluid when compared to PANS and SST turbulence models. It can be seen that the time average quantities is delaying the turbulence in the free shear layer, contributing a larger re-circulation region.

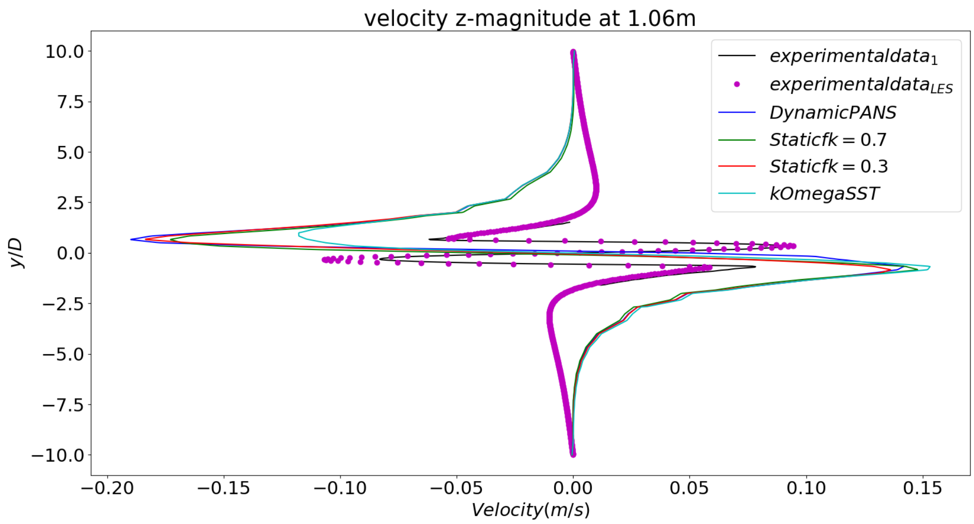

Figure 3.14: Z-Magnitude with Experimental Data at 1.06

The accuracy of the velocity magnitude prediction in the PANS turbulence model can be increased by simulating under a more finer mesh which can help in increasing the velocity prediction of PANS model making it more closer to that of the experimental data.

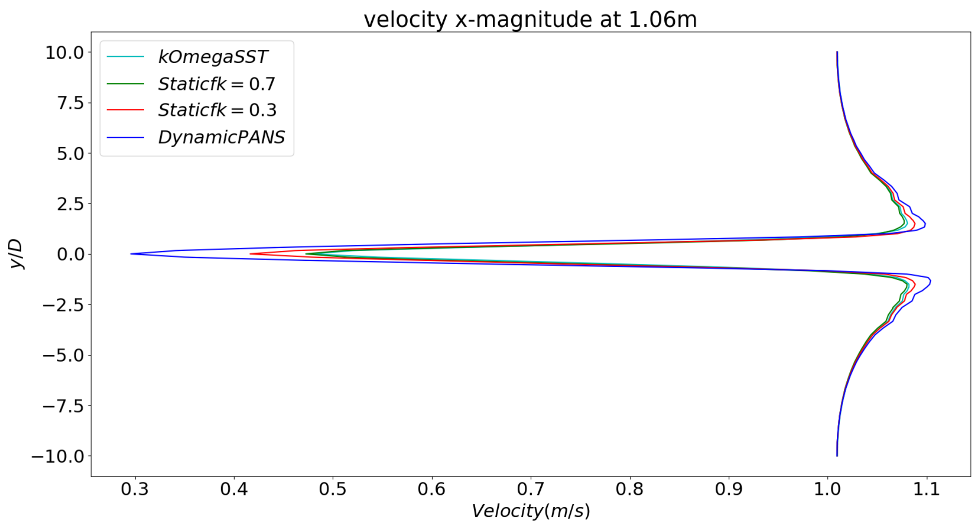

Figure 3.15: X-Magnitude without Experimental Data at 1.06

When the data for only the PANS and SST models are visualised, it can be seen form 3.16 that the dynamic PANS predicts the time averaged value at the shear layer better than other models followed by static f_k of 0.3 then f_k at 0.7 and the SST model respectively. From this we can conclude that the dynamic PANS has a better accuracy at predicting the velocity magnitude at the 1.06 m.

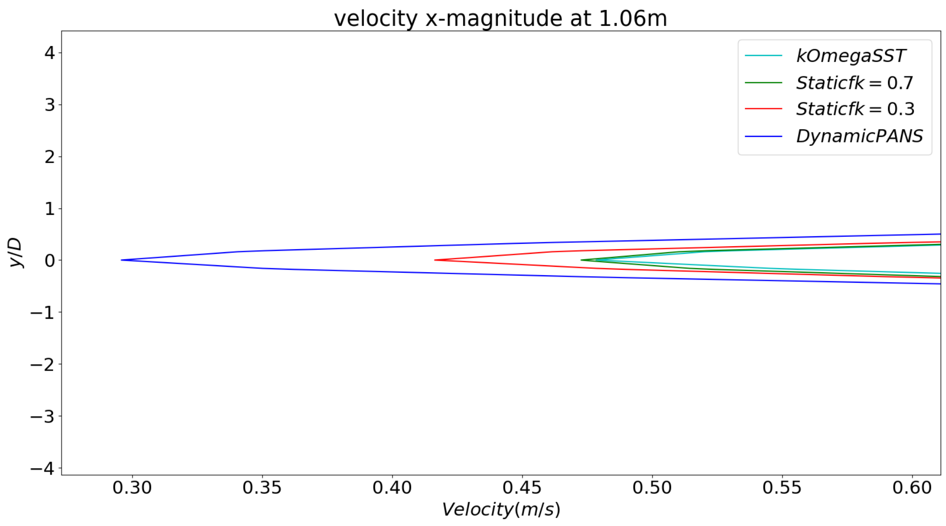

Figure 3.16: X-Magnitude without Experimental Data Zoomed at 1.06

Similarly, the z-magnitude 3.17 also resembles similar behaviour where the dynamic PANS predicts the velocity magnitude in the shear layer better, when compared to the other considered turbulence models.

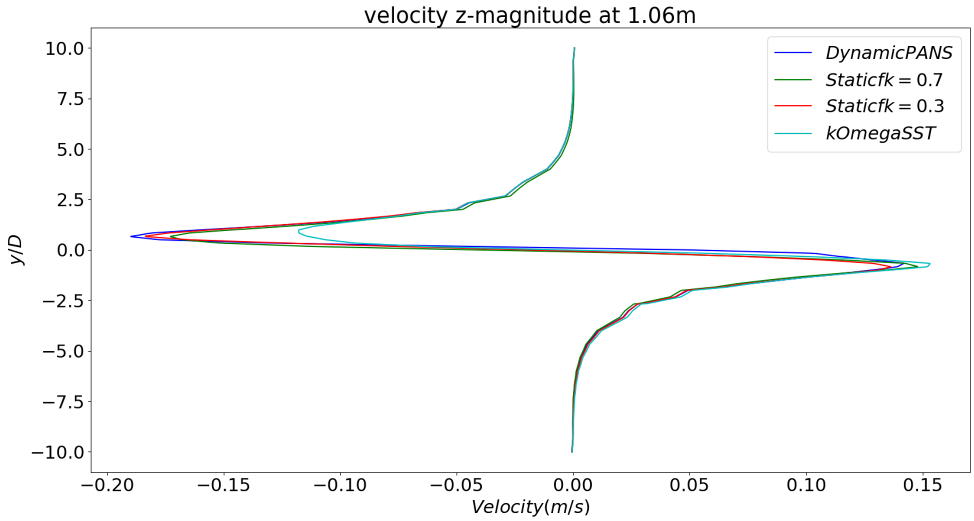

Figure 3.17: Z-Magnitude without Experimental Data at 1.06

Time Averaged Velocity Comparison at 1.54m

The second comparison was performed for the time averaged velocity of the turbulence models at a location of 1.54 m from the center of the cylinder in the streamwise direction. Similar to 1.06m the data was initially compared with the experimental data and a comparison was made within the PANS and SST models.

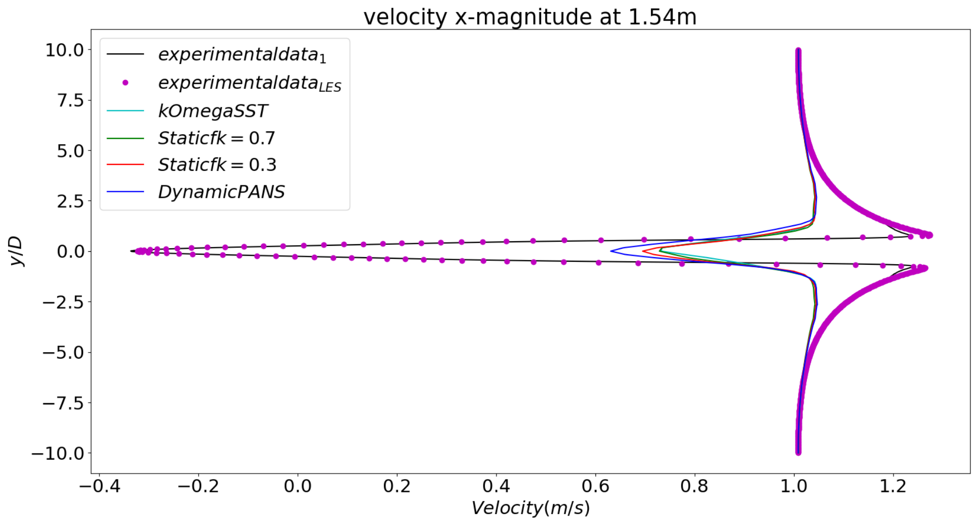

Figure 3.18: X-Magnitude with Experimental Data at 1.54

The data for both the x-magnitude and the z-magnitude from 3.18 and 3.19 shows that the prediction of the different PANS and the SST models are not close to that of the experimental data. This can be rectified by running the simulation with a more finer mesh to predict more accurate results.

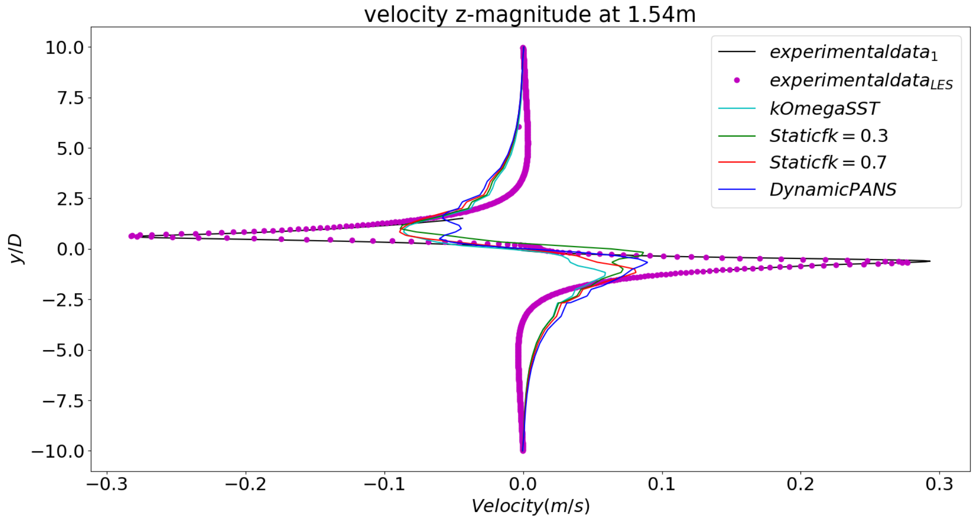

Figure 3.19: Z-Magnitude with Experimental Data at 1.54

When the data extracted from the turbulence models were compared without consideration of the experimental data, it was observed that the dynamic PANS model performed the best in predicting the time averaged velocity in shear layer at 1.54m when compared to other PANS models and the SST model. 3.21

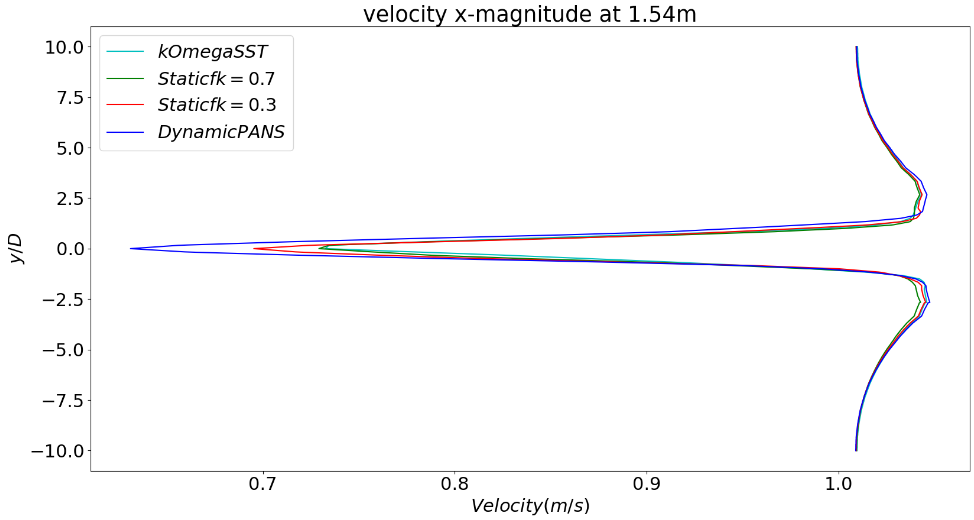

Figure 3.20: X-Magnitude at 1.54

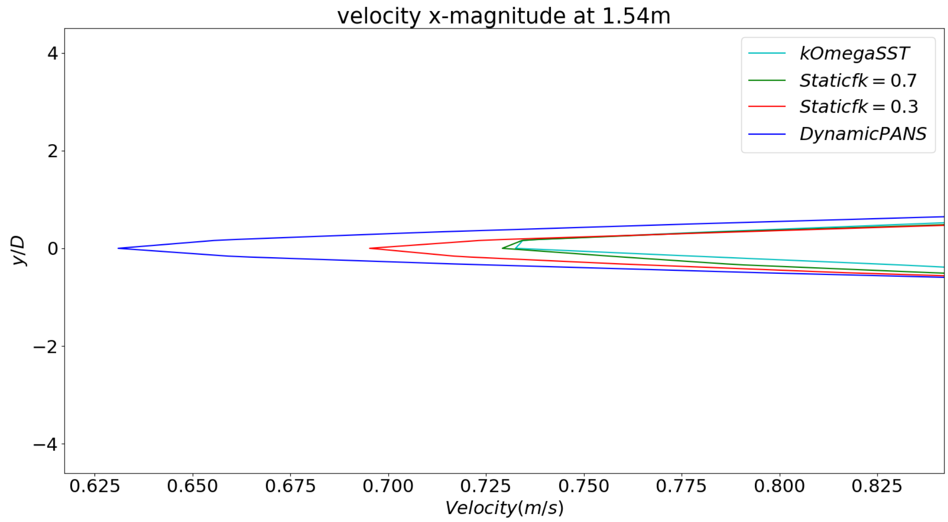

Figure 3.21: X-Magnitude zoomed at 1.54

Time Averaged Velocity Comparison at 2.02

The third comparison in predicting the accuracy of the time averaged velocity of the turbulence models was performed at a location of 2.02 m from the center of the cylinder in the streamwise direction. Similar to other comparisons, the data was initially compared with experimental data.

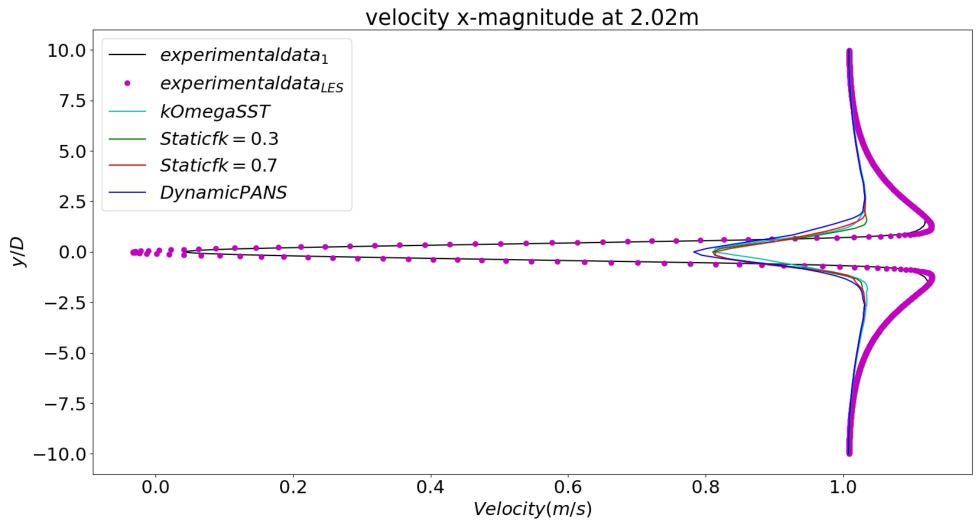

Figure 3.22: X-Magnitude with Experimental Data at 2.02

When comparing with the experimental data, the simulated data have a poor accuracy of turbulence in the shear layer which can be seen form the figures 3.22 and 3.23, this is because of the grid resolution. In order to increase the accuracy of the simulated data, an increase in the grid resolution which is making the mesh more finer can result in the increase in the accuracy of the average velocity prediction of the turbulence models.

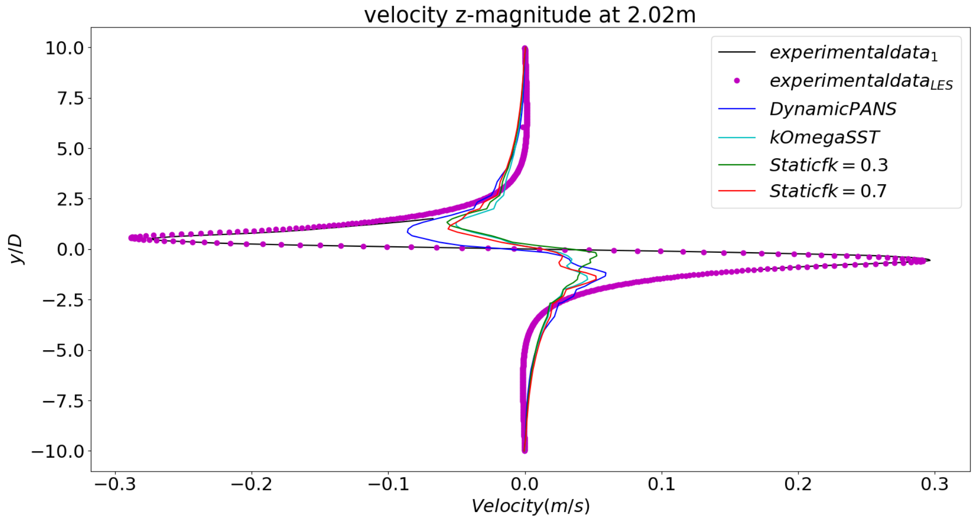

Figure 3.23: Z-Magnitude with Experimental Data at 2.02

When the comparison of the data is considered without taking into account the experimental data, it can be seen that the dynamic PANS model predicts the time averaged velocities more accurately in the shear layer when compared to other turbulence models considered.

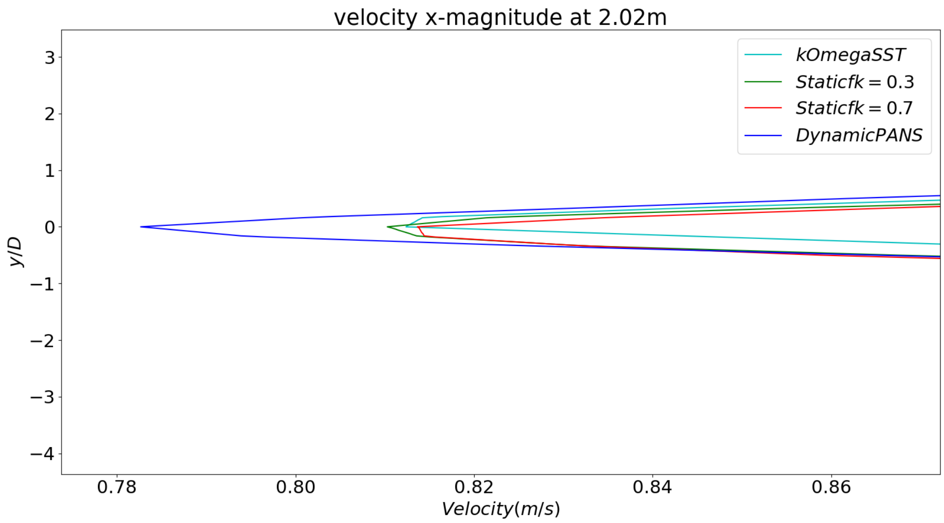

Figure 3.24: X-Magnitude Zoomed at 2.02

From figures 3.24 and 3.25 it can be seen that at a distance of 2.02m the SST model and the PANS model at f_k=0.7 are equal. This can because of the effects of the blending functions considered in the SST turbulence model.

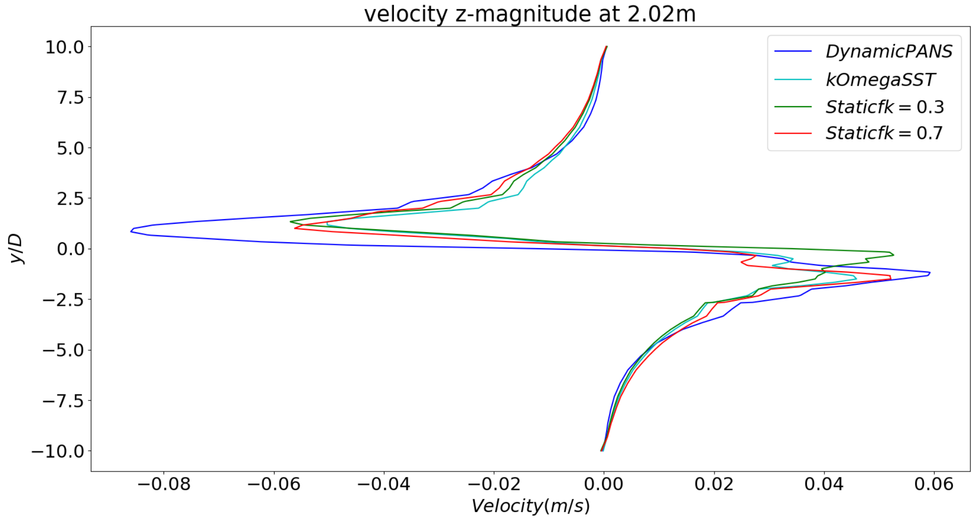

Figure 3.25: Z-Magnitude at 2.02

Mesh-2

The second comparison between the turbulence models was performed for the spatial grid resolution containing $9 * 10^6$ cells. The mesh at the wake was refined to 2 refinement stages by reducing the refinement zone of the mesh from the surface of the cylinder towards the outlet in the downstream direction. The grid refinement for the second mesh can seen from the figure 3.26.

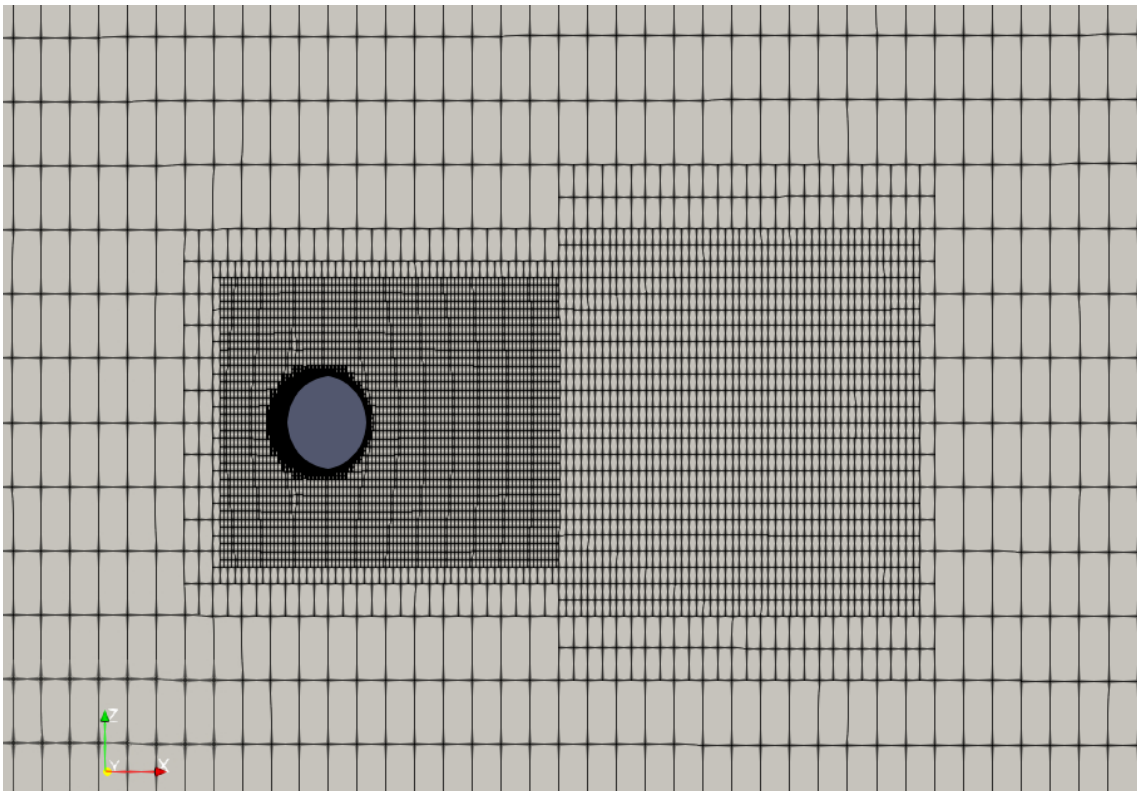

Figure 3.26: Mesh2 Grid Refinement

Drag and Lift Coefficients

Similar to the the Mesh 1, the drag and lift coefficients were computed using the OpenFOAM library. The coefficients were calculated for all the turbulence models considered.

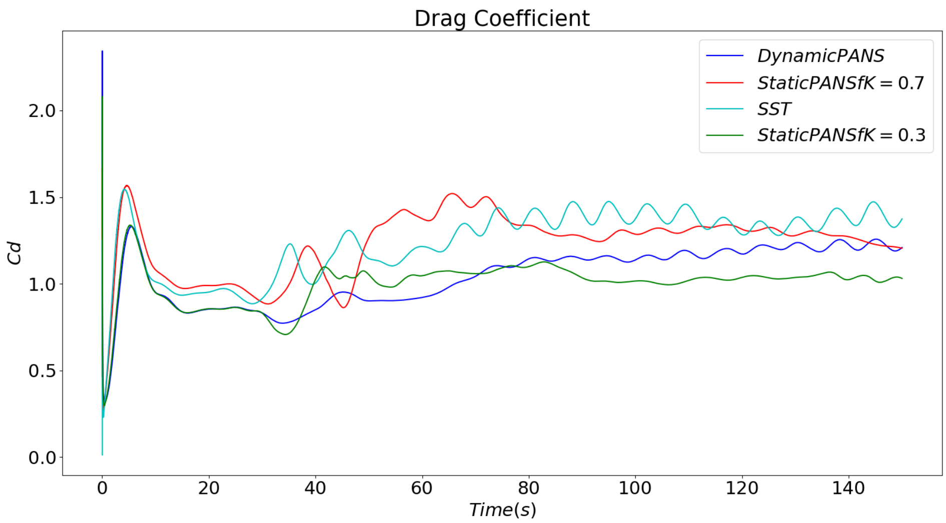

Figure 3.27: Drag Coefficient for Mesh-2

From figure 3.27, it can be seen that the drag coefficient of the SST model fluctuates between higher values of C_D when compared to other turbulence models considered. The lowest fluctuations of C_D can be seen for the static PANS turbulence model with the filter function $f_k = 0.3$.

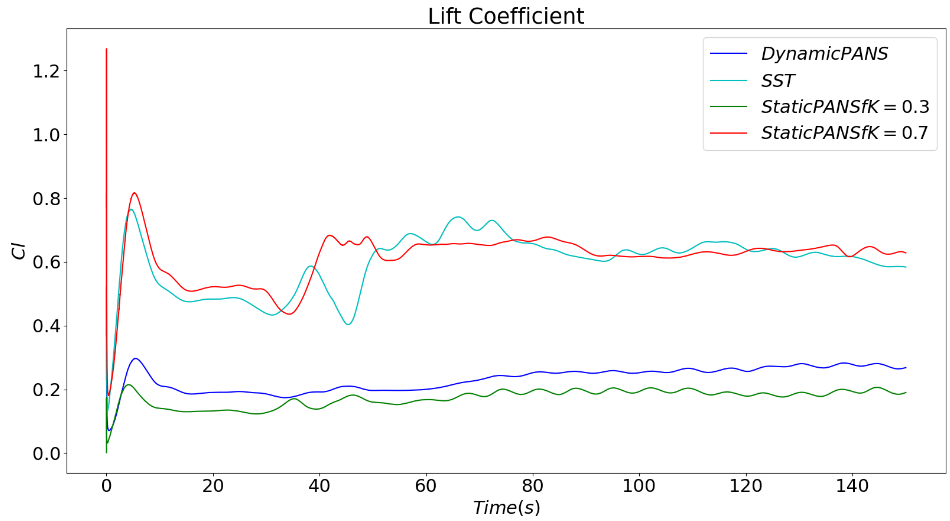

Figure 3.28: Lift Coefficient for Mesh-2

From figure 3.28, the lift coefficient is the lowest for the static PANS model with the filter function $f_k = 0.3$, followed by the dynamic PANS, SST and, static PANS with $f_k = 0.7$ respectively.

Stream-lines Comparison

The stream Lines used to visualise the re-circulation region at the wake of the cylinder to understand the accuracy of prediction of the shear layer development. From figure 3.29 and 3.30, the prediction of the shear layer at the re-circulation region for the SST model is less when compared to the dynamic PANS model. However, the prediction of the static PANS models at $f_k = 0.3$ and 0.7 is better when compared to the dynamic PANS mode.

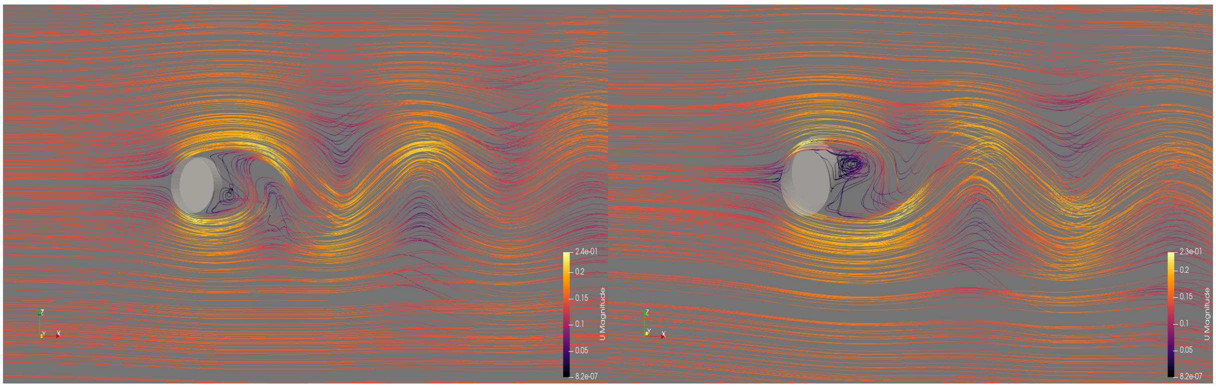

(a) Stream Lines for SST Model M2

(b) Stream Lines for Dynamic PANS Model M2

Figure 3.29: Stream Lines of SST and dynamic PANS for Mesh 2

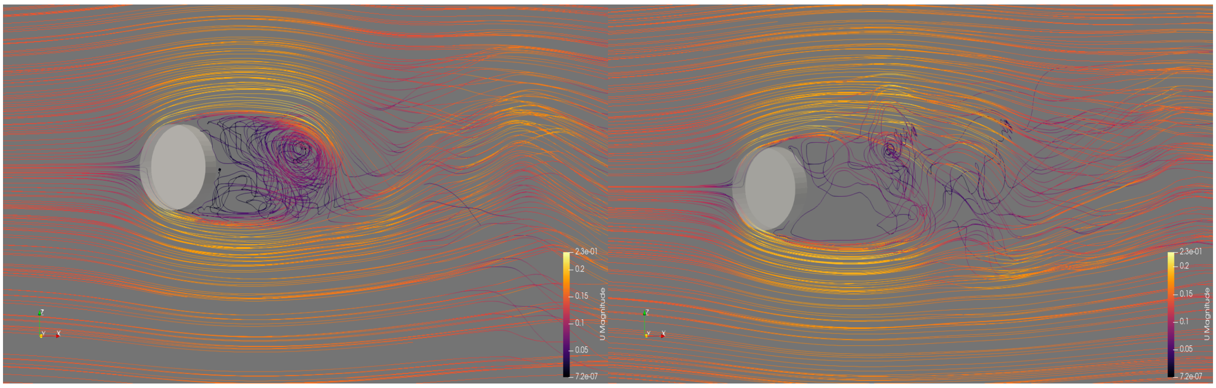

(a) Stream Lines for fk = 0.3 M2

(b) Stream Lines for fk = 0.7 M2

Figure 3.30: Stream Lines for fk = 0.3 and 0.7 for Mesh 2

When comparing the stream lines developed for Mesh 1 and Mesh 2, due to the inclusion of an extra refinement region provided better accuracy the prediction of the re-circulation region.

Q-criterion

Similar to Mesh 1, the Q-criterion was also calculated and visualised. Figure 3.32 and 3.32 depicts the iso-surface of the Q-criterion(Q = 0.1, Q = 0.2 and Q = 0.5).Similar to Mesh 1, the static PANS at f_k = 0.3 provides with a better flow structure followed by dynamic PANS, static PANS at 0.7 and SST respectively.

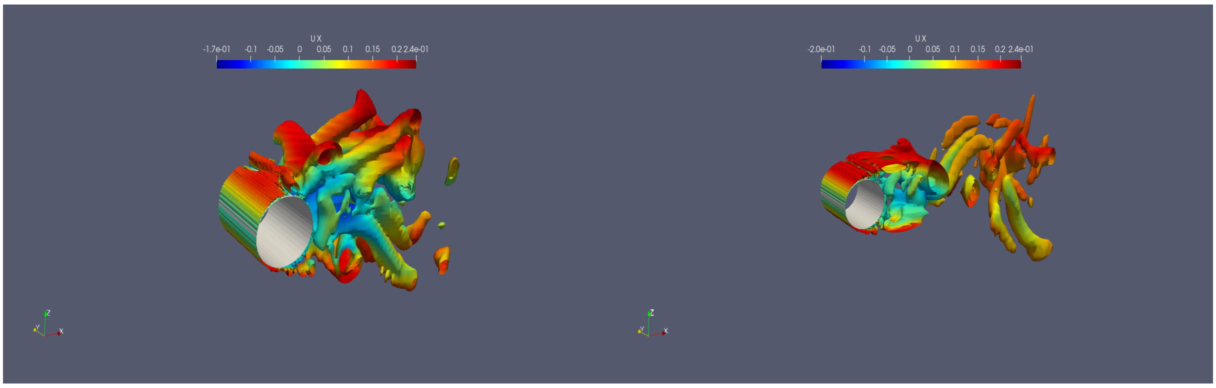

(a) M2 Q-criterion dynamic PANS **(b)** M2 Q-criterion SST

Figure 3.31: M2 Q-criterion for dynamic PANS and SST

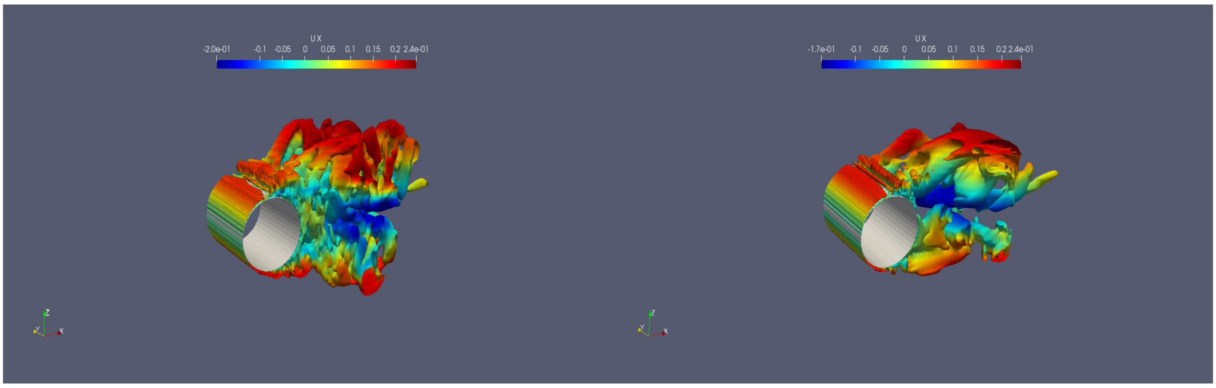

(a) M2 Q-criterion static PANS at 0.3 **(b)** M2 Q-criterion static PANS at 0.7

Figure 3.32: M2 Q-criterion for static PANS at 0.3 and 0.7

Time Averaged Velocity Comparison

The time averaged velocities were extracted using Paraview in streamwise and spanwise direction. The results obtained were extracted and normalized and the velocities were measured and at compared at three different locations at the wake of the cylinder similar to that done for mesh 1. The average velocity comparison was first performed for the location 1.06 m from the cylinder center in the streamwise direction. The comparison of the results for the locations 1.54 and 2.02 m can be seen in the Appendix.

From figure 3.33 and 3.34, it can be seen that the static PANS at $f_k = 0.3$ turbulence model predicts better when compared to the dynamic PANS model for mesh 2. However, when compared with mesh 1 3.15 and 3.17 the results show other wise where the dynamic PANS model predicts better when compared to the other models.

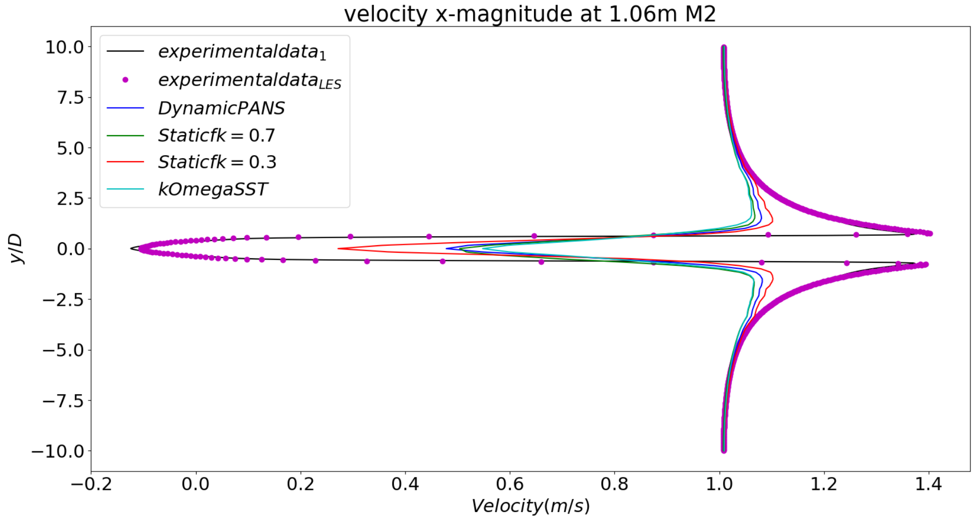

Figure 3.33: X-Magnitude at 1.06 M2

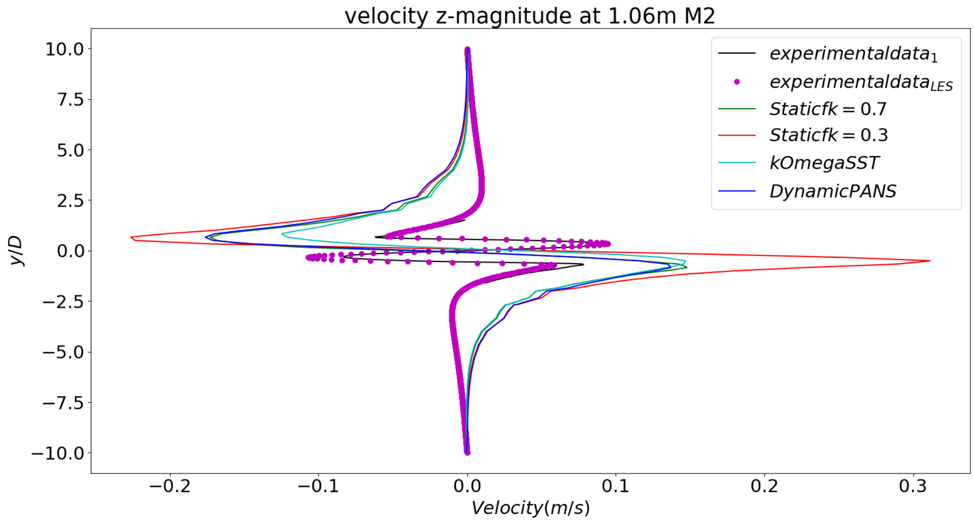

Figure 3.34: Z-Magnitude at 1.06 M2

The change in difference in the prediction of the Averaged Velocities of the turbulence models from Mesh 1 to Mesh 2 can be the fact for the reduced refinement zone for Mesh 2. In the dynamic PANS model, the varying parameter f_k is calculated based on the cell size.Since, Mesh 1 has comparatively more refined cells than Mesh 2, the prediction accuracy is much better.

Forces Comparison

The forces computed for all the turbulence models for both the grid resolutions are compared with values from other reference papers.

References	Models	$\overline{C_D}$	$\overline{C_L}$
Mesh 1	SST	1.280	0.588
	dynamic PANS	1.037	0.234
	fk = 0.3	0.989	0.159
	fk = 0.7	1.313	0.614
Mesh 2	SST	1.244	0.597
	dynamic PANS	1.04	0.232
	fk = 0.3	0.998	0.173
	fk = 0.7	1.229	0.612
Scale-Resolving Simulations of Turbulent flows [12]	SST	1.25	0.664
	fk = 0.5	1.04	0.287
	fk = 0.25	0.93	0.095
Effect of the Closure Partially-Averaged Navier–Stokes Equations[13]	fk = 1.0	1.25	0.66
	fk = 0.75	1.25	0.67
	fk = 0.5	1.04	0.28
	fk = 0.25	0.93	0.10
	fk = 0.15	0.92	0.08
experimental	-	0.98	0.10

Table 3.1: Comparison of forces for the cylinder

From the table 3.1, the average values for the forces can be seen. $\overline{C_D}$ represents the average drag coefficient and $\overline{C_L}$ represents the average lift coefficient for all the turbulence models considered at a Reynolds's number 3,900. The force coefficients are compared with two reference papers [12] and [13]. In [12], the drag and lift coefficients are computed for the SST model and static PANS model at f_k 0.5 and 0.25 where as in [13], the force coefficients are computed for static PANS SST turbulence models at f_k 1.0, 0.75, 0.5, 0.25 and 0.15. Form figures 3.11 and 3.12 it is clear that static PANS at $f_k = 1.0$ mimics SST turbulence model. From the tabular column it is cleat that SST turbulence model predicts higher frag and lift coefficients when compared to the PANS version of the SST models. The force coefficients computed by the dynamic PANS model is similar to that of static PANS at $f_k = 0.5$. For static turbulence models at $f_k = 0.3$ and below have much lower values and are more close to the force coefficient values obtained by experimental analysis.

Variable f_k Comparison

The PANS turbulence model with the variable dynamic filter function was used for both Mesh 1 and Mesh 2. The variable f_k filter function was plotted for both the mesh in the streamwise direction and compared.

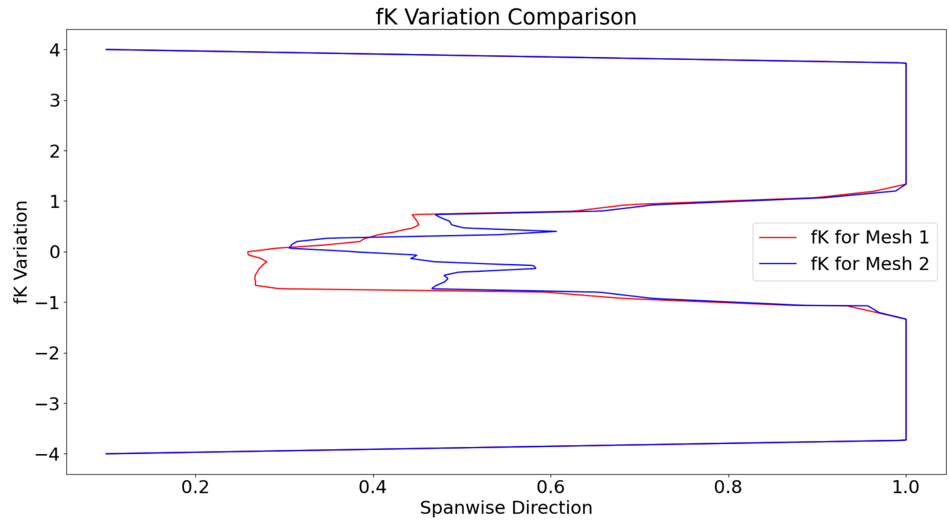

Figure 3.35: f_k Variation Comparison

In Figure 3.35, The fluctuation of the f_k in the spanwise direction for both meshes at a location 1.06m from the center of the cylinder is shown. It can be seen that the f_k parameter changes constantly in the wake of the cylinder where the mesh is refined. Mesh 1 has more mesh refinement at the wake than Mesh 2, and its f_k value falls below 0.3, indicating the complete LES region, but Mesh 2's f_k value falls below 0.4, indicating the start of the LES region.

Conclusion

The PANS turbulence model with a dynamic filter function and two models with static filter function at 0.3 and 0.7 when compared with the SST turbulence models at two different meshes predicted the following results:
The Mesh 1 with higher grid resolution predicted the laminar to turbulent switch better when compared to the Mesh 2 for the varying f_k. Comparing the stream lines, the generation of the re-circular region is better identified for Mesh 1. The time average velocity prediction yielded better and convincing results for Mesh 1 when compared to Mesh 2. Finally the Mesh-1 provided better flow structure when compared to Mesh 2.

The dynamic PANS turbulence model with the dynamic filter function f_k predicts better depending on the refinement of the mesh. This parameter is calculated based on the cell size. The change form the LES region to the RANS region is better seen for more refined grid resolutions.

4

BB02 Generic Submarine

In this chapter, the investigation for the flow around a submarine is carried out. This submarine model chosen is the BB2 generic hull.

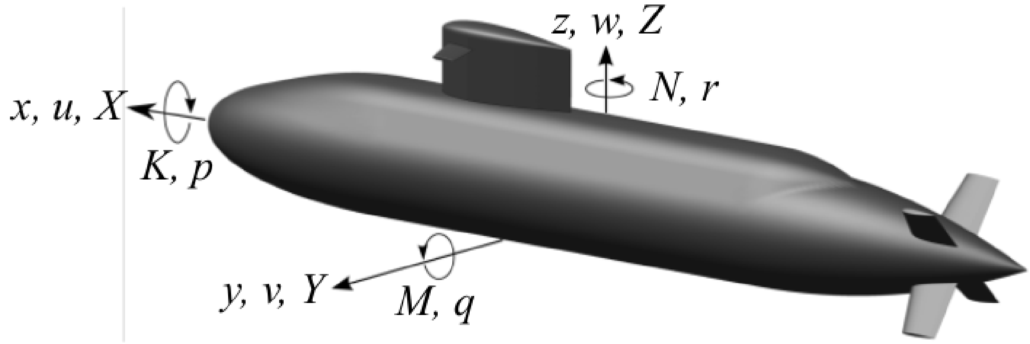

Figure 4.1: Hull Form

The geometry chosen for the CFD analysis of the BB2 can be seen in figure 4.1.The overall length of the submarine is 70.2 m.
The coordinate system for all the global forces and moments can be seen in the figure 4.1. The coordinate system is right handed, where the origin is located at the intersection of the longitudinal axis of symmetry of the hull, mid ship and center-plane with x directed forward, y to the port-side and z vertically upwards. All the integrated forces X,Y,Z and moments K,M,N are non-dimensional.
The CFD simulation was performed for two different phases being straight flight and 10 degree yaw respectively. The submarine hull model was tested using the k-ω SST and the PANS turbulence models developed and compared for a given set of quantities.

4.1 Submarine Geometry and Flow Properties

The submarine form considered in this test case is the BB2 hull form, see 4.1. The design has an overall length of $L_{oa} = 70.2$ m. It is the modified version of the BB1 hull form. The main particulars of the submarine geometry can be found from table 4.1 . The simulations are carried out for a scale factor of 1:35.1.

Table 4.1: Particulars of BB2

Description	Symbol	Full Scale	Model Scale	Unit
Length Overall Submerged	L_{oa}	70.2	2.0	m
Beam	B	9.6	0.2737	m
Depth(to deck)	D	10.6	0.3020	m
Depth(to top of sail)	D_{sail}	16.2	0.4615	m

The hull geometry was first meshed using the snappyHexMesh dictionary file using OpenFOAM. Once the mesh was generated, the mesh was transformed to model scale 1:35.1.
The flow properties for running the simulations can be seen in the table 4.2.

Table 4.2: Flow properties of BB2

Description	Symbol	Value	Unit
Flow velocity	V_∞	28.5	m/s
Density	ρ	1.225	$\frac{kg}{m^3}$
Viscosity	ν	$1.46 * 10^-5$	$\frac{m^2}{s}$
Reynolds	R_e	$3.9 * 10^6$	

4.2 Solving

To solve the integrated equations of the turbulence models, the equations fist needs to be discretized into algebraic equations. the numerical discretization schemes used for this submarine are as follows:

- **Time-Derivative Scheme**: The time derivative scheme used for the SST and the PANS models is backward scheme.
- **Gradient Scheme**: he gradient scheme used for the discretization of the integrated equations is Gauss linear scheme which is the Gaussian integration with central differencing, which is a second order, unbounded scheme.
- **Divergence Scheme**: The divergent scheme used in discretization for velocity, pressure, turbulent kinetic energy, turbulent frequency omega is Bounded Gauss Limited Linear scheme.
- **Laplacian Scheme**: The Laplacian scheme used in this project when discretizing the equations for turbulence is Gauss Linear Corrected, which is Gaussian integration with central differencing and a blend of corrected and uncorrected numerical behaviour.

- **Interpolation Scheme**: Linear interpolations scheme which is also called as the central differencing scheme, which is second order accurate was used for the interpolation of the discretized equations.

The following are the linear solvers used for the simulation,

- **Generalised geometric algebraic multi-grid (GAMG)** with a Gauss-Seidel smoother for the pressure p.
- **Smoother solver** with a symmetric Gauss-Seidel smoother for the velocity U , the turbulent kinetic energy k and the specific dissipation rate ω.

4.3 Post-Processing

The post processing of the simulations were visualised using paraview. The quantities of interest visualised can be seen in the figure 4.2

Original quantity		Data reduction	Datafile name
Coordinates	$p\ h$	$\tilde{x}' = \tilde{x}/L_{\mathrm{oa}}$, same for y' and z'	x, y, z
Velocities	p	$u' = u/V_\infty$, same for v' and w'	u, v, w
Vorticities	p	$\omega'_x = \omega_x \cdot L_{\mathrm{oa}}/V_\infty$, same for ω'_y and ω'_z	vortx, vorty, vortz
Pressure	$p\ h$	$c_p = (p - p_\infty) / \left(\frac{1}{2}\rho V_\infty^2\right)$	cp
TurbulentEnergyKinetic	p	$k' = k/V_\infty^2$	k
SkinFriction	h	$\tau'_x = \tau_x / \left(\frac{1}{2}\rho V_\infty^2\right)$	taux, tauy, tauz
Q	p	$Q' = Q \cdot (L_{\mathrm{oa}}/V_\infty)^2$	Q
H	p	$H' = \frac{\mathrm{helicity}}{\lvert\omega\rvert \cdot \lvert V\rvert}$	H

Figure 4.2: BB2 Flow Quantities

The quantities of interests were visualised for both straight flight and 10 degree yaw respectively.

4.4 Submarine with Straight Flight

The simulation was performed for the submarine hull form with a straight flight phase. The turbulence models used in the simulation of this phase were the kOmegaSST turbulence model and the PANS model with dynamic filter function and two constant filter functions at 0.3 and 0.7.

The submarine mesh for the straight flight can be seen from the figure 4.3

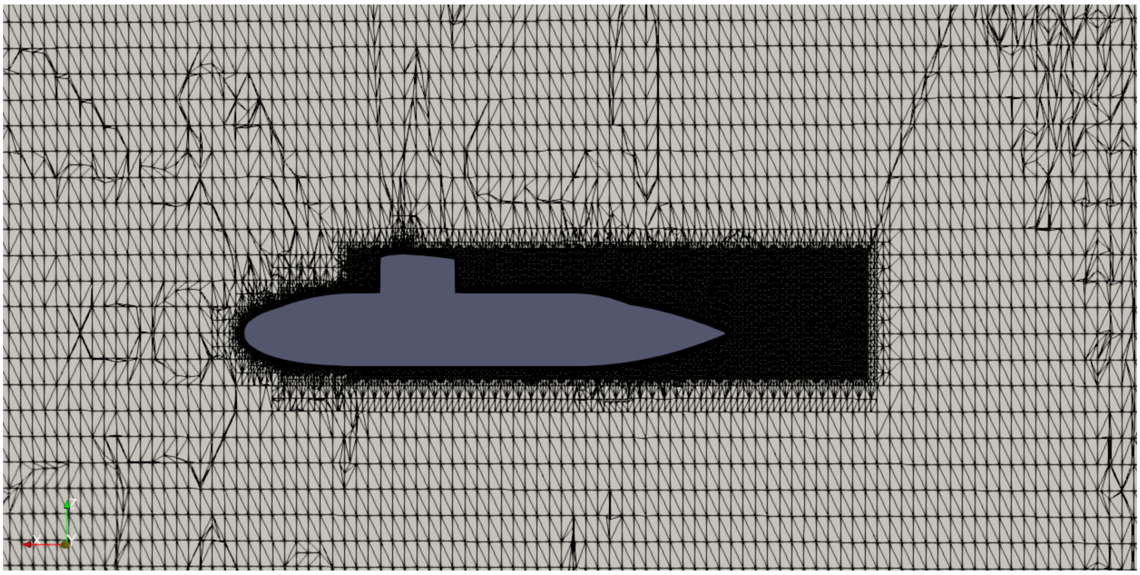

Figure 4.3: BB2 Grid resolution for Straight Flight

A refinement region is used across the submarine model in order to predict the flow quantities better with the developed PANS turbulence models. The total number of cells used is 8M cells. The simulation results for all the different turbulence models according to the flow quantities needed for better understanding of the accuracy of the turbulence models are discussed below.

Drag and Lift Forces

The drag and lift forces computed for the submarine under straight flight was calculated and can be seen from the graphs below.

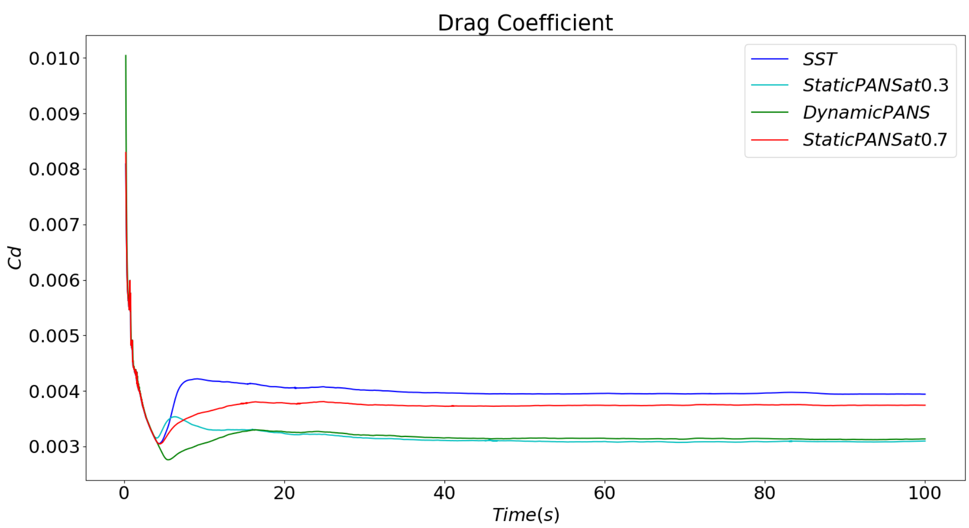

Figure 4.4: Drag Force for straight flight

From figure 4.4, it can be seen that the drag force is the highest for SST turbulence model where as it is the least for both dynamic PANS and static PANS model at f_k = 0.3 turbulence models. For the lift force, from figure 4.5, it can be seen that the static PANS at f_k = 0.7 has the highest value for lift force when compared to other turbulence models.

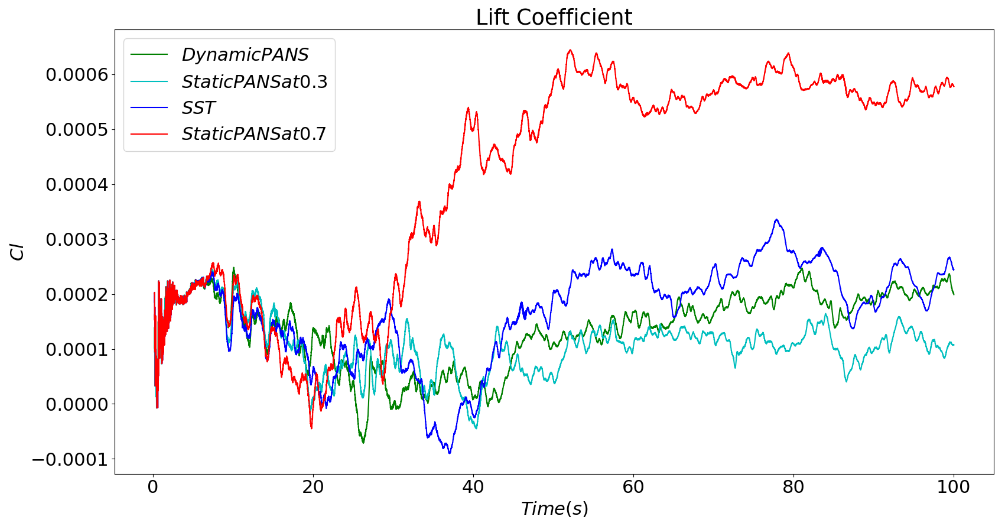

Figure 4.5: Lift Force for straight flight

Vortices

Data for the three vortex components, vortx, vorty, and vortz, were visualized for all of the turbulence models to be compared, with vortx measured in the streamwise direction and vorty and vortz measured in the spanwise order.
The phenomenon known as boundary layer separation causes vortex generation. The SST turbulence model has a higher flow separation than the PANS turbulence models.

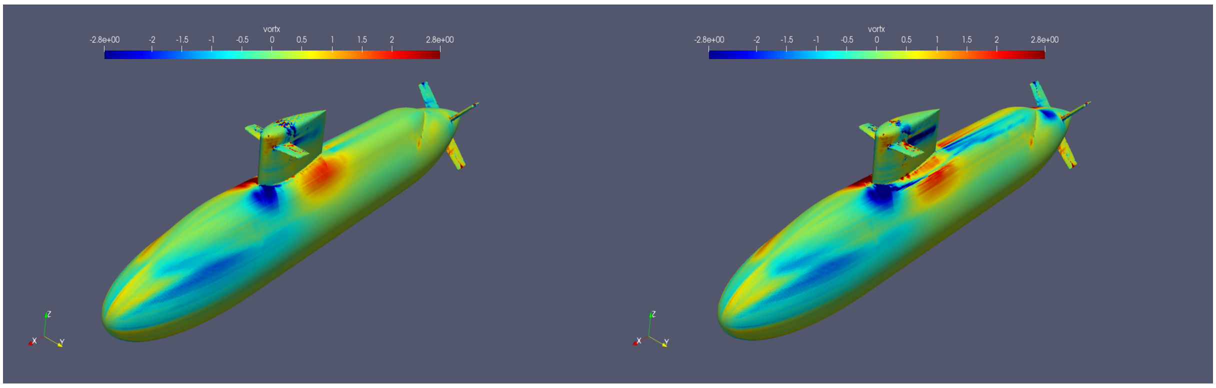

(a) Vorticity x for dynamic PANS Straight Flight **(b)** Vorticity x for SST Straight Flight

Figure 4.6: Vorticity x for dynamic PANS and SST Straight Flight

Figures 4.6 and 4.7 show the vorticity in the x-direction for all the turbulence models considered. For the SST turbulence model, the vortex formations are much more significant when compared to the PANS models. At the leading edge of the sail the vortices formed are weaker compared to the trailing edge of the sail as it should be.

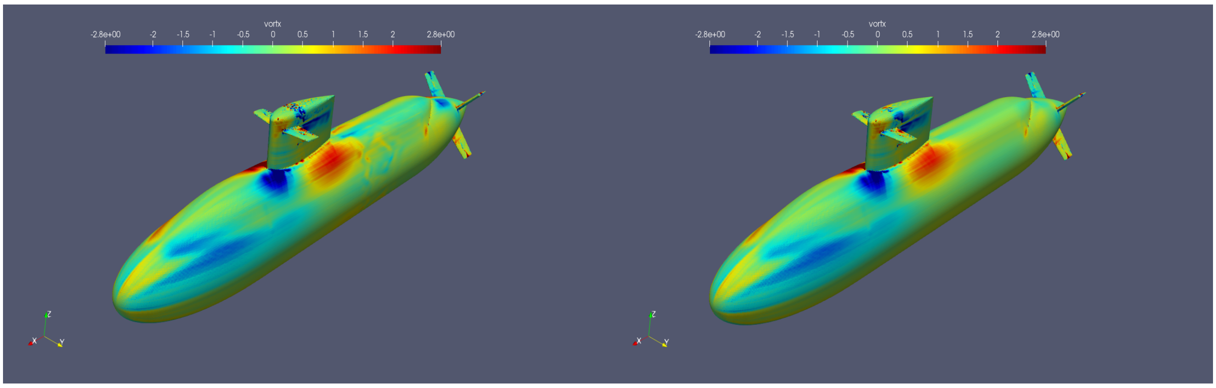

(a) Vorticity x for static PANS at 0.3 Straight Flight **(b)** Vorticity x for static PANS at 0.7 Straight Flight

Figure 4.7: Vorticity x for static PANS at 0.3 and 0.7 Straight Flight

The vortex forming region at the wake of the sails is significantly smaller in PANS models, and this may be due to the need for a more refined mesh at the boundary layer to satisfy the y+ condition. The vortex formation in the spanwise directions have been visualised and can be viewed in the Appendix.

Pressure

All turbulence models had their pressure coefficient C_P computed and visualized. The pressure coefficient, abbreviated as C_P, is a dimensionless number that characterizes the relative pressures in a flow field. This pressure coefficient is used to figure out where the submarine's critical points are.

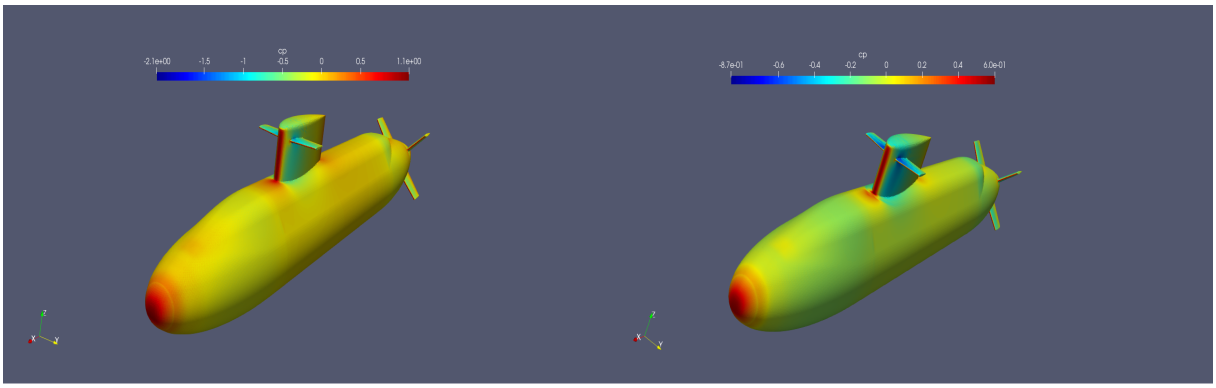

(a) Pressure for dynamic PANS Straight Flight **(b)** Pressure for SST Straight Flight

Figure 4.8: Pressure for dynamic PANS and SST Straight Flight

Figures 4.8 and 4.9 show the pressure distribution along the submarine. All of the turbulence models have a similar pressure distribution. The leading tip of the submarine and the leading edge of the sails are the key places or points where a high-pressure occurrence is possible. The velocity of the fluid increases as it moves with the sails. As the velocity increases, the pressure decreases, and the pressure distribution decreases along the sails.

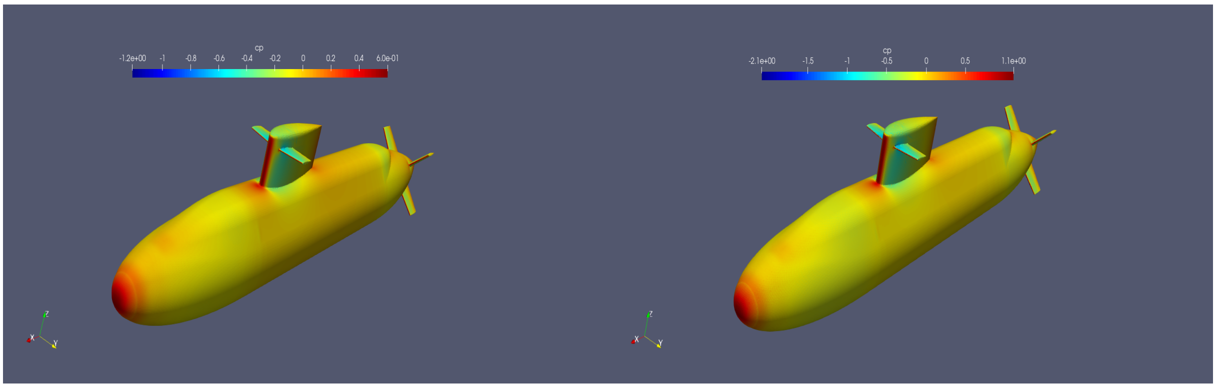

(a) Pressure for static PANS at 0.3 Straight Flight **(b)** Pressure for static PANS at 0.7 Straight Flight

Figure 4.9: Pressure for static PANS at 0.3 and 0.7 Straight Flight

Skin Friction

The skin friction is computed for the submarine taking the wall shear stress into consideration. The shear stress at the wall is an important quantity that is used to measure the force exerted by the wall. The wall shear stress is computed for the streamwise direction taux and the spanwise directions tauy and tauz.
When a fluid flows across the surface of the hull, there is an outward force produced in the orthogonal direction by the surface which produces a shear stress on the surface of the hull. This shear stress causes some friction for the fluid flowing across the surface of the hull which is called as skin friction.

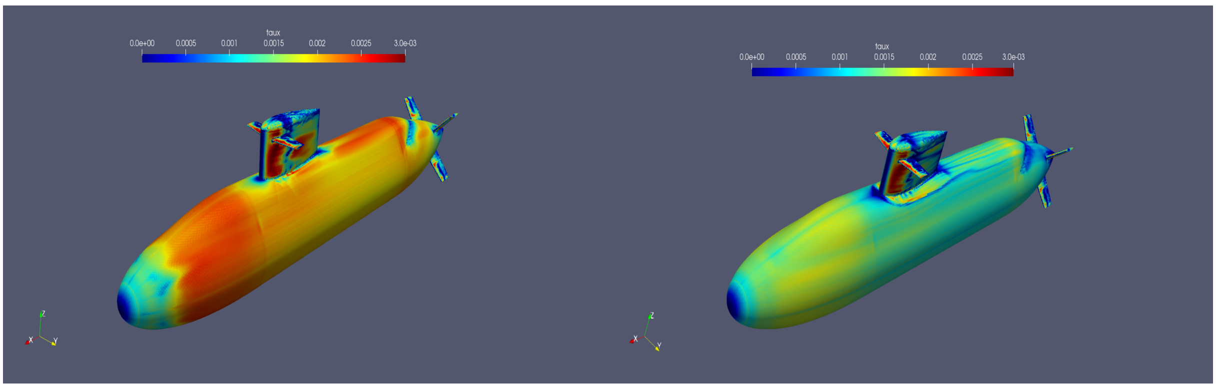

(a) taux for dynamic PANS Straight Flight **(b)** taux for SST Straight Flight

Figure 4.10: taux for dynamic PANS and SST Straight Flight

Figures 4.10 and 4.11 show the wall shear stress in the streamwise direction along the surface of the submarine. From these figures, it is evident that the static PANS model at f_k 0.3 and the SST turbulence model have lower shear stress distribution along the surface of the submarine when compared to the dynamic PANS and the static PANS at f_k 0.7 turbulence models. The differences in the shear stress distribution can also be observed at the leading edge of the sails. This difference of the shear stress observed on the surface of the hull for all the turbulence models can be due to the fact that shear stresses can be quite sensitive to grid quality of the first cells.

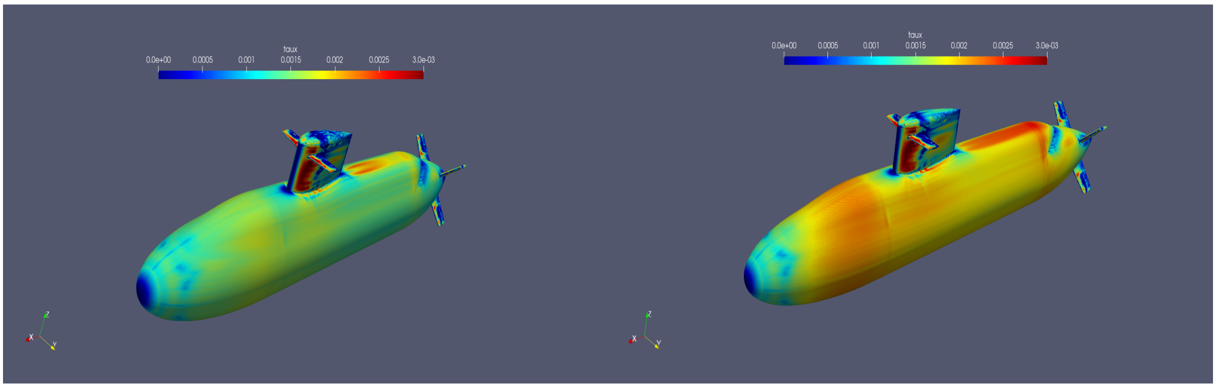

(a) taux for static PANS at 0.3 Straight Flight

(b) taux for static PANS at 0.7 Straight Flight

Figure 4.11: taux for static PANS at 0.3 and 0.7 Straight Flight

Q-Criterion

Similar to the cylinder, the Q-criterion was also calculated and visualised. Figures 4.12 and 4.13 depict the iso-surface of the normalised Q-criterion at 0.1.

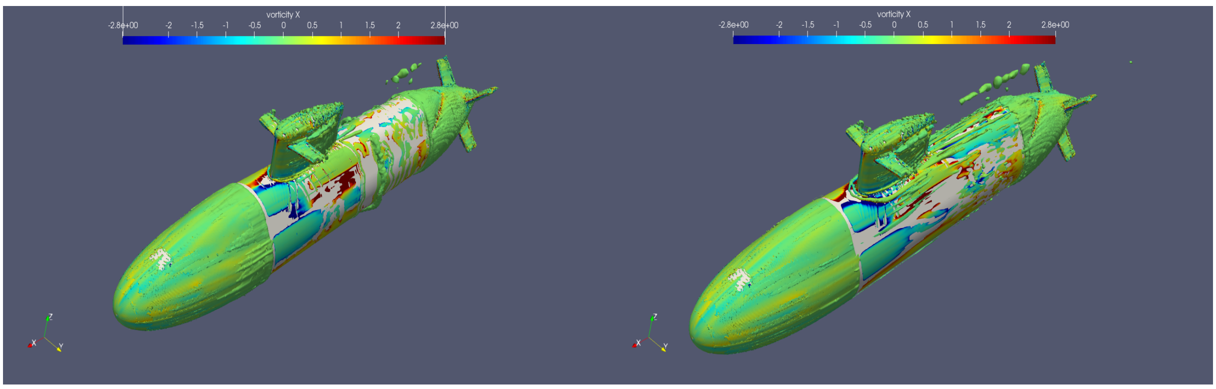

(a) Q Criterion for dynamic PANS Straight Flight

(b) Q Criterion for SST Straight Flight

Figure 4.12: Q Criterion for dynamic PANS and SST Straight Flight

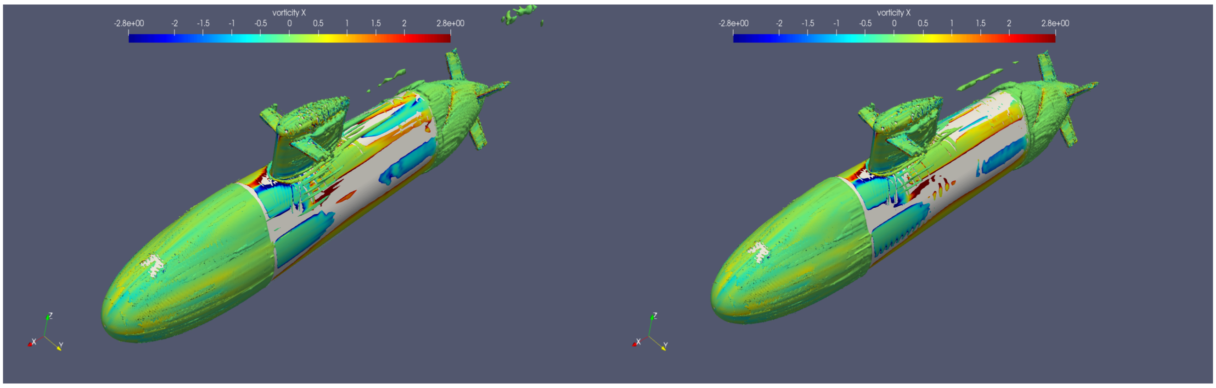

(a) Q Criterion for static PANS at 0.3 Straight Flight

(b) Q Criterion for static PANS at 0.7 Straight Flight

Figure 4.13: Q Criterion for static PANS at 0.3 and 0.7 Straight Flight

The SST model still predicts the development of the vortices better when compared to the PANS turbulence models. The vortex prediction on the PANS models can increase by using a more refined mesh at the wake of the sails.

4.5 Submarine with 10 degree yaw

The simulation was performed for the submarine hull model with a positive 10 degree yaw in the spanwise direction. The turbulence models used in the simulation of this phase are k-ω SST model and the static PANS turbulence models at f_k 0.3 and 0.7. The submarine mesh for 10 degree ya can be seen from the figure 4.14

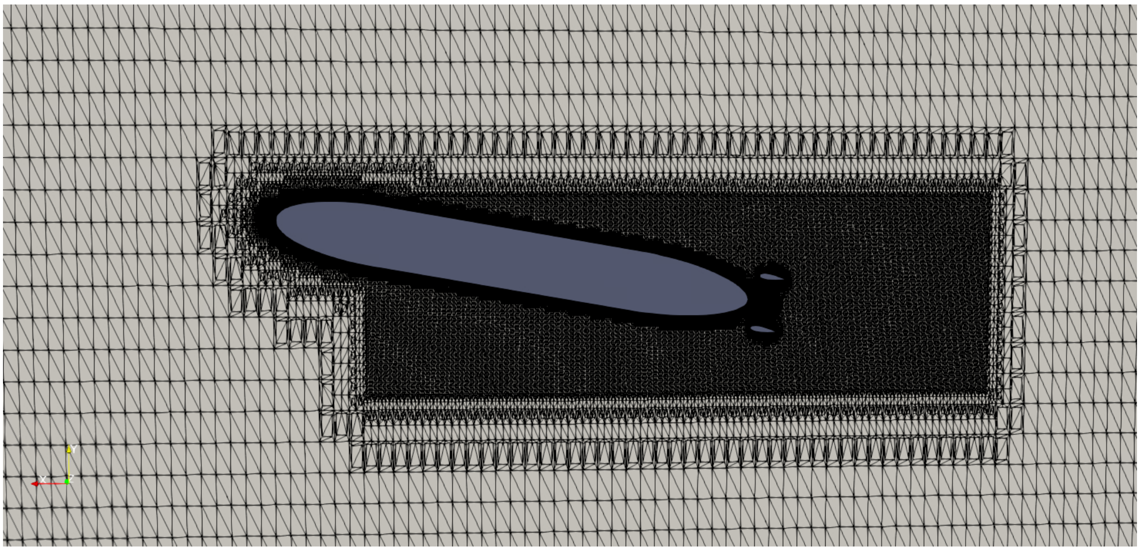

Figure 4.14: BB2 Grid resolution for 10 degree yaw Flight

Similar to the straight flight mesh, a refinement region is used across the submarine model to predict the flow quantities better with the developed PANS models. The total number of cells used is 9M cells. The simulation results for all the different turbulence models according to the flow quantities needed for better understanding of the accuracy of the turbulence models are discussed below.

Drag and Lift Forces

The drag and lift forces for the submarine under 10 degree yaw was calculated and can be seen from the figures below.

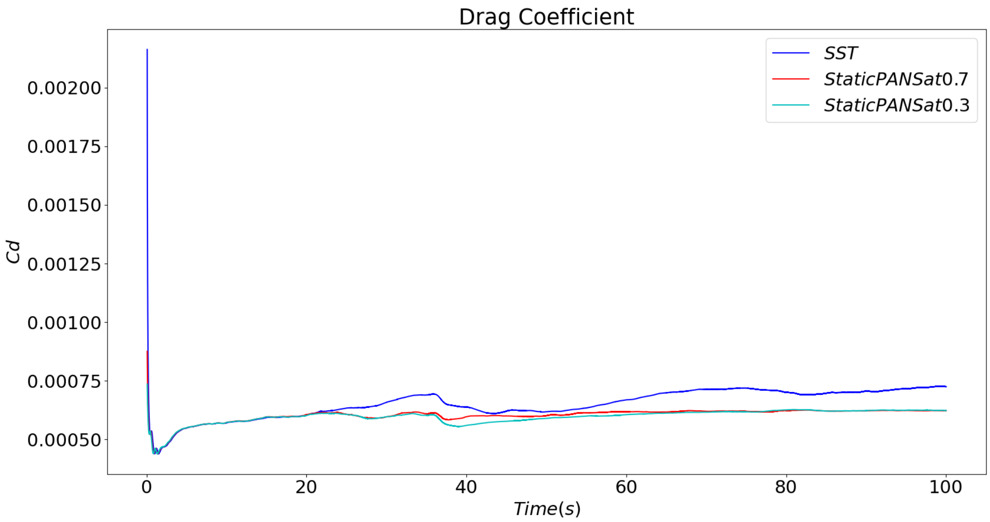

Figure 4.15: Drag Force for SST for 10 degree yaw Flight

From figure 4.15, it can be seen that SST predicts slightly higher drag force compared to the static PANS models. The yaw force for the oblique flow can be seen from figure 4.16, The yaw force predicted by SST and static PANS 0.7 is a bit higher than the static PANS 0.3 turbulence model.

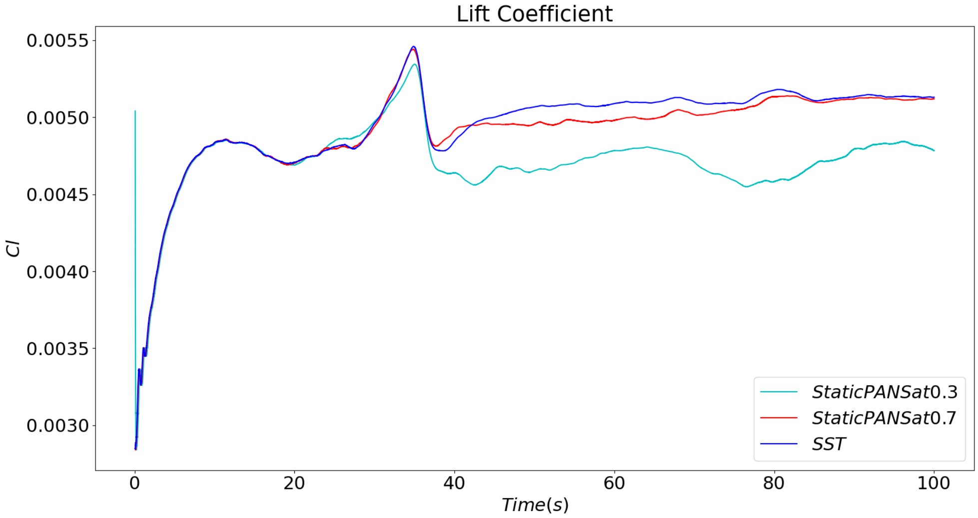

Figure 4.16: Yaw for SST for 10 degree yaw Flight

Vorticies

Data for the three vortex components, vortx, vorty, and vortz, were visualized for all of the turbulence models to be compared, with vortx measured in the streamwise direction and vorty and vortz measured in the spanwise order.

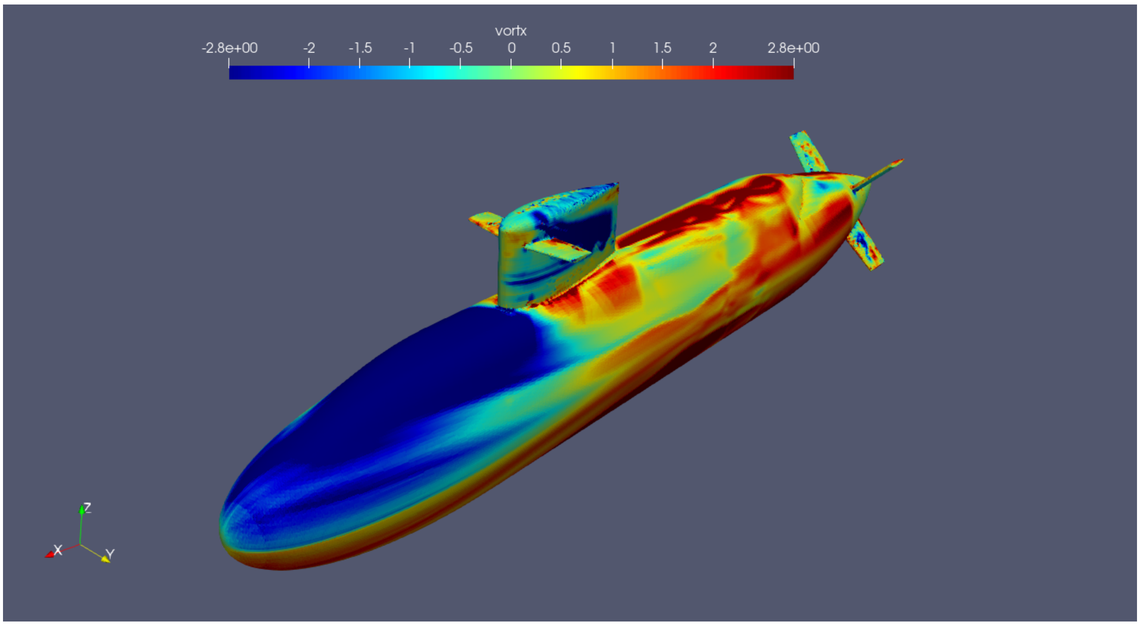

Figure 4.17: Vorticity x for SST for 10 degree yaw Flight

Figures 4.17 and 4.18 show the vorticity in the x-direction for all the turbulence models considered. It can be seen that at the front of the hull the vorticies formed are much weaker compared to the vortices formed at the wake of the sail.

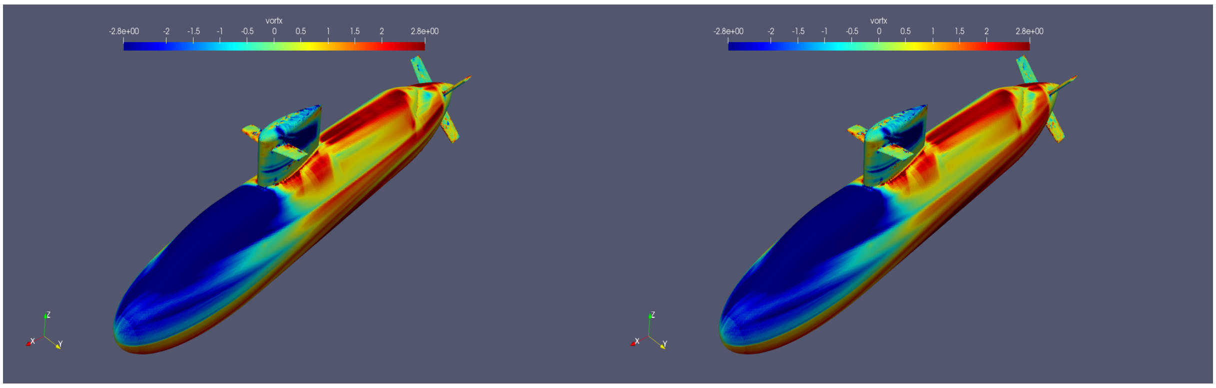

(a) Vorticity x for static PANS at 0.3 for 10 degree yaw Flight

(b) Vorticity x for static PANS at 0.7 for 10 degree yaw Flight

Figure 4.18: Vorticity x for static PANS at 0.3 and 0.7 for 10 degree yaw Flight

Pressure

All turbulence models had their pressure coefficient C_P computed and visualized.The pressure coefficient, abbreviated as C_P, is a dimensionless number that characterizes the relative pressures in a flow field. This pressure coefficient was used to figure out where the submarine's critical points were.

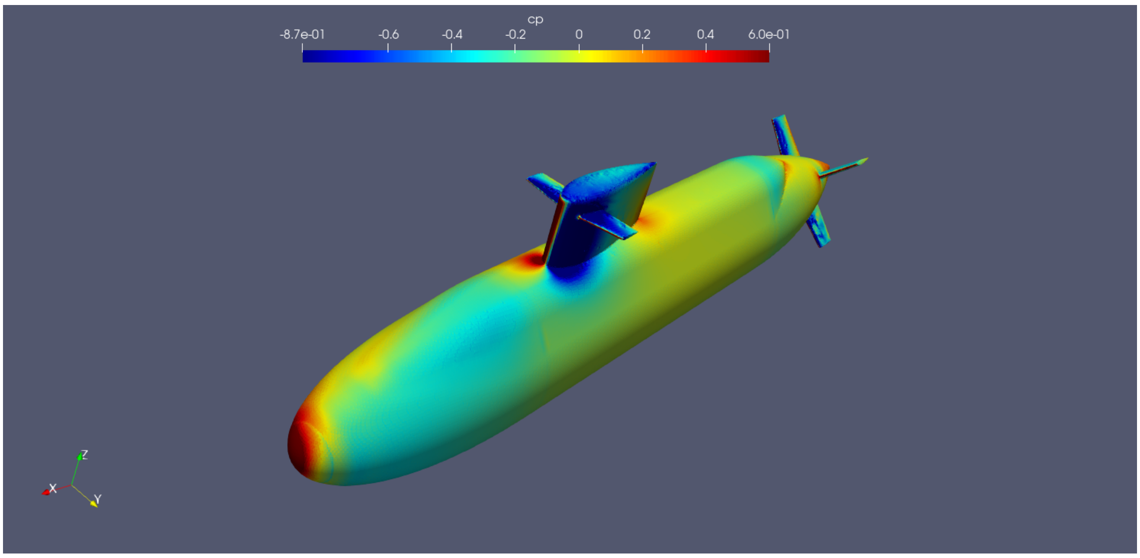

Figure 4.19: Pressure for SST for 10 degree yaw Flight

Figures 4.19 and 4.20 show the pressure distribution along the submarine for 10 degree yaw. It can be observed that at the leading edge of the submarine there is a high pressure and low pressure point because of the 10 degree yaw and the leading tip there is a high pressure point. On the region of low pressure the velocity increases and at the high pressure point the velocity reduces.

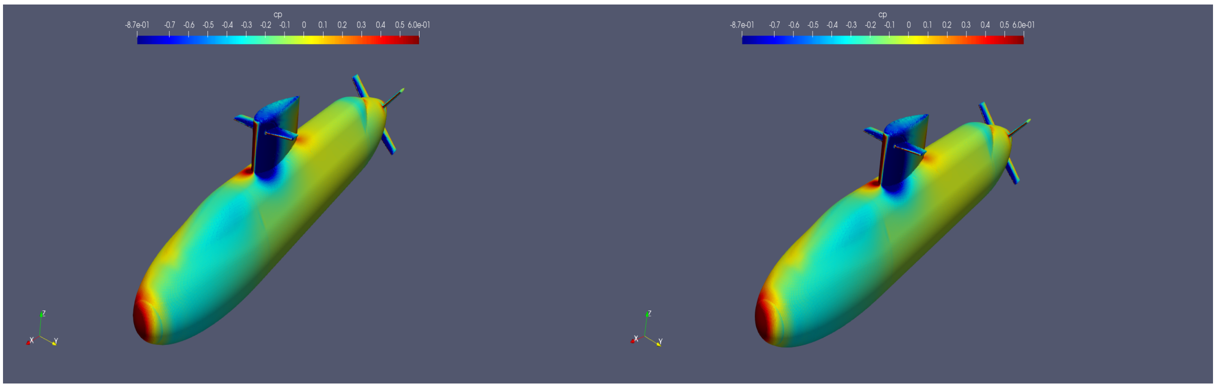

(a) Pressure for static PANS at 0.3 for 10 degree yaw Flight **(b)** Pressure for static PANS at 0.7 for 10 degree yaw Flight

Figure 4.20: Pressure for static PANS at 0.3 and 0.7 for 10 degree yaw Flight

Skin Friction

The skin friction is computed for the submarine taking the wall shear stress into consideration. The shear stress at the wall is an important quantity that is used to measure the force exerted by the wall. The wall shear stress is computed for the streamwise direction taux and the spanwise directions tauy and tauz.

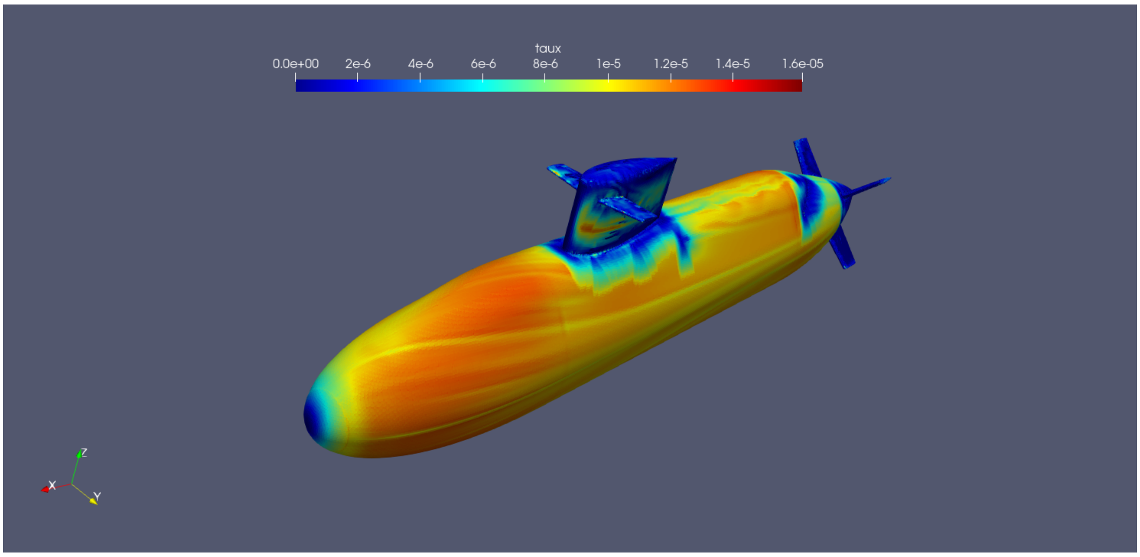

Figure 4.21: taux for SST for 10 degree yaw Flight

Figures 4.21 and 4.22 show the wall shear stress in the streamwise direction along the surface of the submarine at 10 degree yaw. From the visualisation it is clear that the SST turbulence model and the static PANS models show similar wall shear stress along the surface of the submarine at 10 degree yaw. When observed closely at the wake of the sail, the SST model predicts comparatively lesser wall shear stress compared to the static PANS models.

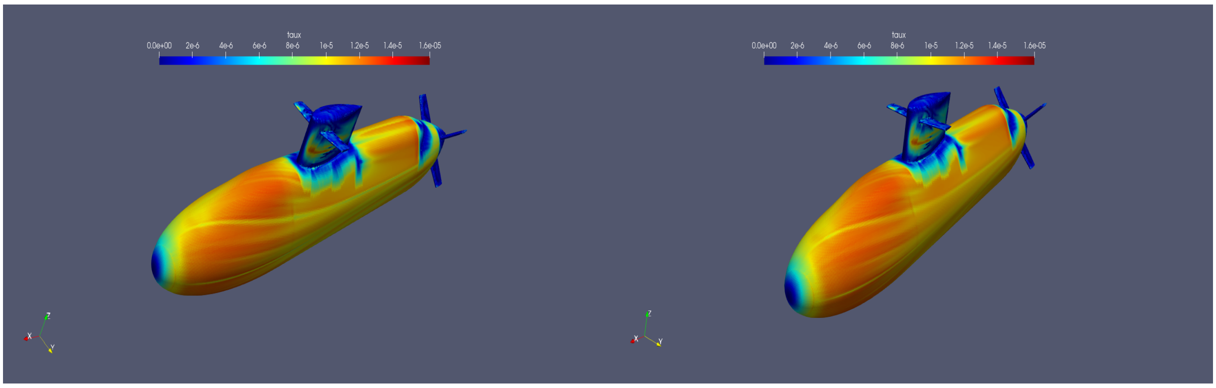

(a) taux for static PANS at 0.3 for 10 degree yaw Flight

(b) taux for static PANS at 0.7 for 10 degree yaw Flight

Figure 4.22: taux for static PANS at 0.3 and 0.7 for 10 degree yaw Flight

Q-Criterion

The Q-criterion was calculated and visualised for the submarine at the 10 degree yaw. Figures A.29 and 4.24 depict the iso-surface of the normalised Q-criterion at 0.1.

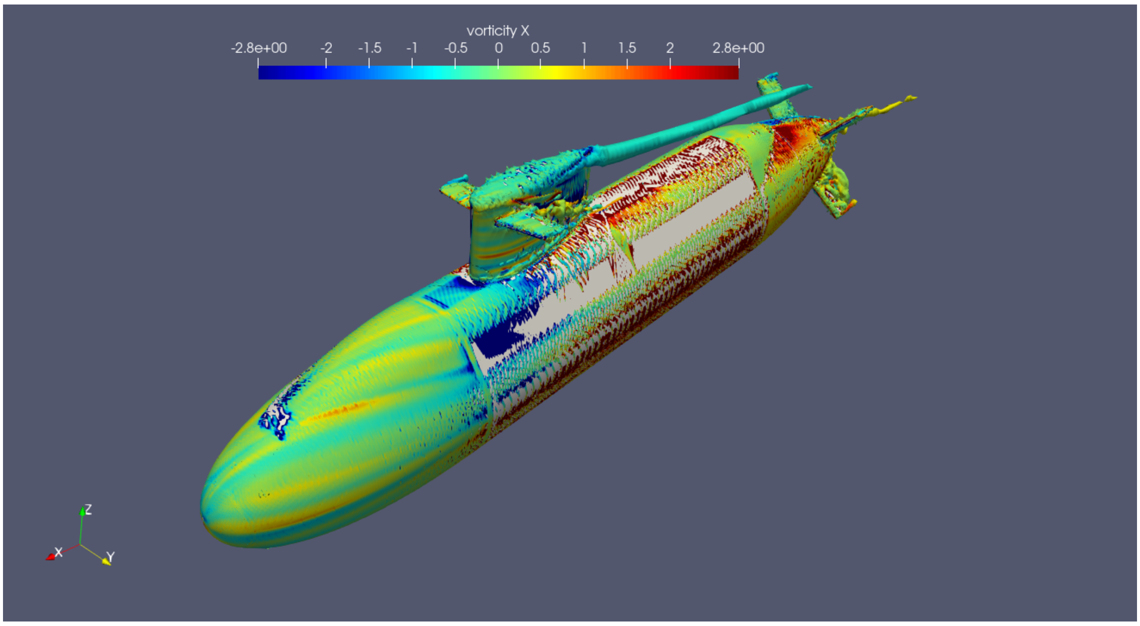

Figure 4.23: Q-Criterion for SST for 10 degree yaw Flight

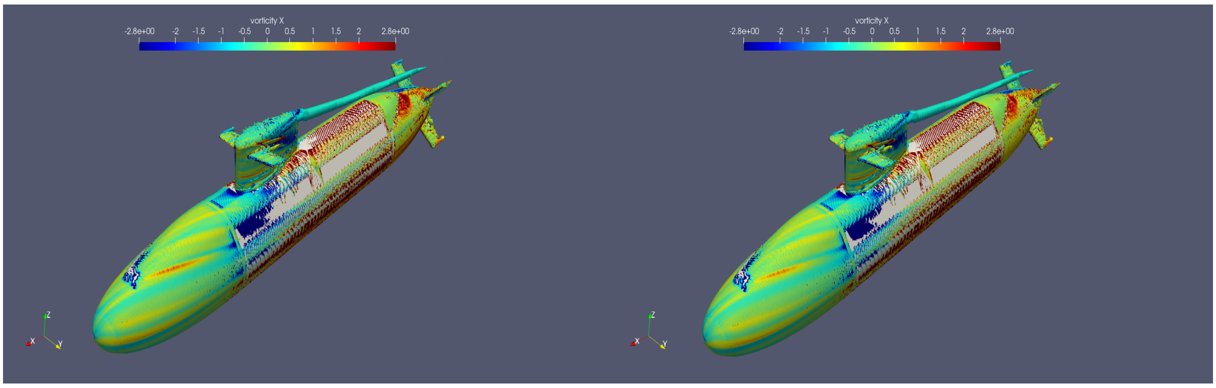

(a) Q-Criterion for static PANS at 0.3 for 10 degree yaw Flight

(b) Q-Criterion for static PANS at 0.7 for 10 degree yaw Flight

Figure 4.24: Q-Criterion for static PANS at 0.3 and 0.7 for 10 degree yaw Flight

Similar to the straight flight, the SST model still predicts the development of the vortices better when compared to the PANS turbulence models. The vortex prediction on the PANS models can increase by using a more refined mesh at the wake of the sails.

Forces Comparison

The forces computed for both the straight and the oblique flow were compared with the results from the initial test of the submarine hull.

References	Models	$\overline{C_D}$	$\overline{C_L}$
Straight flow	SST	0.0057	0.00016
	dynamic PANS	0.0031	0.00013
	$f_k = 0.3$	0.0031	0.00010
	$f_k = 0.7$	0.0037	0.00041
Phase 0 straight flow	SST	0.00156	0.000127
References	Models	$\overline{C_D}$	$\overline{C_{yaw}}$
10 degree yaw	SST	0.00064	0.0123
	$f_k = 0.3$	0.00059	0.0117
	$f_k = 0.7$	0.0006	0.0122
phase 0 oblique flow	SST	0.00055	-0.0144

Table 4.3: Comparison of forces for the Submarine

From the table it can be seen that for the straight flow, the drag and lift forces and quite large when compared to the test results from phase 0. The static PANS with $f_k = 0.7$ gives the highest drag and lift force when compared to other models and static f_k at 0.3 gives the least. Similarly, for the oblique flow, SST predicts a bit higher force when compared to the static PANS models and the values for the oblique flow is quite similar to that of the test results obtained in the phase 0 simulations of the hull.

5

Conclusion and Future Work

The present work has investigated the ability of turbulence prediction of the PANS implementation for the kωSST model. The PANS model is implemented for a static filter function and dynamic filter function for the kωSST turbulence model and compared with the actual kωSST model. Initially, the PANS version was validated by investigating the flow around a circular cylinder at a Reynolds number of 3900. Two different grid resolutions were considered, where one had a refined mesh, and the other had a comparatively coarse mesh. The results obtained for both the grid resolution provided a better understanding of the PANS implementation for the kωSST model. The refined mesh provided better outcomes for the dynamic PANS when compared with the coarse mesh, and this may be due to the fact that for the dynamic PANS, the filter function fk switches between the RANS and LES mode based on the size of the cell and hence for an increased number of cells the filter function switches between the RANS and the LES mode better when compared to the coarser mesh. As a result, the dynamic PANS performed better than the standard SST turbulence model. After validating the PANS implementation for the kωSST turbulence model, an investigation was carried out for a BB2 generic submarine where the submarine model was chosen within the NATO AVT-301 group. The CFD analysis for this hull was performed using the standard kωSST turbulence model and the developed PANS model. This CFD investigation was conducted for two phases in which one of the phases was for the submarine at straight flight, whereas the second phase was for the sub at 10-degree yaw. The flow quantities measured are Velocity distribution, Vortices, Pressure, Turbulent Kinetic Energy, Skin Friction along the hull surface and the forces were computed and compared. The results obtained for the submarine shows that the static PANS model at fk 0.3 predicted better results when compared to other turbulence models used. In contrast, for 10-degree yaw, the PANS model and the SST model predicted similar results.

A different implementation of the dynamic filter function for the dynamic PANS model can be considered to obtain a more accurate inflow prediction for the laminar transition to turbulence. Furthermore, a variable resolution PANS model can also be considered to get a smoother transition from RANS to LES mode. The variable resolution model acts as a bridging factor and helps provide closure to the dynamic PANS model, also called the zonal approach. Another way to improve the flow prediction is to implement a more refined mesh since the filter function depends on the size of the cell.

Bibliography

[1] B Basara, S Krajnović, and S Girimaji. Near-wall formulation of the partially averaged navier– stokes turbulence model aiaa j. page 49, 2011.

[2] L Davidson. Zonal pans: evaluation of different treatments of the rans–les interface. page 283, 2016.

[3] L Davidson. Fluid mechanics, turbulent flow and turbulence modeling. page 176, 2019.

[4] S Girimaji, E. Jeong, and R. Srinivasan. Partially averaged navier-stokes method for turbulence: Fixed point analysis and comparison with unsteady partially averaged navier-stokes. pages 422—-429, 2005.

[5] S Kenjeres and K Hanjalic. Les, t-rans and hybrid simulations of thermal convection at high ra numbers. int j heat fluid flow. page 27, 2006.

[6] S. Lakshmipathy and S Girimaji. Partially-averaged navier-stokes method for turbulent flows: k model implementation. pages 9–12, 2006.

[7] F.R. Menter. Two-equation eddy-viscosity turbulence models for engineering applications. page 32, 1994.

[8] A Molland and S R Turnock. Marine rudders and control surfaces. 2008.

[9] F S. Pereira. Towards predictive scale-resolving simulations of turbulent external flows. page 1, 2018.

[10] F S. Pereira. Towards predictive scale-resolving simulations of turbulent external flows. pages 4–5, 2018.

[11] F S. Pereira. Towards predictive scale-resolving simulations of turbulent external flows. pages 29–30, 2018.

[12] F S. Pereira. Towards predictive scale-resolving simulations of turbulent external flows. pages 58–59, 2.18.

[13] F S. Pereira, L Eça, and G Vaz. Investigating the effect of the closure in partially-averaged navier–stokes equations. pages 7–8, 2019.

[14] H K Versteeg and W Malalasekera. An introduction to computational fluid dynamics. pages 1–2, 2007.

A

Appendix 1

A.1 Cylinder

The Time Average Velocity for Mesh 2 at 1.54m.

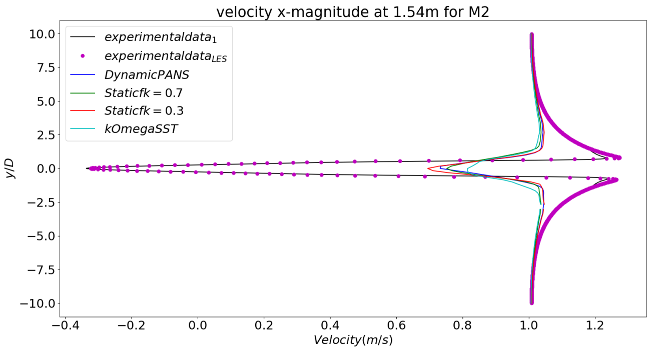

Figure A.1: X-Magnitude with Experimental Data at 1.54m for Mesh 2

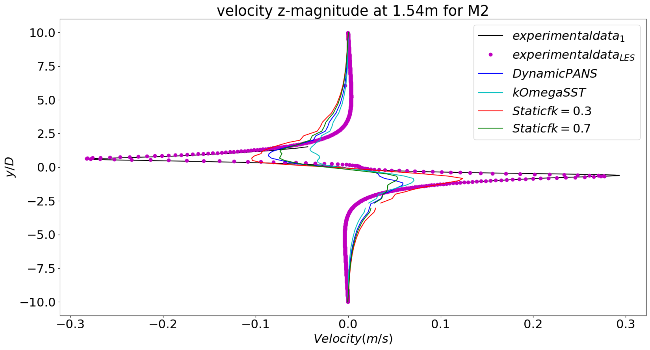

Figure A.2: Z-Magnitude with Experimental Data at 1.54m for Mesh 2

The Time Average Velocity for Mesh 2 at 2.02m.

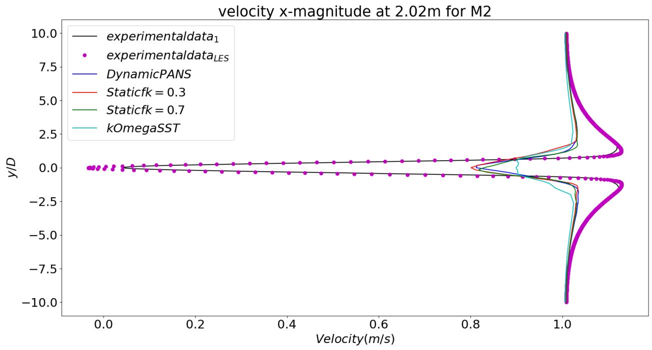

Figure A.3: X-Magnitude with Experimental Data at 2.02m for Mesh 2

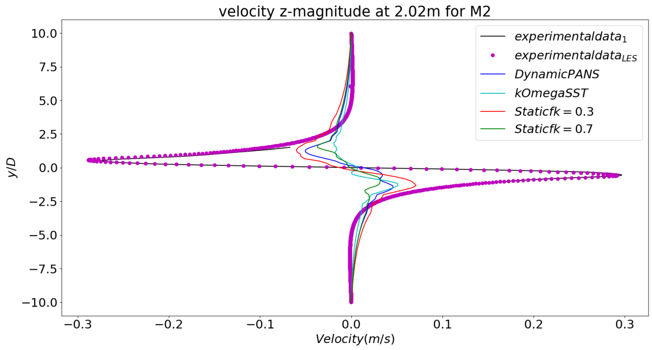

Figure A.4: Z-Magnitude with Experimental Data at 2.02m for Mesh 2

A.1.1 Velocity profile for Mesh 1

Velocity profile for all the four turbulence models considered for Mesh 1.

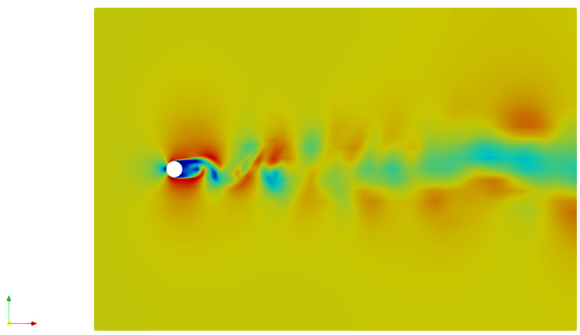

Figure A.5: Velocity profile for SST Turbulence model for Mesh 1

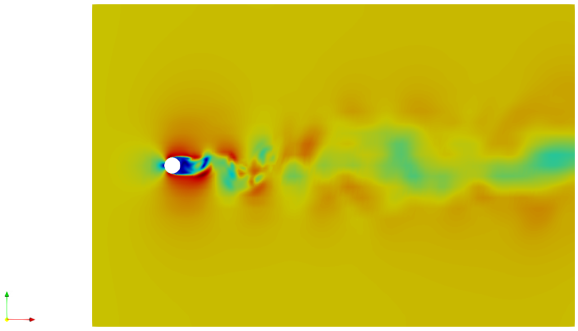

Figure A.6: Velocity profile for dynamic PANS Turbulence model for Mesh 1

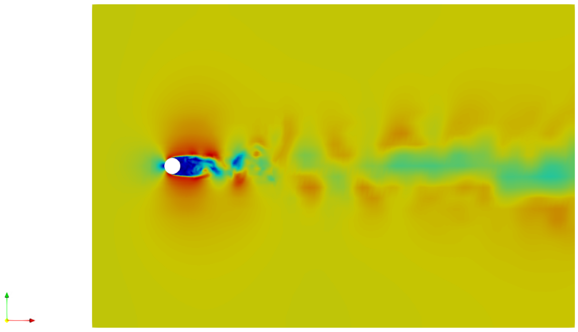

Figure A.7: Velocity profile for static PANS at 0.3 Turbulence model for Mesh 1

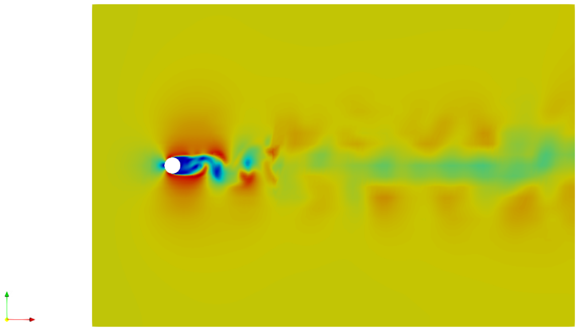

Figure A.8: Velocity profile for static PANS at 0.7 Turbulence model for Mesh 1

A.1.2 Unresolved Turbulent Kinetic Energy for Mesh 1

Unresolved Turbulent Kinetic Energy for all the four turbulence models considered for Mesh 1

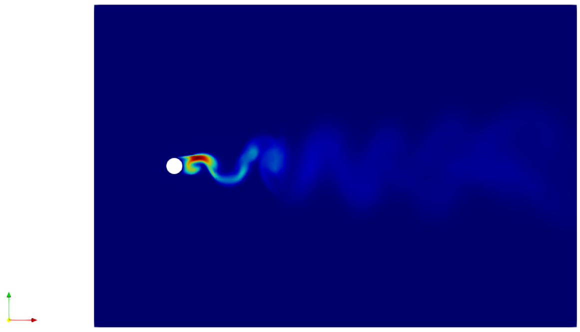

Figure A.9: Turbulent Kinetic Energy for SST Turbulence model for Mesh 1

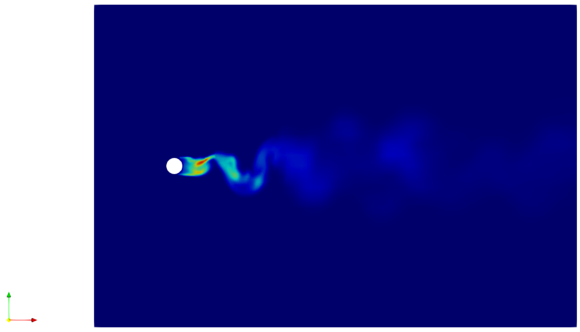

Figure A.10: Unresolved Turbulent Kinetic Energy for dynamic PANS Turbulence model for Mesh 1

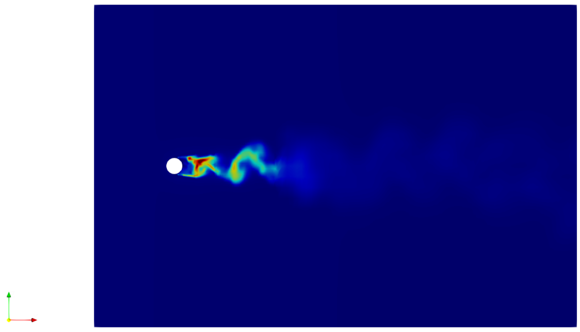

Figure A.11: Unresolved Turbulent Kinetic Energy for static PANS at 0.3 Turbulence model for Mesh 1

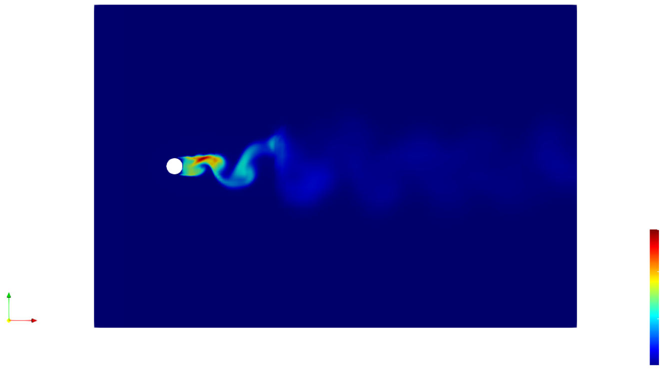

Figure A.12: Unresolved Turbulent Kinetic Energy for static PANS at 0.7 Turbulence model for Mesh 1

A.1.3 Velocity profile for Mesh 2

Velocity profile for all the four turbulence models considered for Mesh 2.

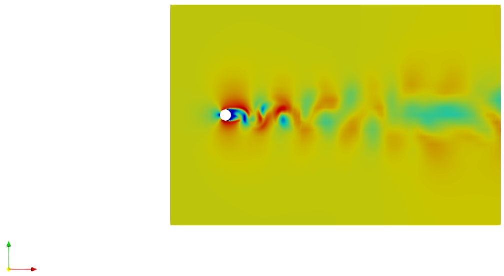

Figure A.13: Velocity profile for SST Turbulence model for Mesh 2

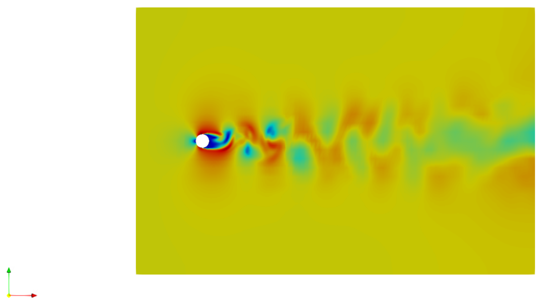

Figure A.14: Velocity profile for dynamic PANS Turbulence model for Mesh 2

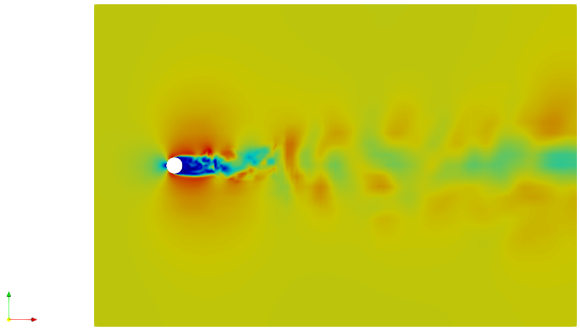

Figure A.15: Velocity profile for static PANS at 0.3 Turbulence model for Mesh 2

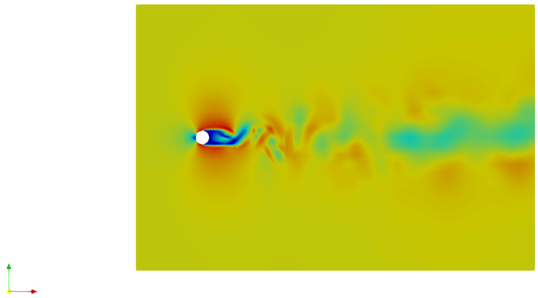

Figure A.16: Velocity profile for static PANS at 0.7 Turbulence model for Mesh 2

A.1.4 Unresolved Turbulent Kinetic Energy for Mesh 2

Unresolved and resolved Turbulent Kinetic Energy for all the four turbulence models considered for Mesh 2.

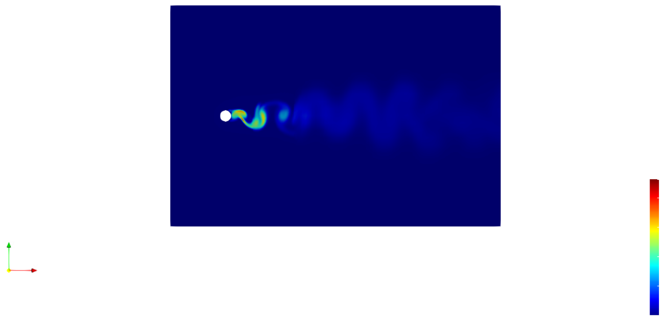

Figure A.17: Turbulent Kinetic Energy for SST Turbulence model for Mesh 2

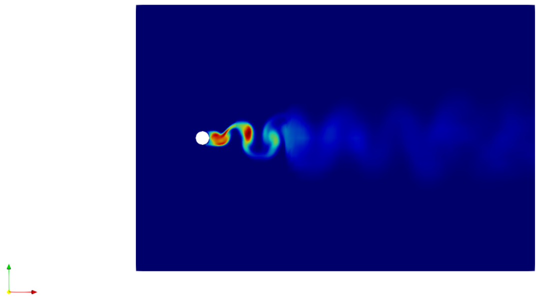

Figure A.18: Unresolved Turbulent Kinetic Energy for dynamic PANS Turbulence model for Mesh 2

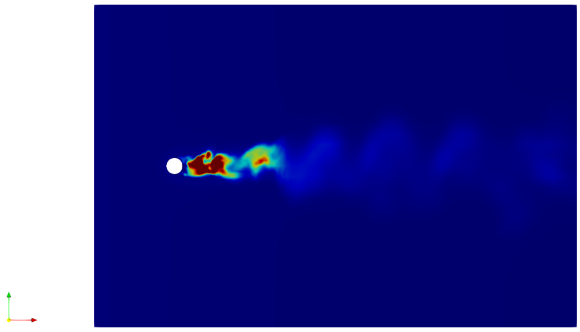

Figure A.19: Unresolved Turbulent Kinetic Energy for static PANS at 0.3 Turbulence model for Mesh 2

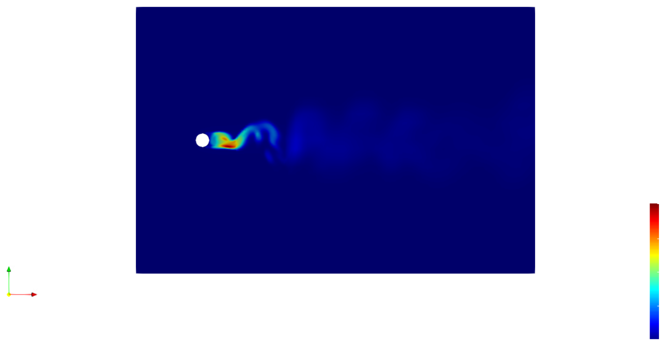

Figure A.20: Unresolved Turbulent Kinetic Energy for static PANS at 0.7 Turbulence model for Mesh 2

A.2 Submarine Straight

A.2.1 Vorticies

The Vorticies in spanwise direction vorty and vortz are visualised

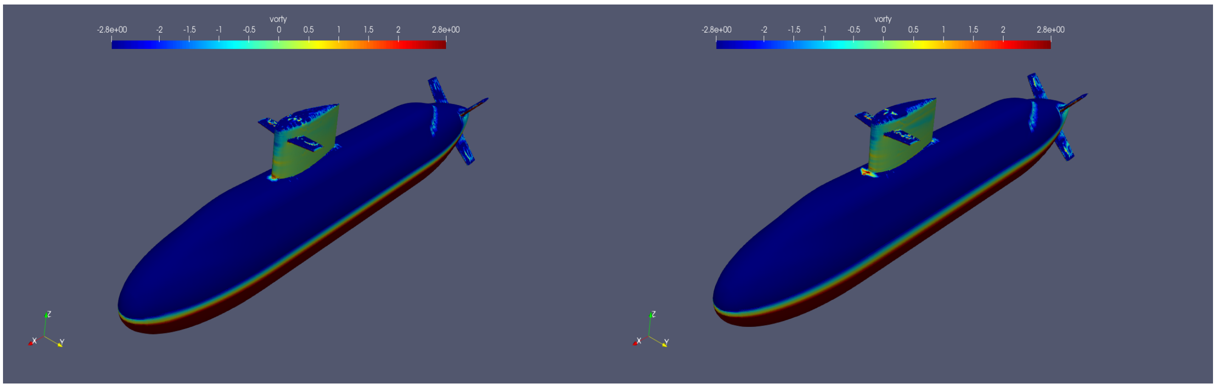

(a) vorty for dynamicPANS **(b)** vorty for SST

Figure A.21: vorty for dynamicPANS and SST

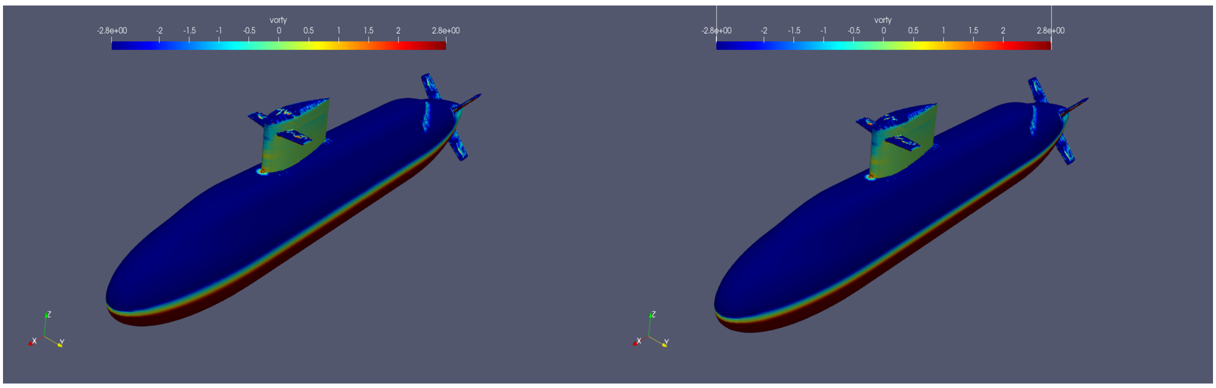

(a) vorty for staticPANS at 0.3 **(b)** vorty for staticPANS at 0.7

Figure A.22: vorty for staticPANS at 0.3 and 0.7

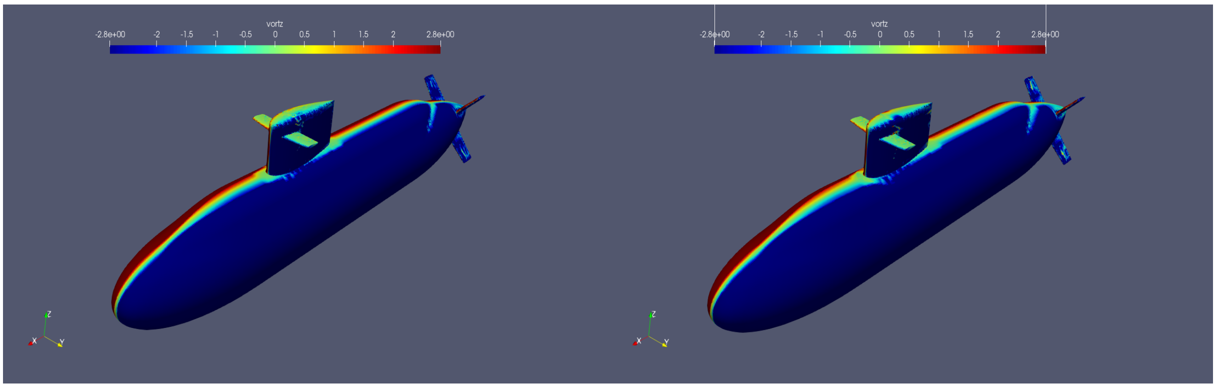

(a) vortz for dynamicPANS (b) vortz for SST

Figure A.23: vortz for dynamicPANS and SST

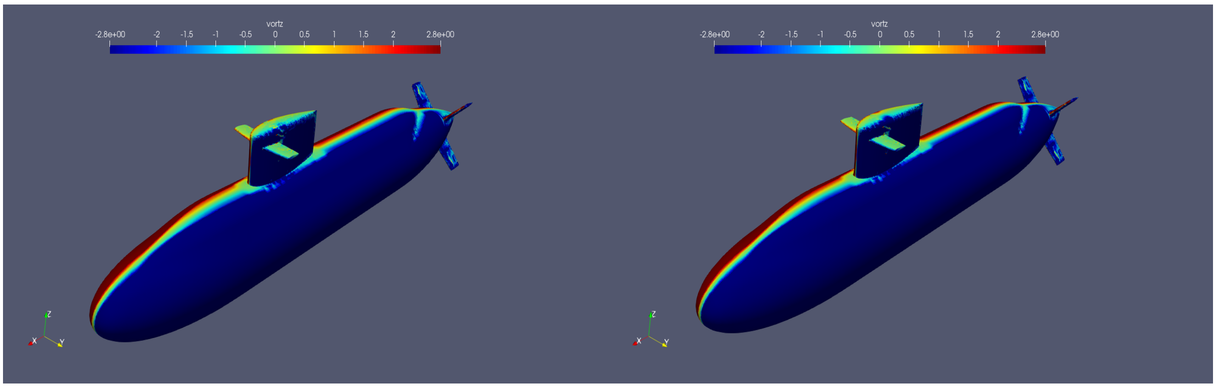

(a) vortz for staticPANS at 0.3 (b) vortz for staticPANS at 0.7

Figure A.24: vortz for staticPANS at 0.3 and 0.7

A.2.2 Skin Friction

The Skin Friction in spanwise direction tauy and tau z are visualised

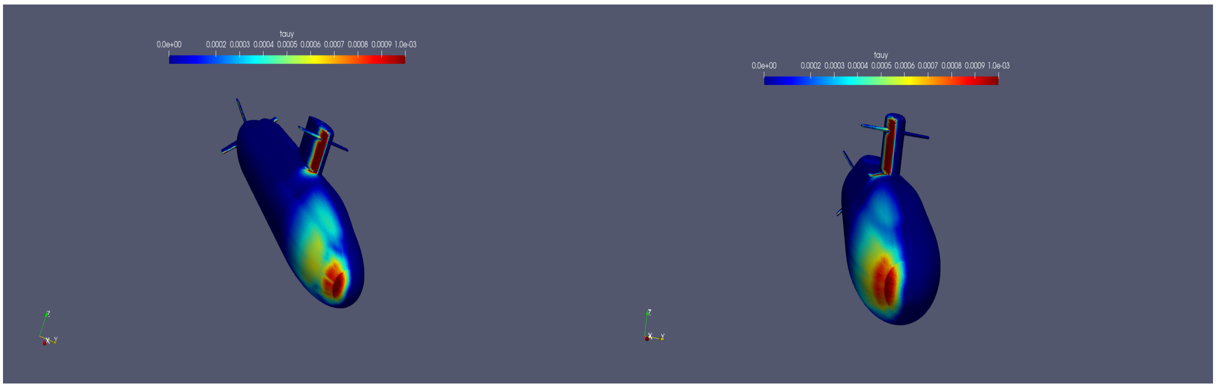

(a) tauy for dynamicPANS (b) tauy for SST

Figure A.25: tauy for dynamicPANS and SST

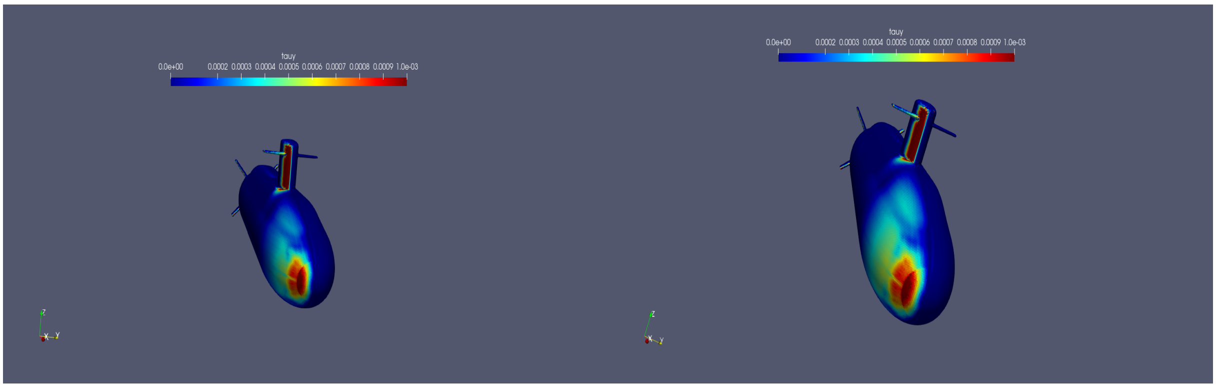

(a) tauy for staticPANS at 0.3 (b) tauy for staticPANS at 0.7

Figure A.26: tauy for staticPANS at 0.3 and 0.7

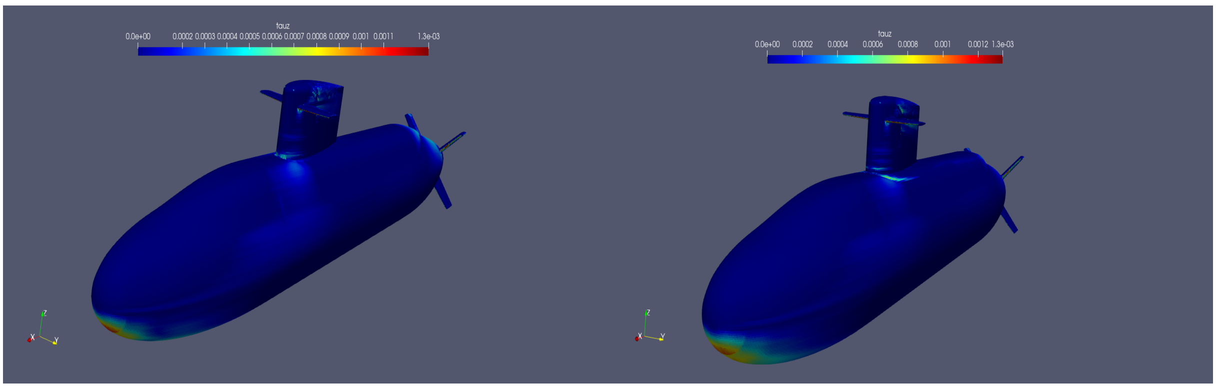

(a) tauz for dynamicPANS (b) tauz for SST

Figure A.27: tauz for dynamicPANS and SST

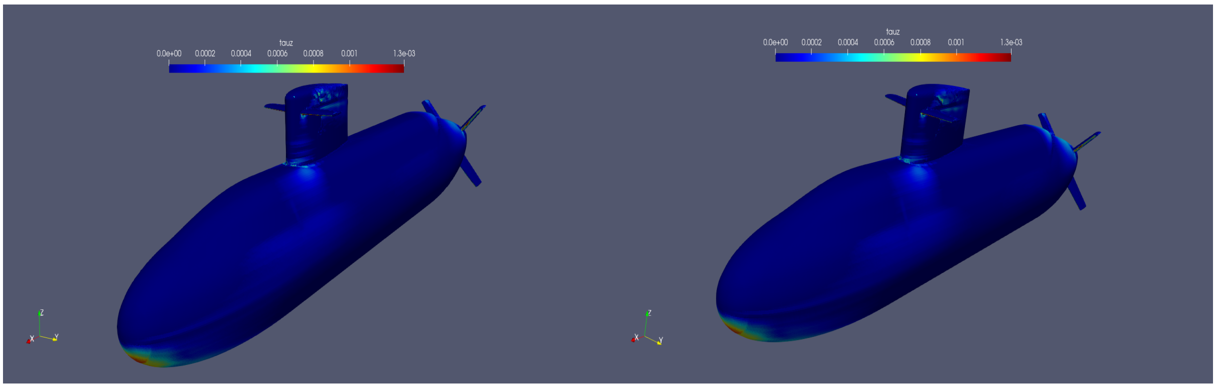

(a) tauz for staticPANS at 0.3

(b) tauz for staticPANS at 0.7

Figure A.28: tauz for staticPANS at 0.3 and 0.7

A.2.3 Unresolved Turbulent Kinetic Energy

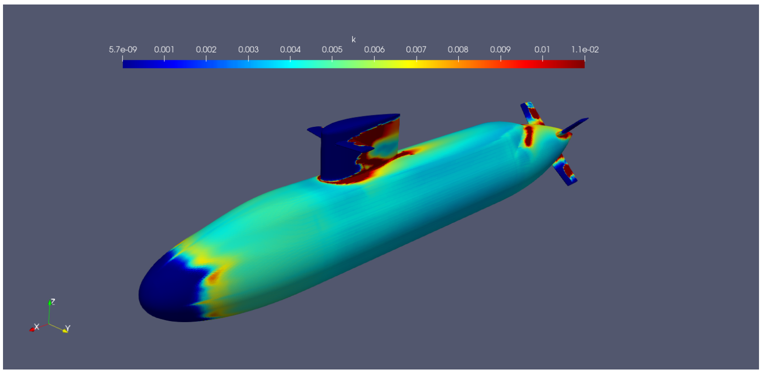

Figure A.29: Unresolved Turbulent Kinetic Energy for Dynamic PANS

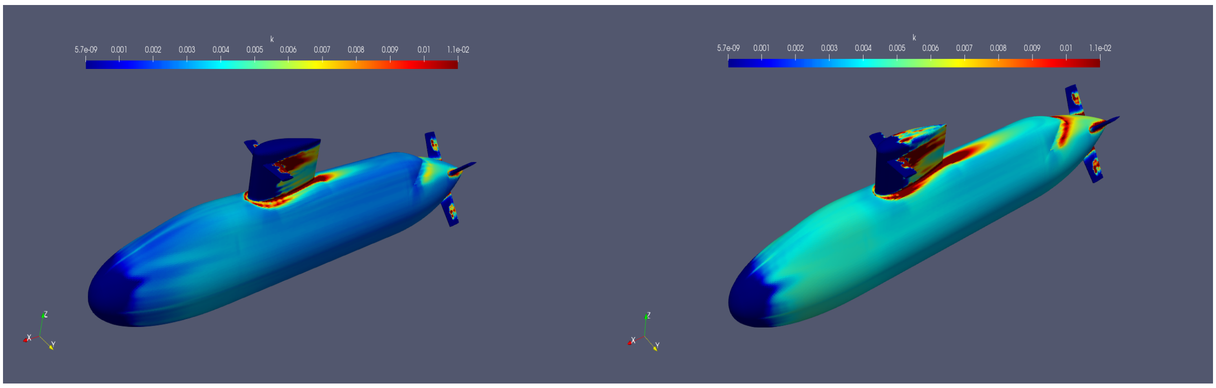

(a) Unresolved Turbulent Kinetic Energy for staticPANS at 0.3

(b) Unresolved Turbulent Kinetic Energy for staticPANS at 0.7

Figure A.30: Unresolved Turbulent Kinetic Energy for staticPANS at 0.3 and 0.7

A.3 Submarine 10 Degree Yaw

A.3.1 Co-Ordinates

The co-ordinates for y and z of the submarine at 10 degree yaw are visualised

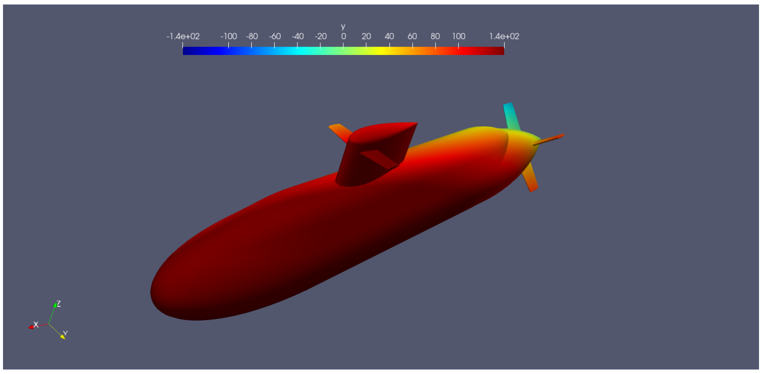

Figure A.31: y Co-Ordinate for SST 10 degree yaw

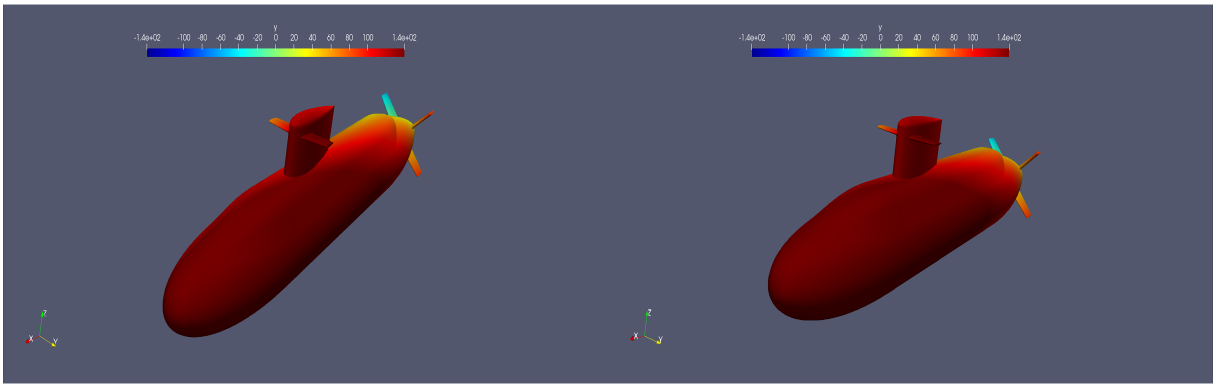

(a) y Co-Ordinate for staticPANS at 0.3 10 degree yaw

(b) y Co-Ordinates for staticPANS at 0.7 10 degree yaw

Figure A.32: y Co-Ordinates for staticPANS at 0.3 and 0.7 10 degree yaw

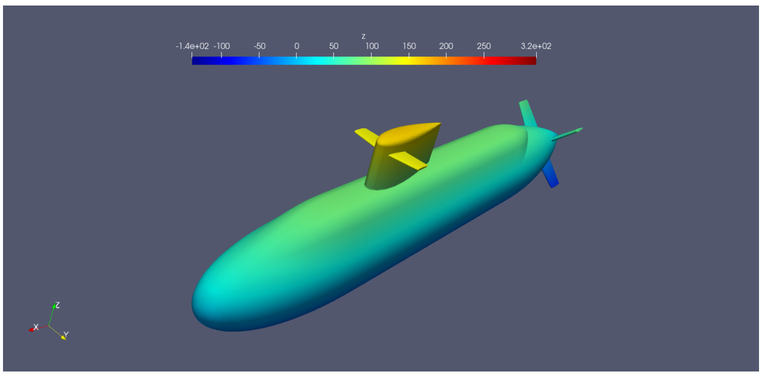

Figure A.33: z Co-Ordinate for SST 10 degree yaw

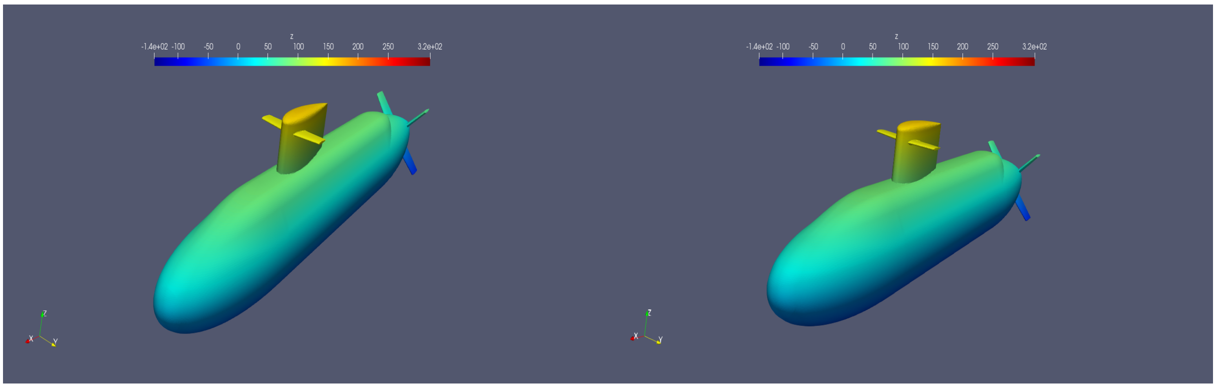

(a) z Co-Ordinate for staticPANS at 0.3 10 degree yaw

(b) z Co-Ordinates for staticPANS at 0.7 10 degree yaw

Figure A.34: z Co-Ordinates for staticPANS at 0.3 and 0.7 10 degree yaw

A.3.2 Vorticies

The Vorticies in spanwise direction vorty and vortz are visualised for 10 degree yaw.

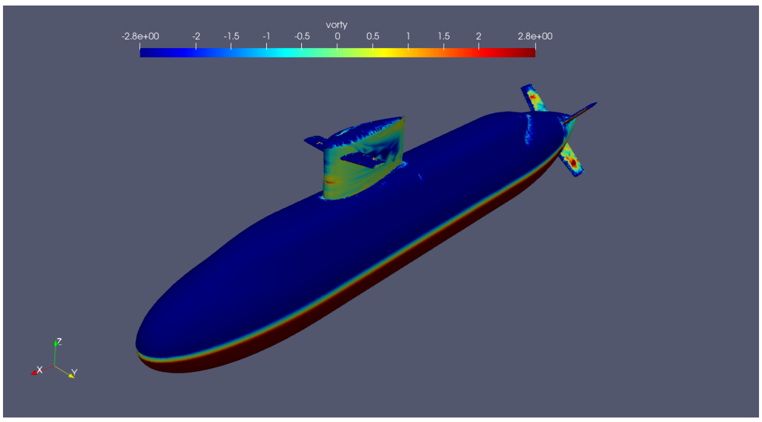

Figure A.35: vorty for SST 10 degree yaw

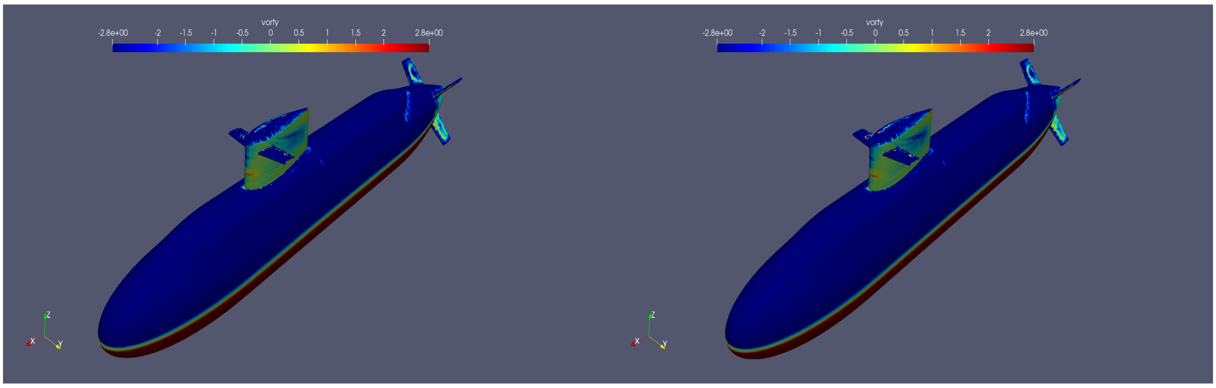

(a) vorty for staticPANS at 0.3 10 degree yaw **(b)** vorty for staticPANS at 0.7 10 degree yaw

Figure A.36: vorty for staticPANS at 0.3 and 0.7 10 degree yaw

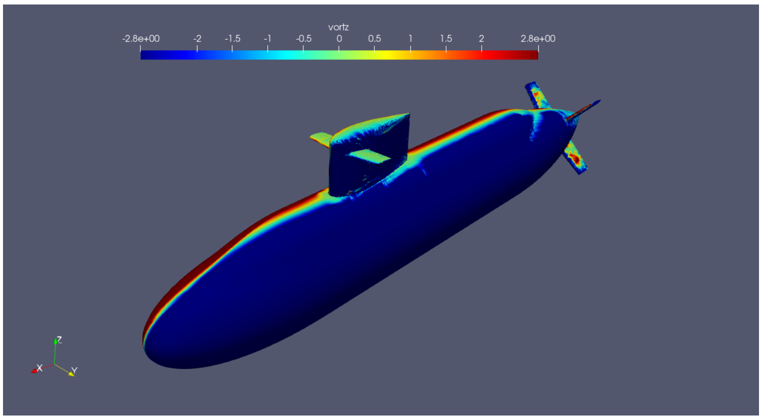

Figure A.37: vortz for SST 10 degree yaw

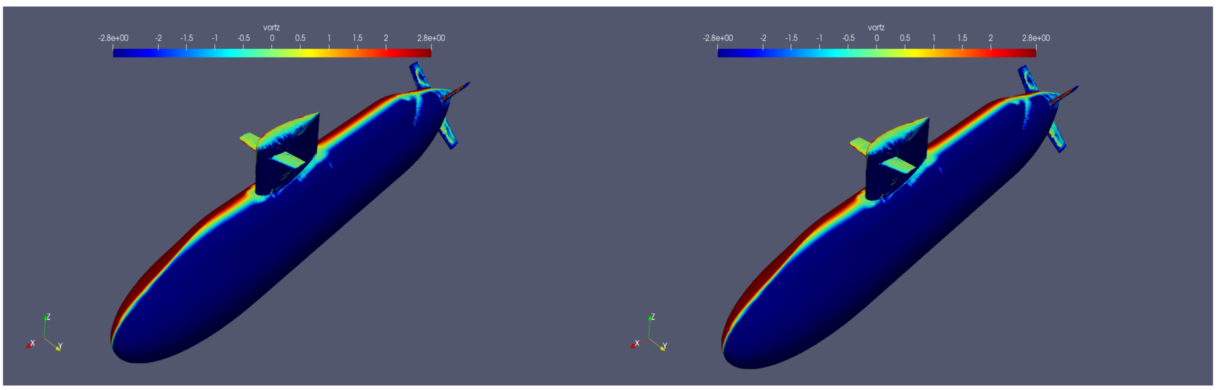

(a) vortz for staticPANS at 0.3 10 degree yaw **(b)** vortz for staticPANS at 0.7 10 degree yaw

Figure A.38: vortz for staticPANS at 0.3 and 0.7 10 degree yaw

A.3.3 Skin Friction

The Skin Friction in spanwise direction tauy and tau z are visualised for 10 degree yaw.

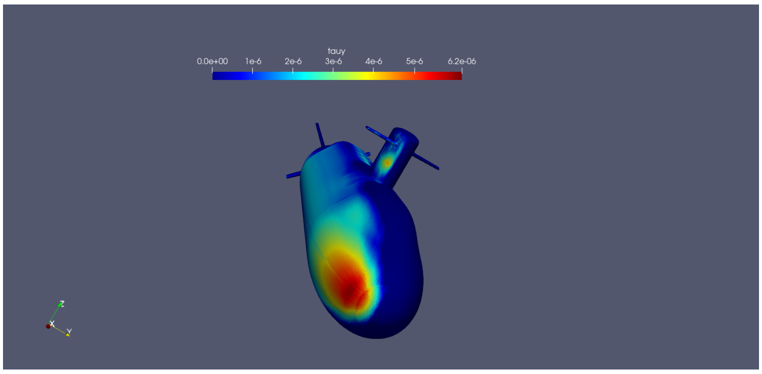

Figure A.39: tauy for SST 10 degree yaw

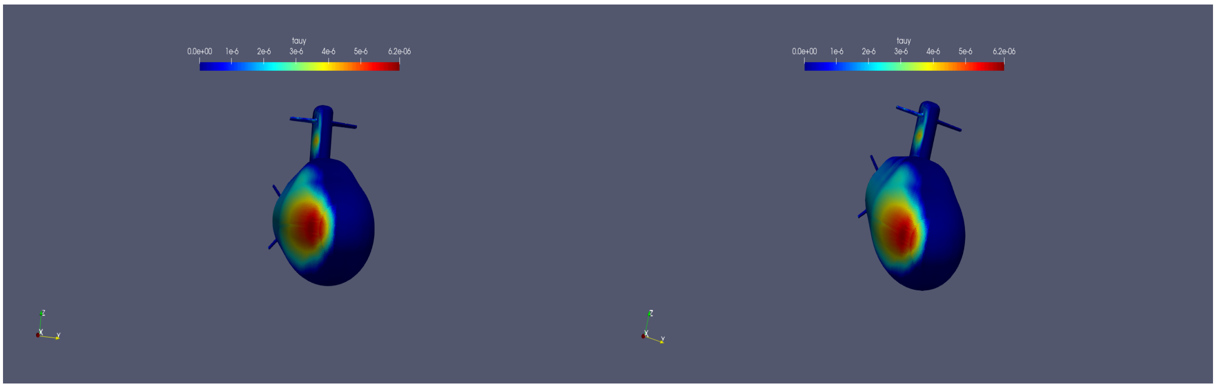

(a) tauy for staticPANS at 0.3 10 degree yaw **(b)** tauy for staticPANS at 0.7 10 degree yaw

Figure A.40: tauy for staticPANS at 0.3 and 0.7 10 degree yaw

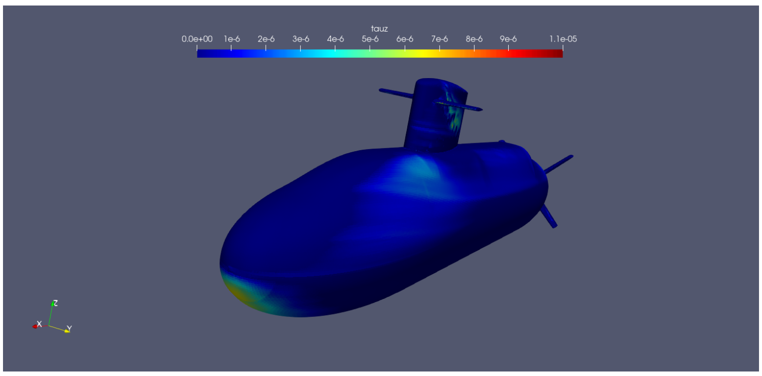

Figure A.41: tauz for SST 10 degree yaw

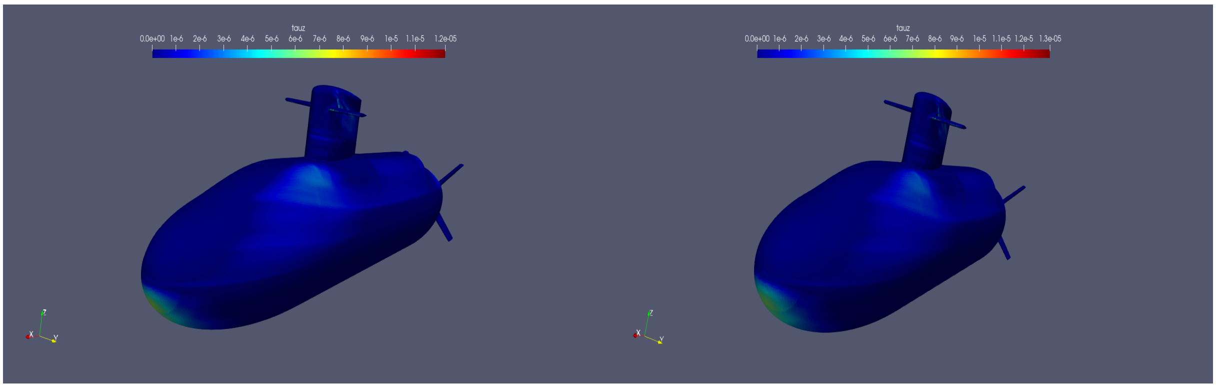

(a) tauz for staticPANS at 0.3 10 degree yaw **(b)** tauz for staticPANS at 0.7 10 degree yaw

Figure A.42: tauz for staticPANS at 0.3 and 0.7 10 degree yaw

A.3.4 fK Variation

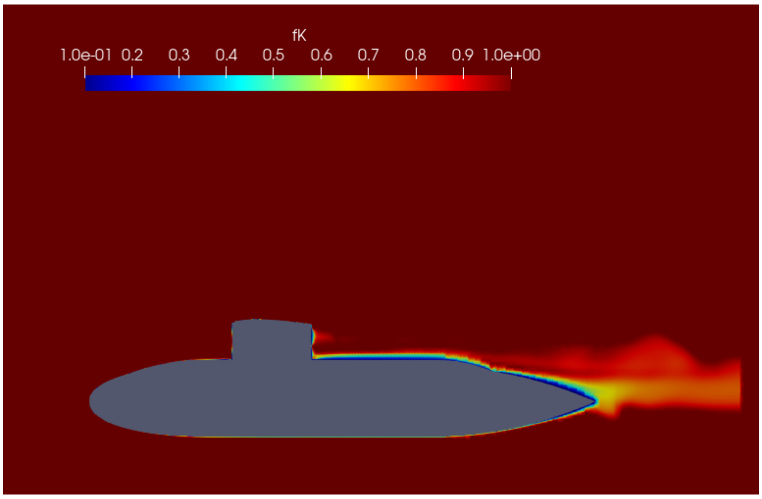

Figure A.43: fk variation

DEPARTMENT OF SOME SUBJECT OR TECHNOLOGY
CHALMERS UNIVERSITY OF TECHNOLOGY
Gothenburg, Sweden
www.chalmers.se

AVANCEZ
1829

CHALMERS
UNIVERSITY OF TECHNOLOGY